SUPPORTED PHOSPHOLIPID MEMBRANES AS BIOMETRIC LABS-ON-A-CHIP: ANALYTICAL DEVICES THAT MIMIC CELL MEMBRANE ARCHITECTURES AND PROVIDE INSIGHT INTO THE MECHANISM OF BIOPRESERVATION

A Dissertation

by

FERNANDO ALBERTORIO

Submitted to the Office of Graduate Studies of
Texas A&M University
in partial fulfillment of the requirements for the degree of

DOCTOR OF PHILOSOPHY

May 2006

Major Subject: Chemistry

SUPPORTED PHOSPHOLIPID MEMBRANES AS BIOMETRIC LABS-ON-A-CHIP: ANALYTICAL DEVICES THAT MIMIC CELL MEMBRANE ARCHITECTURES AND PROVIDE INSIGHT INTO THE MECHANISM OF BIOPRESERVATION

A Dissertation

by

FERNANDO ALBERTORIO

Submitted to the Office of Graduate Studies of
Texas A&M University
in partial fulfillment of the requirements for the degree of

DOCTOR OF PHILOSOPHY

Approved by:

Chair of Committee,	Paul S. Cremer
Committee members,	David H. Russell
	Paul A. Lindahl
	Debjyoti Benerjee
Head of Department,	Emile A. Schweikert

May 2006

Major Subject: Chemistry

ABSTRACT

Supported Phospholipid Membranes as Biometric Labs-on-a-Chip: Analytical Devices That Mimic Cell Membrane Architectures and Provide Insight into the Mechanism of Biopreservation. (May 2006)

Fernando Albertorio, B.S., Pontifical Catholic University of Puerto Rico

Chair of Advisory Committee: Dr. Paul S. Cremer

This dissertation focuses on the applications of solid supported phospholipid membranes as mimics of the cellular membrane using lab-on-a-chip devices in order to study biochemical events such as ligand-receptor binding and the chemical mechanism for the preservation of the biomembrane. Supported lipid bilayers (SLBs) mimic the native membrane by presenting the important property of two-dimensional lateral fluidity of the individual lipid molecules within the membrane. This is the same property that allows for the reorganization of native membrane components and facilitates multivalent ligand-receptor interactions akin to immune response, cell signaling, pathogen attack and other biochemical processes.

The study is divided into two main facets. The first deals with developing a novel lipopolymer supported membrane biochip consisting of Poly(ethylene glycol) (PEG)-lipopolymer incorporated membranes. The formation and characterization of the lipopolymer membranes was investigated in terms of the polymer size, concentration and molecular conformation. The lateral diffusion of the PEG-bilayers was similar to the control bilayers. The air-stability conferred to SLBs was determined to be more

effective when the PEG polymer was at, or above, the onset of the mushroom-to-brush transition. The system is able to function even after dehydration for 24 hours. Ligand-receptor binding was analyzed as a function of PEG density. The PEG-lipopolymer acts as a size exclusion barrier for protein analytes in which the binding of streptavidin was unaffected whereas the binding of the much larger IgG and IgM were either partially or completely inhibited in the presence of PEG.

The second area of this study presents a molecular mechanism for *in vivo* biopreservation by employing solid supported membranes as a model system. The molecular mechanism of how a variety of organisms are preserved during stresses such as anhydrobiosis or cryogenic conditions was investigated. We investigated the interaction of two disaccharides, trehalose and maltose with the SLBs. Trehalose was found to be the most effective in preserving the membrane, whereas maltose exhibited limited protection. Trehalose lowers the lipid phase transition temperature and spectroscopic evidence shows the intercalation of trehalose within the membrane provides the chemical and morphological stability under a stress environment.

DEDICATION

Dedicated to the people who believed in me the most, my parents:

Sarah Isabel Carpintero

and

Ramon Enrique Albertorio

for their loving support in teaching me the value of an education

and

to my friend Amado A. Pereira for always telling me:

“Yes, you can.”

ACKNOWLEDGEMENTS

With highest regards and gratitude to my advisor, Dr. Paul S. Cremer, for his guidance, support and for providing a wonderful atmosphere for doing research in his group. Most importantly, the intellectual freedom with which he has allowed me to pursue my work has given me the opportunity to further grow as a young investigator. His enthusiasm toward science is contagious and he has always been an example of hard-work, dedication and creativity.

I sincerely thank my fellow Cremer group members and friends, for your support and help during these years and for providing a unique and fun work atmosphere. Dr. Tinglu Yang, thank you for your help, guidance and so many hours of helpful discussions. Thanks to Dr. Sho Kataoka, for many hours of insightful discussions, help and training on the SFG and for more countless hours of fun discussions. I especially thank, my good friends, those who have worked closely with me: Vanessa Chapa, Dr. Susan Daniel, Arnaldo Diaz and Kelly Martinez for you sincere friendship, patience, dedication and scientific contributions to my work.

I also wish to thank my many mentors and advisors I was privileged to have throughout a decade of my research career: Dr. Anraldo Carrsquillo, for your true love and enthusiasm towards science and for giving me the opportunity of a MARC fellowship. Dr. Matas and his group for giving me my first research experience, and Dr. Philip Oldham for allowing me to pursue research for two summers at Mississippi State University. Finally, but with sincere gratitude to Dr. Josh Zimmerberg for giving me

the great opportunity of a pre-doctoral research fellowship at the National Institutes of Health (NIH). Thank you for opening the door to biophysics and allowing me to explore new and exiting fields of research. To Dr. Jens Coorssen and Paul Blank, I thank you for being such a positive influence as scientists and mentors.

Finally, I thank my family. To my brothers, Carlos, Ricardo and Enrique Albertorio, I am grateful for their understanding in my choice of a career and for being, each in their own way, role models. To my parents I dedicate my Doctorate of Philosophy Degree in Chemistry. I thank Sarah and Ramon for their loving support, understanding and countless sacrifices they have made to insure I pursue my goals and for teaching me that the most valuable asset in life is your education.

Financial support for this work was provided by the Army Research Office ARO and the National Institutes of Health NIH. Other support was provided by the Defense Advanced Research Project Agency DARPA.

TABLE OF CONTENTS

CHAPTER Page

LIST OF FIGURES

FIGURE Page

FIGURE Page

FIGURE Page

LIST OF TABLES

CHAPTER I

INTRODUCTION

1.1. Purpose/Objective

The study reported in this dissertation has focused on improving the technology of artificial solid supported phospholipid membranes as a mimic of the cellular biomembrane. The need for an improved bio-mimic system is evident in the recent focus of various areas of research in more complex systems such as transmembrane proteins[1], ion channels[2], ligand-receptor interactions, protein-lipid interactions, and membrane dynamics. Therefore, improvements within this field will allow for the creation of better biosensors and model systems for biophysical research.[3, 4] This work is divided into two areas where the first focuses on the incorporation of poly(ethylene glycol) PEG-lipopolymers within solid supported lipid bilayers for the development of a novel biosensing platform. The second area is centered in employing solid supported lipid membranes as an alternative model system in which to elucidate a molecular mechanism of biopreservation.

We have employed various analytical techniques that are surface selective. The importance and need for surface selective analytical methodology arises from the fact

---

This dissertation follows the style and format of the *Journal of the American Chemical Society.*

that most of the biochemical processes that take place on the biomembrane occur at an interface. Therefore, the solid supported membrane system provides an advantage over bulk techniques, in which the biological interface is still defined, in this case, at the bilayer/aqueous interface, and the surface biochemical reactions that take place on the biomembrane can be studied in a native-like environment. The techniques employed interrogate chemical structure, function and morphology of the system, and will be described in chapter II. Briefly, they include vibrational sum frequency spectroscopy, which allows us to probe the chemical structure at an interface while fluorescence microscopy is employed to assay the function of the supported membrane, and atomic force microscopy provides morphological information and structure of our system. The combination of these and other analytical techniques, along with Lab-on-a-Chip technology, allows us to acquire data on various levels, thus permitting us to formulate molecular mechanisms of the biochemical phenomena under investigation.

1.2. The Biological Membrane

The biomembrane has been observed since the early 1900s.[5] However, earlier observations of the nature of oil/water mixtures have been recorded more than a century ago. Benjamin Franklin, in 1774, first observed the behavior of oil droplets on water and noticed that the oil spread, and formed a thin film over the water surface.[6] In 1890, Lord Raleigh conducted the first quantitative experiment of oil/water mixtures attempting to determine the thickness of the oil film. However, the most noted

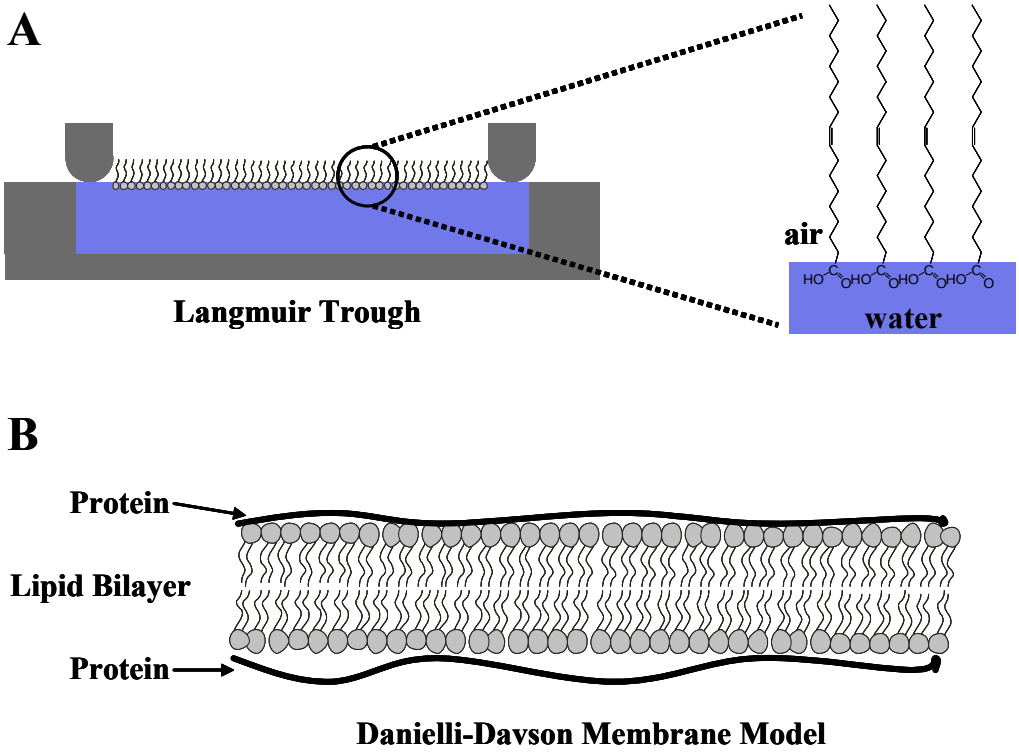

Figure 1.1. (A) The Langmuir trough apparatus with a monolayer of fatty acids. Oleic acid is shown to align itself at the air/water interface. The hydrophobic portion points towards the air while the carboxylic acid interacts with the underlying water. (B) The Danielli-Davson model of the biomembrane.

contribution was made by Irving Langmuir[7], who made quantitative measurements of the area and thickness of oil films employing an improved apparatus, initially developed by Agnes Pokels, known today as a Langmuir trough.[6, 7] Langmuir turned his attention to the behavior of fatty acids and proposed that the fatty acids spontaneously orient themselves at the air/water interface by pointing their hydrophobic chains toward the air, while the carboxylic group interacts with the underlying water as illustrated in figure 1.1.

The first to study the lipids found in biomembranes was Evert Gorter.[8] Using extracted lipids from red blood cells, Gorter and Grendel demonstrated that lipid molecules can form a double layer or bilayer as well as a monolayer and also noted that the surface area of the extracted lipids was twice the area of the native cell.[8] Based on these observations, Danielli and Davson proposed the first model of the biological membrane, shown in figure 1.1., in which the lipids form a bilayer while proteins are adsorbed on both sides of the membrane.[9] However, this model was incomplete and did not account for the functionality of the biomembrane. This and other models were further refined through observations made by light microscopy and electron microscopy.[10]

Singer and Nicolson in 1972 presented the fluid mosaic model of the biomembrane.[11] The model incorporates the basic bilayer structure of Gorter and Grendel, but is modified in that the proteins are incorporated within the bilayer and are as fluid as the lipid molecules that constitute the membrane.[8] This model suggests the complexity of the biomembrane, and the key property that the lipid molecules that constitute the bilayer exhibit lateral diffusion. In fact, such lateral

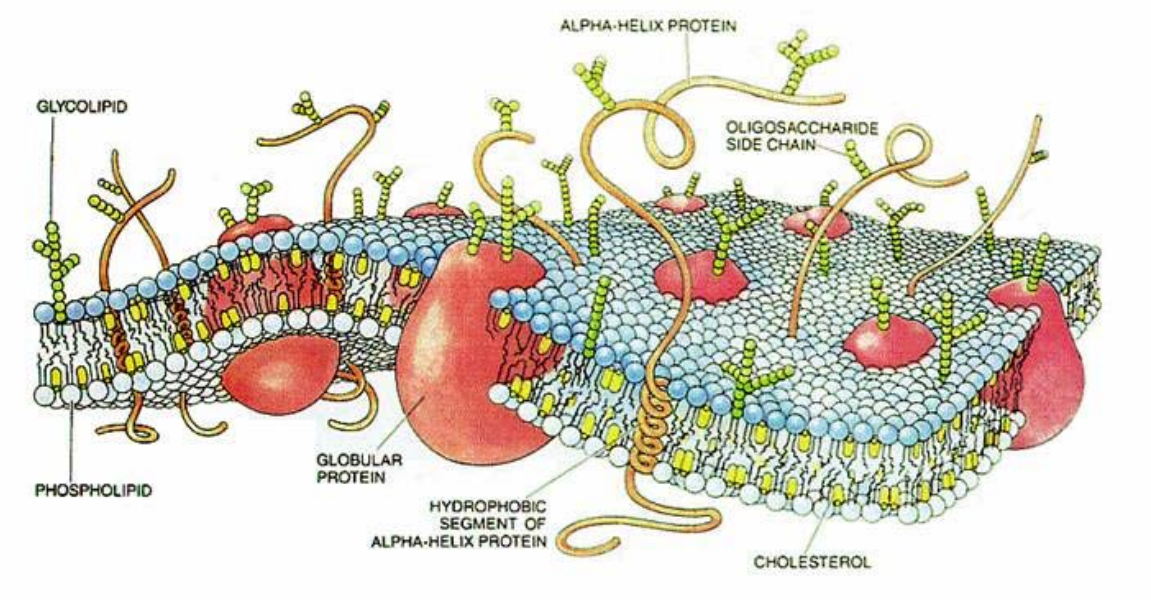

Figure 1.2. The fluid mosaic model of the biomembrane. The phospholipids form a bilayer and the proteins are globular and are incorporated within the fluid membrane.

diffusion allows for the reorganization of the membrane constituents such as membrane associated proteins, transmembrane proteins and other biomolecules.[11] The fluid mosaic model is represented in figure 1.2.

The chemical nature of the biomembrane is manly composed of phospholipids, which are amphiphilic molecules that posses a hydrophilic head and hydrophobic tails.[12] The amphiphilic nature of lipids allows them to reorganize into bilayers, for example, where the hydrophobic tails exclude water and the hydrophilic heads orient toward the aqueous environment. Fatty acids, in esterified form, are the major components of lipids and are carboxylic acids with a long chain hydrocarbon side group. The most common are palmitic, oleic, linoleic and stearic acid. The physical chemical properties of fatty acids vary with their degree of unsaturation. Saturated fatty acids are very flexible and the hydrocarbon chain exists in a fully extended conformation in order to minimize steric interaction between neighboring methylene groups. Their melting temperature increases with molecular weight. The first site of unsaturation usually occurs between the C_9-C_{10} position. Double bonds are usually in the cis configuration. This reduces the effective packing of the hydrocarbon chains by reducing van der Waals interactions, thus inducing a lowering of the melting temperature as the degree of unsaturation increases. Lipid fluidity is dependent on the melting temperature of the fatty acid residues. Therefore, the degree of unsaturation plays an important role in the membrane properties.

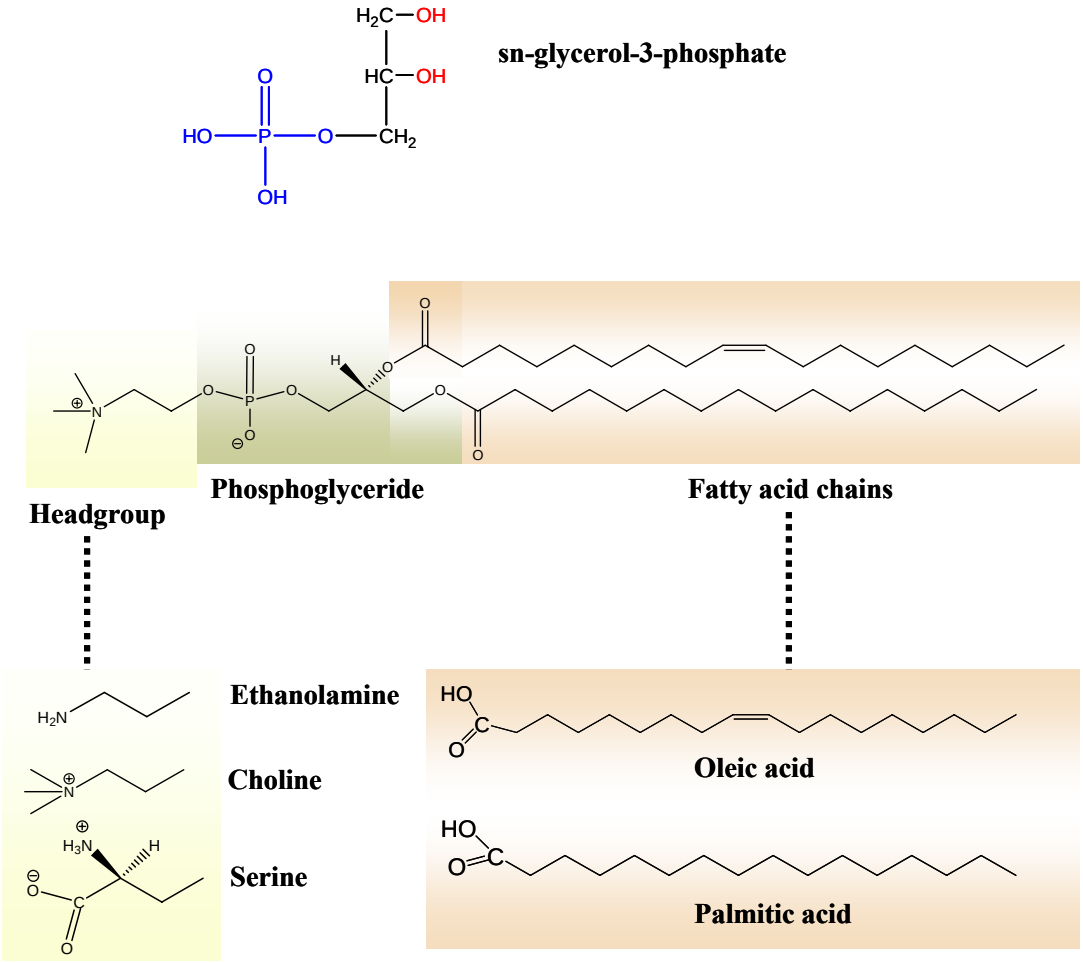

Figure 1.3. The chemical structure of a phosphocholine lipid.

Glycerol is the other building block in the chemical make-up of lipids. Triesters of glycerol form triacylglycerides, which are neutral fats that function as energy reservoirs in animals and plants. Although they are a class of lipids, they are not a component of the biomembrane. Phosphoglycerides consist of sn-glycero-3-phosphate esterified at its C_1 and C_2 positions to fatty acids as shown in figure 1.3. A phosphoryl group is linked at the C_3 position that has a group X at its other end. Group X may consist of a variety of other molecules such as a choline, ethanolamine or serine group. This is the basic chemical structure of a phospholipid that constitutes the biological membrane.[12]

In summary, the amphiphilic nature of the lipid molecules that self-arrange to form the lipid bilayer which is the unit structure of the biomembrane allows for various key properties of the biomembrane.[10] The membrane is a semi-permeable barrier allowing for the selective passage of certain molecules.[6, 12] It provides a fluid and dynamic surface for biochemical reactions to take place and finally, a variety of biomolecules other than lipids are incorporated within the biomembrane. These may be, for example, cholesterol, and sphingolipids which allow for phase segregation, for lipid rafts formation, transmembrane proteins which may be embedded within the bilayer, membrane-associated proteins, glycolipids, proteoglycans, and other molecules that share the biomembrane environment.[11]

1.3. Solid Supported Phospholipid Membranes

The biomembrane is an integral part of the cell physiology.[13] Many biochemical reactions such as cell signaling, ligand-receptor[14] binding, immune response, pathogen attack and endo/exocytosis among others, occur at the membrane surface.[12, 15, 16] These biochemical processes are of great importance in the areas of pharmaceutical industry, and medical and biophysical research.[17] It is therefore important to develop *in vitro* strategies that closely mimic the native biomembrane.

Since their inception in the mid 1980s, solid supported lipid bilayers[18-20] (SLBs) introduced by McConnell[21] and co-workers[22], have proven to be useful mimics of the cell biomembrane.[21, 23] They preserve the lateral fluidity of the lipid molecules which is a fundamental property of native membranes.[24, 25] This allows for the reorganization of membrane components and thus facilitates the investigations of a variety of biochemical and biophysical phenomena, such as ligand-receptor[26-28] interactions and protein-lipid interactions, among others.

The formation and methods of preparation of solid supported lipid bilayers has been discussed in the literature.[29-34] The use of synthetic or natural extracts of lipids is common in the formulation of this *in vitro* system. They are typically formed by either Langmuir-Schaffer techniques[35] or via vesicle fusion[36]. In the Langmuir-Schaffer technique, the bottom leaflet of the bilayer is first formed by pulling a substrate, for example a borosilicate slide, through a lipid monolayer as shown in figure 1.4.[37] The aliphatic portion of the lipids will orient themselves toward the air, while the polar

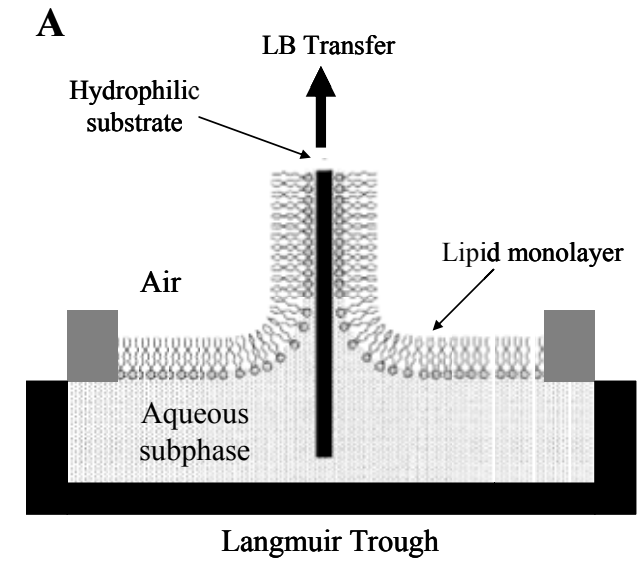

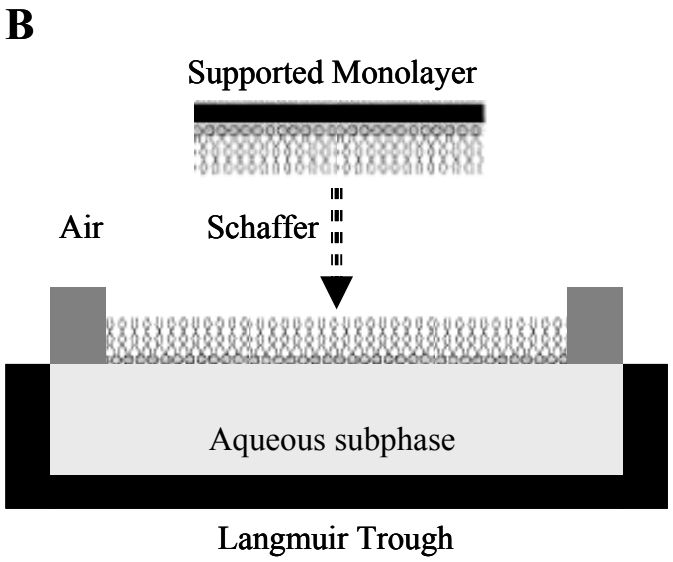

Figure 1.4. The assembly of a solid supported lipid bilayer by Langmuir-Blodget (A) followed by the Schaffer technique (B).

headgroups orient towards the hydrophilic substrate. The upper leaflet can either be formed by a schaffer technique or via vesicle fusion.[36] Although this methodology has not been employed for these studies, this technique has proven useful for the formation of hybrid-lipid bilayers[38], cushioned membranes[1, 39] and for the incorporation of transmembrane helices and peptides within the supported membrane.[39, 40]

The method employed in this study for the assembly of solid supported membranes is the technique of vesicle fusion.[41] In this technique, small unilamellar vesicle solutions are prepared following a similar protocol for the preparation of liposomes.[42] Briefly, a lipid in chloroform solution is dried under vacuum. During this stage, a packing of lipids occurs as the solvent is removed. The next step involves the resuspension of the packed lipids in aqueous buffer solution. Herein, the lipids tend to form a stable structure called liposomes, which are micrometers in size and are multilamellar.[43] Repeated freeze-thaw is done in order to break-up the multilamellar vesicles and form large unilamellar vesicles (LUVs).[43] Finally, the process of extrusion at high pressure through a polycarbonate filter membrane is performed in order to obtain small unilamellar vesicles (SUVs) of sizes that range from fifty to hundreds of nanometers. The size of the vesicles can be tailored by employing membranes of different pore sizes. It should also be noted that a similar product may be achieved by using probe sonication.[42]

Because of their size, small unilamellar vesicles possess a high radius of curvature.[41] The vesicle fusion method exploits this property by using vesicles with a

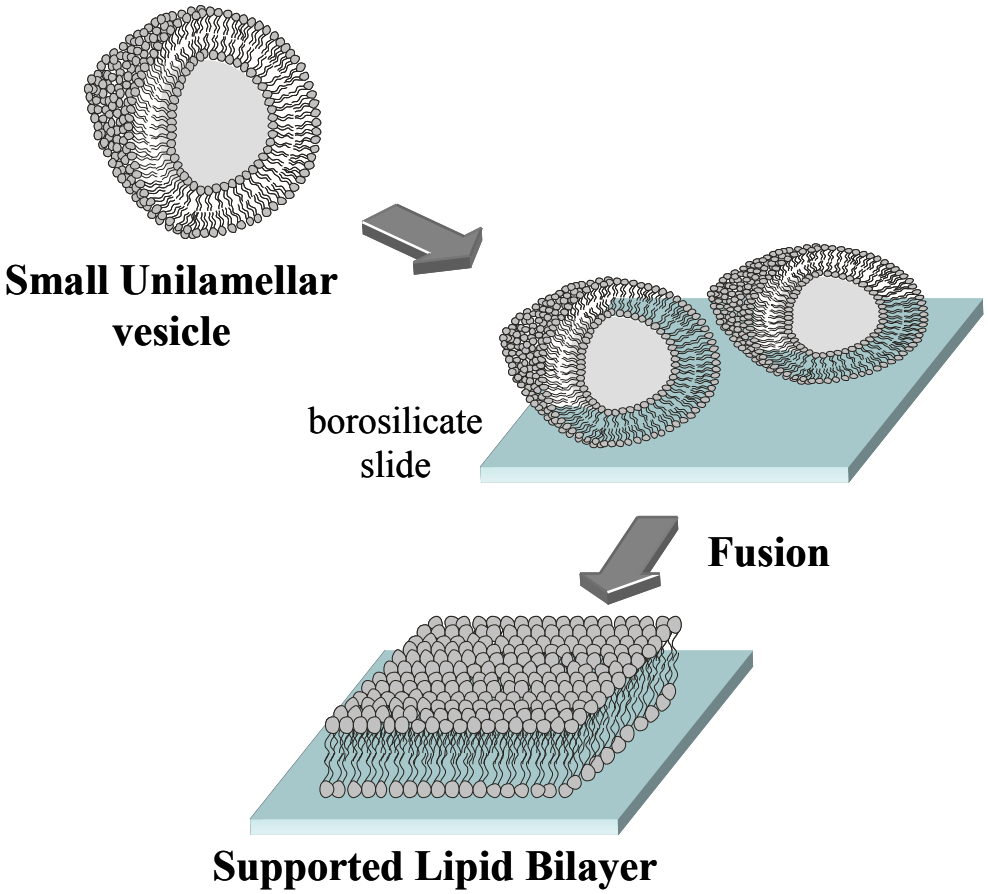

Figure 1.5. The fusion of small unilamellar vesicles to a planar borosilicate substrate.

typical size of 50-100 nm.[41, 44] Generally, these vesicle solutions are exposed to a planar hydrophilic substrate such as silicon, borosilicate, quartz or mica.[41] The SUVs spontaneously fuse to the substrate resulting in a single lipid bilayer.[29, 30, 45] The process of vesicle fusion is illustrated in figure 1.5. However, the exact mechanism of vesicle fusion is still debated in the literature.

Various methods have been employed to study the mechanism of small unilamellar vesicle fusion. Fluorescence microscopy of dye-encapsulated vesicles has been utilized to study the kinetics of membrane fusion.[29, 34, 46] Atomic force microscopy[47] (AFM) has also been employed to elucidate the intermediate steps of fusion while the quartz crystal microbalance with dissipation (QCM-D)[48] technique has proven useful to study the onset, kinetics[49] and pathways of vesicle fusion.[49-51] Other reports have utilized elipsometry or surface plasmon resonance (SPR) microscopy or spectroscopy.[47, 52]

A general mechanism is that vesicles that encounter the solid/aqueous interface of a hydrophilic substrate may proceed via one of two pathways.[52] The first pathway implies that vesicles with a radius greater than the critical radius (r_c) will undergo direct fusion to the underlying substrate. In the second pathway, vesicles with a radius smaller than r_c will undergo vesicle-vesicle fusion until their radius equals the critical radius and then proceed via the first pathway.[53] It should be noted that in order for either pathway to proceed, a minimal surface density of vesicles is required. Known as a percolation threshold, this is the minimal concentration of vesicles needed in order to form an infinitely continuous two-dimensional film.[52, 53]

There are external factors that will affect the mechanism of fusion. These have been studied by QCM-D[48] in which the change in two parameters, frequency and dissipation are monitored as a function of time. The change in frequency is related to the adsorbed mass or surface density, and the dissipation is related to the type of film i.e. hardness or softness of the adsorbed film.[48] The fusion of vesicles to the quartz crystal under aqueous conditions is monitored. Intact adsorbed vesicles or a lipid bilayer can be distinguished with this technique by their respective changes in frequency and dissipation.[54] Therefore, the effects on the kinetics and pathway of fusion may be studied by changing parameters such as vesicle size, charge, lipid composition, concentration, temperature, pH and the electrolyte solution.[55] QCM-D has been compared to other methods such as elipsometry and SPR[50], which do not provide a clear distinction between adsorbed vesicles and a fused lipid bilayer.[56, 57] Fluorescence microscopy is useful in assaying the function of the two-dimensional lipid film. In particular, fluorescence recovery after photobleaching[36] (FRAP) provides information about the 2-D lateral diffusion of the fluorescently labeled lipids within the bilayer.[58] This methodology will be discussed in Chapter II.

The fusion of small unilamellar vesicles to planar substrates depends on various parameters. The size of the vesicles, concentration and charge will affect the vesicle curvature and their interaction with the substrate. The hydrophilicity, surface charge and surface roughness of the substrate play an important role in the assembly of solid supported lipid membranes. Other parameters such as vesicle composition, lipid phase

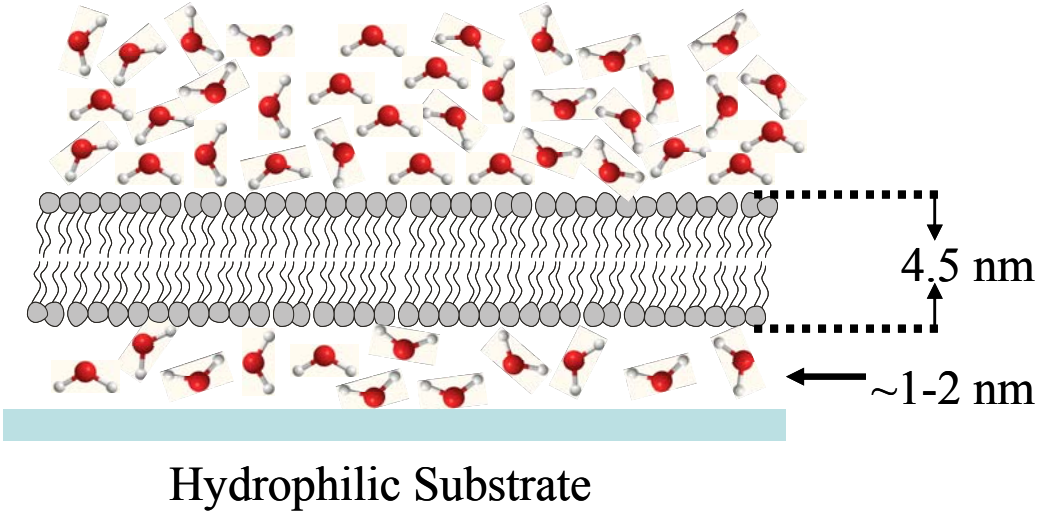

Figure 1.6. Phospholipid membrane supported on a hydrophilic substrate. There is a molecular thin layer of water in between the substrate and lipid bilayer.

transition temperature, and the electrolyte solution will affect, to various degrees, the overall fusion process.

A supported lipid bilayer is characterized by having a thickness of 4.5-5nm.[59, 60] The most important feature is that a thin water layer of ~1-2nm exists between the substrate and the lipid film.[61] The presence of this water layers affords structural stability and maintains two-dimensional lateral fluidity of the supported membrane.[62] A model membrane is shown in figure 1.6.

1.4. Stability of Phospholipid Membranes

Solid supported bilayers preserve the lateral mobility of the individual lipid molecules because a thin water layer resides between the lower leaflet of the membrane and the underlying solid surface.[63] Lateral fluidity makes these platforms ideal for creating biosensors because they can readily mimic the same two-dimensional rearrangements that take place on cell surfaces during ligand-receptor recognition events.[25, 28] The forces that hold the bilayer at the solid/aqueous interface of a glass substrate involve electrostatic, van der Waals, hydrophobic, and steric interactions.[64] A major problem is that the lipid bilayer delaminates from the interface if the thin film is exposed to the air/water interface. This detachment occurs because it is energetically unfavorable to remove the hydrophilic lipid headgroups from solvation waters. Therefore, when an air bubble arrives at the surface, the membrane must reorganize to expose some of its lipid chains to the nascent air/water interface, while the rest of the

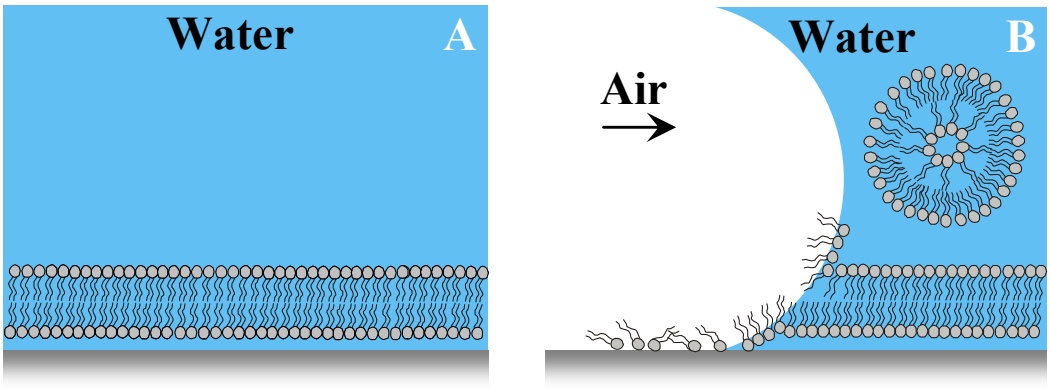

Figure 1.7. The introduction of an air interface destroys the solid supported bilayer by peeling it away from the surface in vesicle sections (note: some lipids also form a monolayer at the air surface).

lipid material becomes part of newly formed vesicles in the aqueous solution as depicted in Figure 1.7.[63]

Attempts to preserve supported bilayers in order to protect them upon exposure to air have been presented in the literature.[65, 66] The main motivation is to present a novel system for biosensing applications. Certain strategies have involved the use of tethered or hybrid bilayers systems.[38, 64] These systems are generally prepared via the Langmuir-Blodgett method in which the bottom leaflet is covalently attached to the underlying support.[35, 67] The type of chemical modification depends on the substrate. thiol or silane modified lipids are employed for either gold or SiO_2 substrates. These chemical modifications help anchor the lipid bilayer to the support. Other methods employ bolaamphiphiles monolayers and substrate modifications in order to achieve air stability.[38] Polymerizable synthetic lipids have also been used to create a new class of stable lipid bilayers.[68] These lipids usually contain dienes and can either be chemically or photo-polymerized, and have been found to be resistant to exposure to air and chemical solvents. Photo-polymerization has also been applied for the spatial addressing of lipid membranes for sensing applications.[69-71] Finally, other attempts to stabilize lipid membranes have been achieved by employing charged lipid vesicles, thus relying on the electrostatic interactions between the bilayer and substrate.[72] Although these methods yield air stable supported bilayers, these systems lack or experience a loss in the lateral mobility of the lipids within the membrane. Hence this affects their performances as biomimics and sensing platforms.

Consistent with the mechanism for lipid bilayer removal that is described above, our laboratory developed a simple method for preventing delamination. The approach involved specifically binding a protein monolayer of streptavidin to a biotin containing phospholipid surface.[63] This should have had two effects on the bilayer stability. First, it would increase the bending elastic modulus (stiffness) of the membrane and thus increase the barrier for lipid patches to roll up into sheets and peel away as vesicles. Second, the presence of the protein coat should make it difficult for the upper leaflet of the bilayer to rearrange to form a monolayer film at the nascent air/water interface.[63]

The strategy described above works exceedingly well at preventing the delamination process from occurring. In fact, the lipid molecules remained mobile when the system was placed in ambient air. The diffusion constant in the lipid membrane before removal from water was $D=1.9 \times 10^{-8}$ cm^2/sec. While in air near 100% relative humidity, $D = 2.9 \times 10^{-9}$ cm^2/sec and returned to the original value upon rehydration in bulk water. Of equal significance was the fact that the mobile fraction of labeled lipids in the membrane was greater than 90%.[63]

Despite the success of the approach described above, it is unsuitable for the creation of biosensors. Unfortunately, it is necessary to blanket the entire bilayer with a relatively close-packed streptavidin film to afford air stability. Therefore, when additional ligands are also incorporated into the film for sensing applications, they are unavailable for binding with their target protein analytes because the protective streptavidin layer sterically blocks additional ligand-receptor binding.

In summary, the methods presented in the literature towards membrane preservation generally consist of chemical modification of the lipid film, substrate modification, a complex assembly method or a steric effect. Therefore these methods can compromise of the underlying characteristics of the system.

1.5. Summary

Solid supported phospholipid membranes are useful mimics of the cell biomembrane. They preserve the property of two-dimensional lateral fluidity of the individual lipid molecules and membrane constituents found in native membranes. As biomimics, they have a vast utility as biosensors and present the opportunity to study cellular biochemical and biophysical processes.

Our interest and main goal of the study reported herein is to improve the technology of solid supported membranes by further mimicking other aspects of the native biomembrane architecture. Primarily, the study focuses on improving the stability of supported phospholipid membranes by employing lipopolymer incorporated bilayers. In order to address this problem, we utilized an alternative membrane coating that stabilizes the lipid bilayer, while still allowing facile ligand-receptor binding to take place.[73] The particular architecture needs to be porous enough to allow access for proteins, toxins, and other large analytes of interest in the solution phase to bind to surface-associated ligands, while still affording the required air stability. Poly(ethylene glycol) PEG conjugated lipids were used for this purpose. The choice of membrane stabilizer is inspired by the elaborate chemistries found on bacterial and eukaryotic cell

surfaces. Cell surfaces are often terminated with a variety of glycosylated proteins, glycolipids, and polymeric structures that can extend tens of nanometers above the plasma membrane.[74] The glycocalyx affords stability to real cells, and plays a role in cell signaling and cell-cell interactions.[75] Such an approach has been notably absent from most model membranes mimics to date.

The second goal of the study was to investigate and model the process of biopreservation using the solid supported membrane system. Herein, SLBs have proven useful in elucidating a molecular level mechanism of biomembrane preservation by small disaccharides.

This study represents and contributes to the improvement of the biosensing capabilities of solid supported phospholipid membranes. It also demonstrates the close biomimicking properties of SLBs and how this model system can be employed to elucidate biomolecular interactions and processes.

CHAPTER II

EXPERIMENTAL

2.1. Synopsis

This chapter presents the methodology employed throughout this study. The goal of all the experimental techniques is to obtain surface specific data of the system under investigation. The experimental techniques explain herein are designed to obtain functional, chemical and morphological information about the system. The use of surface selective analytical methods to study solid supported phospholipid membranes for a variety of applications has been demonstrated.

This chapter discusses the application of microfluidic technology[76] in combination with SLBs as analytical devices.[77] A fluorescence microscopic method used to probe the function of solid supported lipid bilayers in terms of their two-dimensional lateral diffusion[78] will also be presented.

Vibration sum frequency spectroscopy[79] (VSFS) has been employed to investigate the chemical nature of the interface. This spectroscopic technique is useful for the determination of the orientation, alignment and chemical nature of species that are interacting at an interface, such as a solid/aqueous or aqueous/air interface.[80]

Furthermore, atomic force microscopy[81] (AFM) has been used as a morphological probe of the solid supported lipid membrane system. This section presents the methodology employed to probe a solid supported membrane in its native

environment. The instrument design and the experimental technique of fluid AFM is presented.

Other experimental methods such as the conjugation of fluorescent dyes and purification of labeled proteins will be described. The preparation of vesicle solutions and other chemicals employed in this study will be explained in their respective chapters.

2.2. Soft Lithographic Preparation of Microfluidic Devices

Since its development in the 1980s by Whitesides[14, 82] and coworkers, the soft lithographic technique has made it possible to create a wide variety of spatially addressed devices.[32, 45, 83, 84] Soft lithography is defined as a set of methods for the fabrication of structures using elastomeric materials, polymeric stamps or conformable molds. It is an effective and low cost method for the creation of micro- or nano-structures. For these reasons, soft lithography[85] is the method of choice for the development of microfluidic devices. Generally, the process can be divided into three main steps. The first step is photolithography in which a structure is transferred to a photoresist polymer using a photomask; after which a chemical etching or dry etching procedure is performed. The final steps involve the use of an elastomeric material called poly(dimethylsiloxane) PDMS in which, after the curing or cross linking step, a negative image of the photomaster is transferred to the PDMS stamp. The procedure is illustrated in figure 2.1.[76, 86]

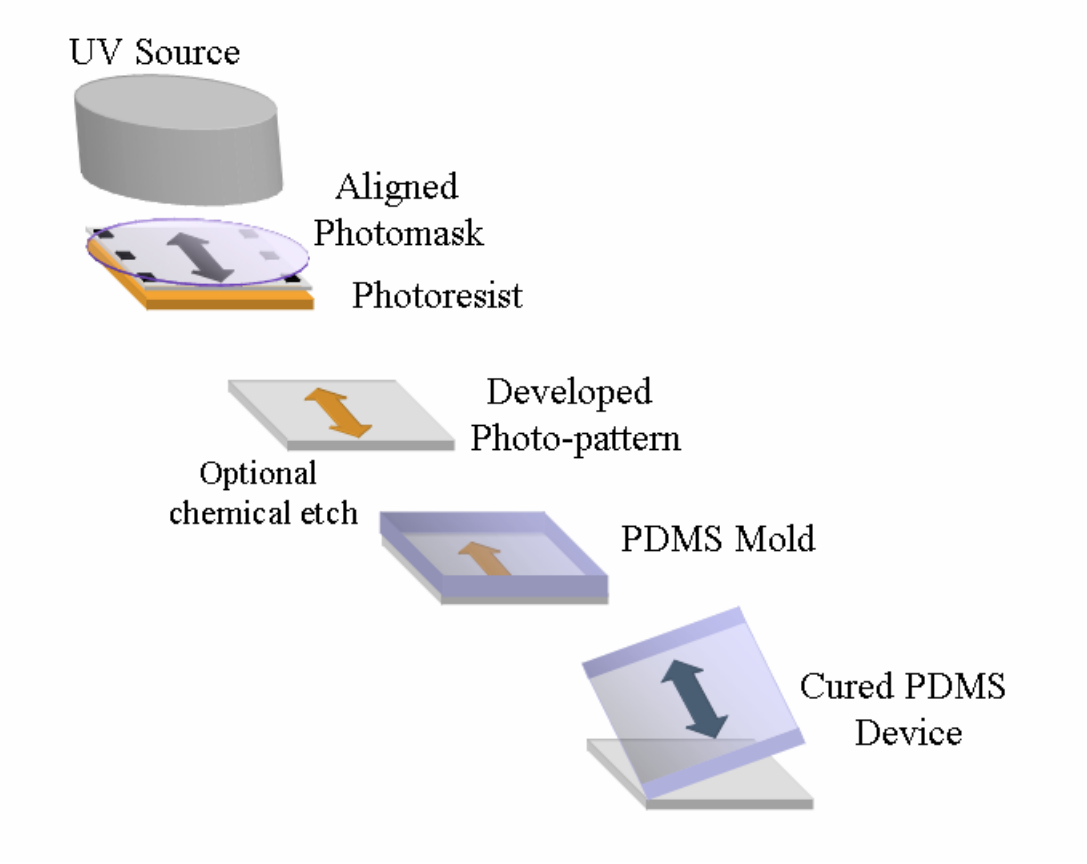

Figure 2.1 Schematic of the soft lithography procedure.

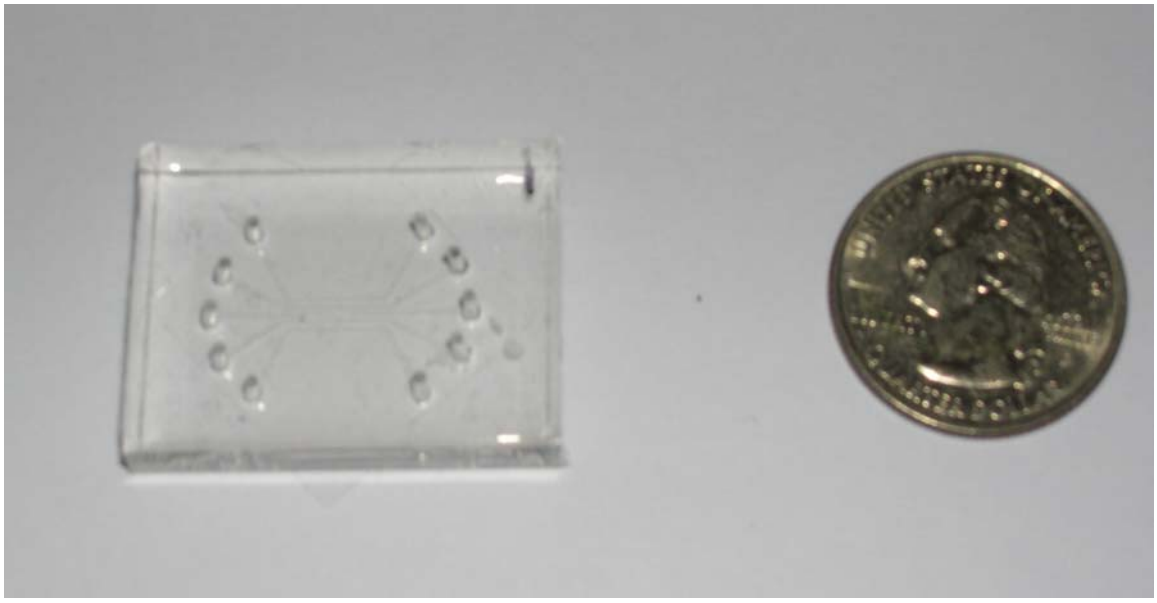

Figure 2.2. Photograph of a 5-channel microfluidic device.

The procedure is useful for creating low aspect ratio microchannels. In this study, we created 5-channel PDMS microfluidic devices as shown in figure 2.2. The devices are manufactured using a similar procedure as described above. An S-1813 photoresist is acquired from Shipley. After exposing the photoresist covered slide to UV radiation, the photoresist is baked, and developed. At this stage a hard baking procedure is done at 100 ^{o}C for 24 hours in order to remove excess solvent; after which a chemical etching procedure is done using hydrofluoric acid solution according to a published procedure.[82] This provides etched microchannels with a height of ~27 μm and a width of ~ 300 μm. A profilometer is used to characterize the finished product. The procedure is finished by pouring the PDMS elastomer followed by curing at 70 ^{o}C for 1 hour. When the device is ready to be used, the PDMS stamp is pealed and the inlets and outlets or perforated. The tall channels allow for the devices to be pumped manually with a syringe and are also reusable.[73]

2.3. Conjugation of Fluorescently Labeled Proteins

The use of reactive fluorescent dyes for the conjugation of proteins to be detected by fluorescence microscopy is an integral part of the systems employed in this study. The careful selection of fluorescent molecules is important in order to achieve high signal-to-noise, and lower limits of detection. Important factors are the quantum efficiency (QE) of the selected dye, excitation and emission wavelength, solubility and reactive moiety. Derivatives of fluorescein, like Rhodamine dyes, Texas Red and the Alexa dye family, have been widely applied in the area of biomedical research because

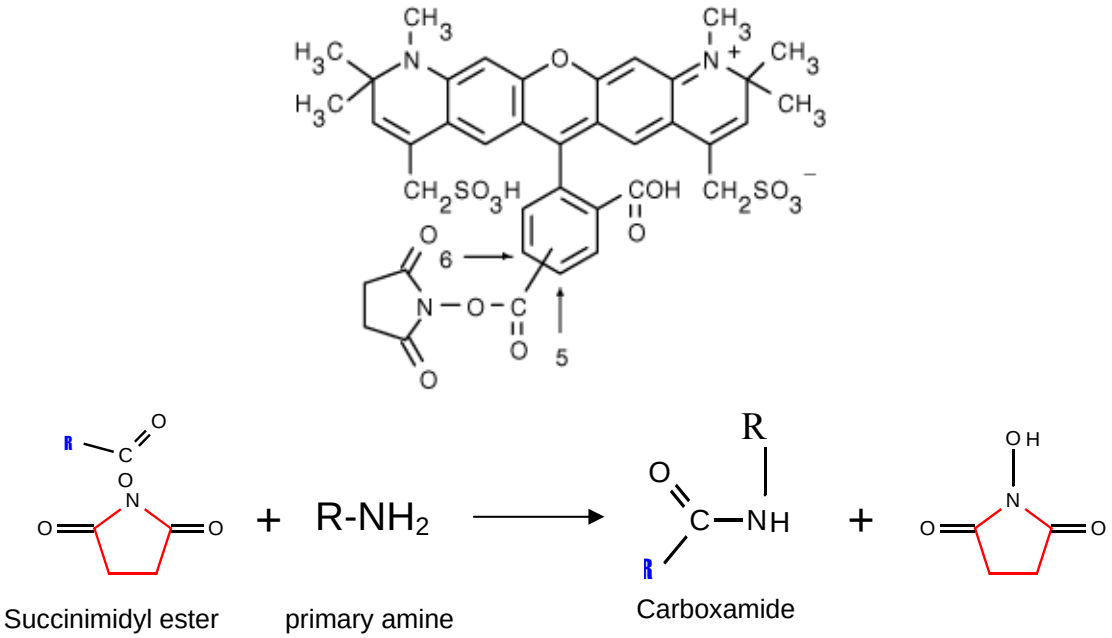

Figure 2.3. The chemical structure of an Alexa-fluor dye with a succinimidyl ester reactive group. The succinimidyl ester reacts with the primary amines of the proteins and thus allows for the fluorescent conjugation of biomolecules.

of their high QE, thermal and chemical stability, solubility in aqueous medium and ease of conjugation. This was achieved by the addition of more conjugated fused rings, amine and carboxylic groups at the ends and the coupling of a reactive group such as a succinimidyl ester.

Figure 2.3 shows the chemical structure of an Alexa-fluor dye, which are acquired from Molecular Probes (Eugine OR.). The reactive group is a succinimidyl ester, which readily reacts with primary amines. Since proteins contain primary amines from amino acids like argenine and lysine, these biomolecules are easily labeled under aqueous conditions. The degree of labeling or mole dye/mole protein can be tailored by changing the solution conditions. The labeling of proteins such as IgG has been performed according to established procedures, typically 1mg/ml protein from 1 hour at room temperature at pH 8.0. The unreacted dye is separated from the analyte by size exclusion chromatography (SEC).

2.4. Fluorescence Recovery after Photobleaching FRAP

The technique of fluorescence recovery after photobleaching FRAP is one of the standard methods to measure the translational dynamics of a fluorescent species.[78] Initially intended to measure the diffusion coefficients of dye molecules[87], FRAP, has been most recently employed in measuring the lateral diffusion on membrane components such as proteins and labeled lipid molecules.[36, 58] The technique is represented in figure 2.4.

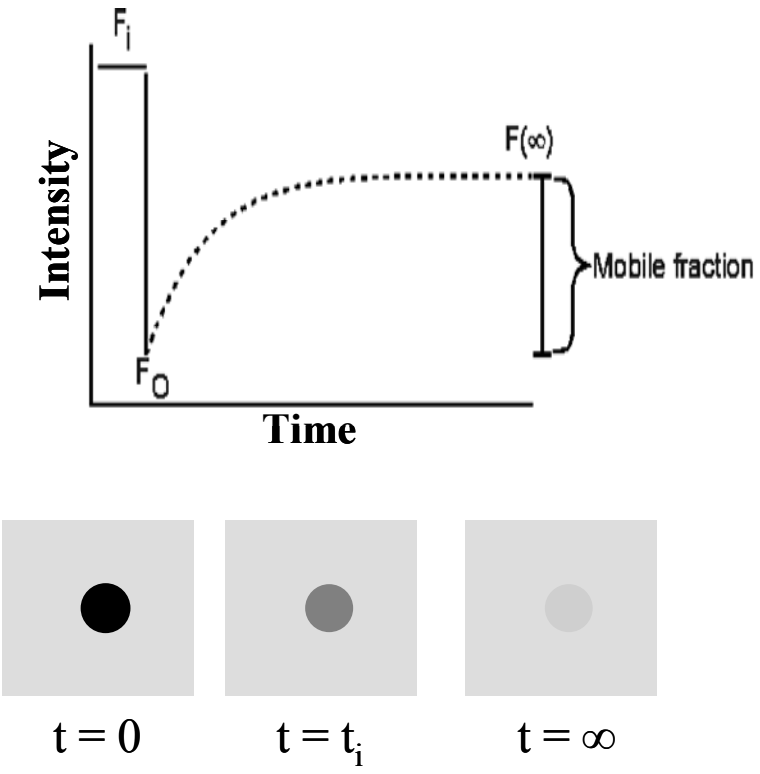

Figure 2.4. A fluorescence recovery after photobleaching curve. An intense laser bleaches part of the sample and the fluorescence recovery of the bleached region is monitored as a function of time. The resulting FRAP curve is used to calculate the diffusion constant and mobile fraction of the analyte.

In a typical FRAP experiment the sample is photobleached with an intense laser for a short period of time; after which the recovery of fluorescence intensity of the bleached region is monitored as a function of time and a FRAP curve is generated. The fluorescence intensity before and during the experiment, are normalized according to the following equation:

$$y = \frac{F_o - F_t}{F_i - F_0} \tag{2.1}$$

where y is the normalized fluorescence intensity, F_i represents the fluorescence intensity before bleaching, F_0 is the intensity of the photobleached region at t = 0, and F_t is the intensity of the bleached region as a function of time. We also assume that the fluorescently labeled component is initially uniformly distributed within an infinite two dimensional plane and that the observable consists of only one component diffusing within the plane.[78] Applying first order kinetics allows us to fit the FRAP curve to a single exponential rise to maximum equation as follows:

$$y = a(1 - e^{-kt}) \tag{2.2}$$

where *a* represents the mobile fraction of the component and k is a constant. To calculate the time at half recovery ($t_{1/2}$), we assume a = 1, then $t_{1/2}$ = ln2/k since the process follows first order kinetics. The diffusion constant (D) is calculated using the following equation[73, 78, 87]:

$$D = \frac{w^2}{4\tau_{1/2}}\gamma_D \tag{2.3}$$

In this equation, w represent the full-width-at-half-max of the Gaussian laser beam and γ_D is a correction factor for the amount of induced photobleaching.

It should be noted that the FRAP experiment depends on the control of various parameters. The laser beam is typically Gaussian and circular, however, variants of this technique may employ an elliptical beam.[58] The laser power and bleach time must remain constant in order to insure consistent results. It is important that for fast diffusing molecules with a $D > 10^{-8}$ cm^2/s, the bleach time must be much less than $t_{1/2}$. Other factors that affect the diffusion measurements by FRAP include temperature and photobleaching of the sample during data acquisition. This may be controlled by adjusting the image acquisition time intervals during the time-laps imaging.

The fluorescence recovery after photobleaching (FRAP) curves used for this study were obtained by exposing the sample to laser irradiation from a 2.5 W mixed gas Ar^+/Kr^+ laser (Stabilite 2018, Spectra Physics). Planar bilayer samples were irradiated at 568.2 nm with 100 mW of power for times not exceeding 1 sec. A 17.0 μm full-width at half-max bleach spot was made by focusing the light onto the bilayer through the 10x objective. The FRAP experiments were performed using an inverted epifluorescence Nikon Eclipse TE2000-U microscope and the bilayers observed with a 10x objective. Images were obtained using a MicroMax 1024b CCD camera (Princeton Instruments) and data analysis was performed with MetaMorph software (Universal Imaging). The fluorescence microscopy system employed for FRAP measurements is shown in figure 2.5.

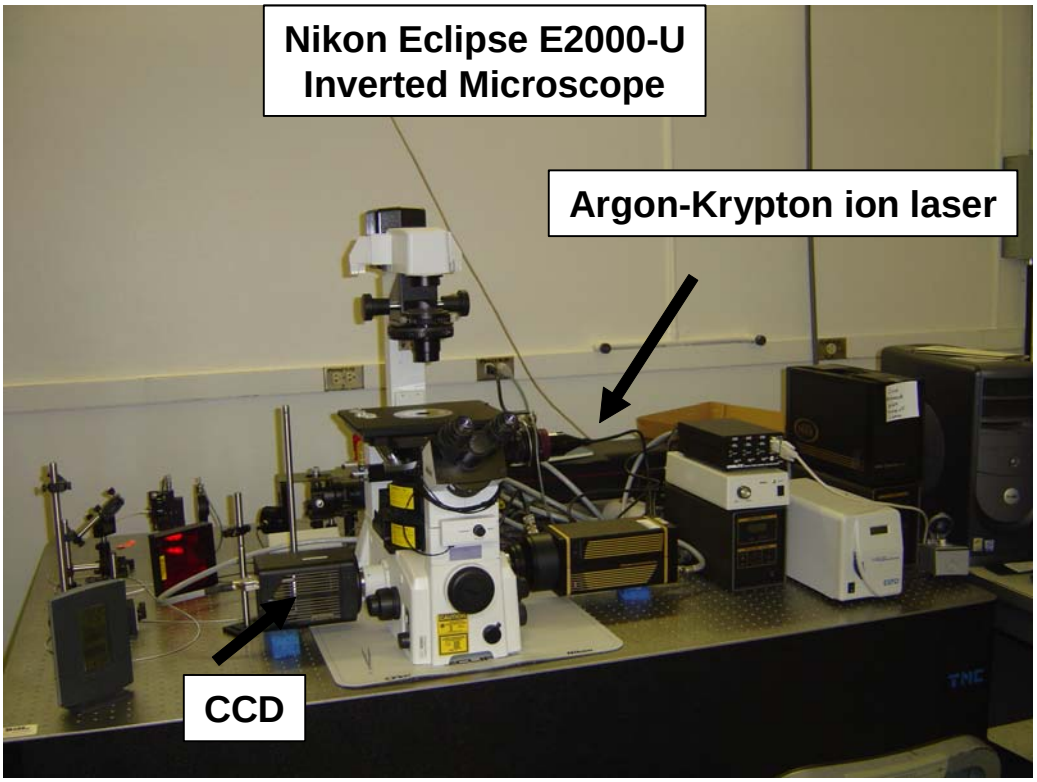

Figure 2.5. The inverted fluorescence microscope system used for acquiring fluorescence recovery after photobleaching measurements of diffusion constants of solid supported phospholipid membranes.

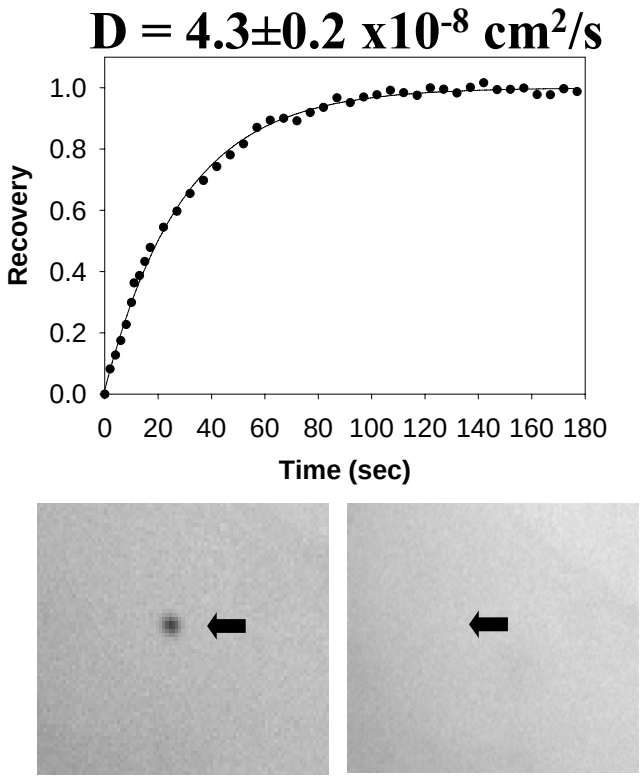

Figure 2.6. The fluorescence recovery after photobleaching curve for a phosphatidylcholine bilayer with 0.1 mole% Texas Red DHPE as a fluorescent probe. A typical value for phospholipid two-dimensional diffusion constant of 4.3±0.2 x 10^{-8} cm^2/s was obtained. The mobile fraction or percent recovery of the fluorescently labeled probe is 97%.

A typical fluorescence recovery after photobleaching experiment for a supported phospholipid membrane is shown in figure 2.6. The bilayer consists of phosphatidylcholine lipids with 0.1 mole% Texas Red DHPE. The lipid bilayer is bleached with an Ar^+/Kr^+ laser at 568.2 nm at a power of 100mW for 1 second. The fluorescence recovery is monitored by time-laps imaging. The resulting FRAP curve gave a diffusion constant of $4.3\pm0.2 \times 10^{-8}$ cm^2/s. The mobile fraction or percent recovery of the labeled fluorophores was 97%.

The FRAP experiments employed in this study are used to determine the function of the supported phospholipid membranes. By monitoring the changes in diffusion constants and mobile fractions, we are able to determine if perturbations to the supported membrane had an overall effect on its function and characteristics.

2.5. Ligand-Receptor Binding Using Microfluidic Technology

Ligand-receptor[26, 88] binding can be investigated using solid supported phospholipid membranes formed inside microfluidic devices.[17, 28] The SLBs are formed via vesicle fusion and may incorporate surface bound receptors that consist of functionalized lipids. One such example is biotin-capped phosphatidylethanolamine (biotin-PE). The surface density of the receptor can be varied inside each microchannel. The system is interrogated by flowing over a fluorescently labeled ligand, such as streptavidin.[88, 89] The levels of binding are quantified using an epi- or total internal reflection (TIRF) fluorescence microscope.[90, 91] A binding curve is generated from the resulting image. The process is shown in figure 2.7.

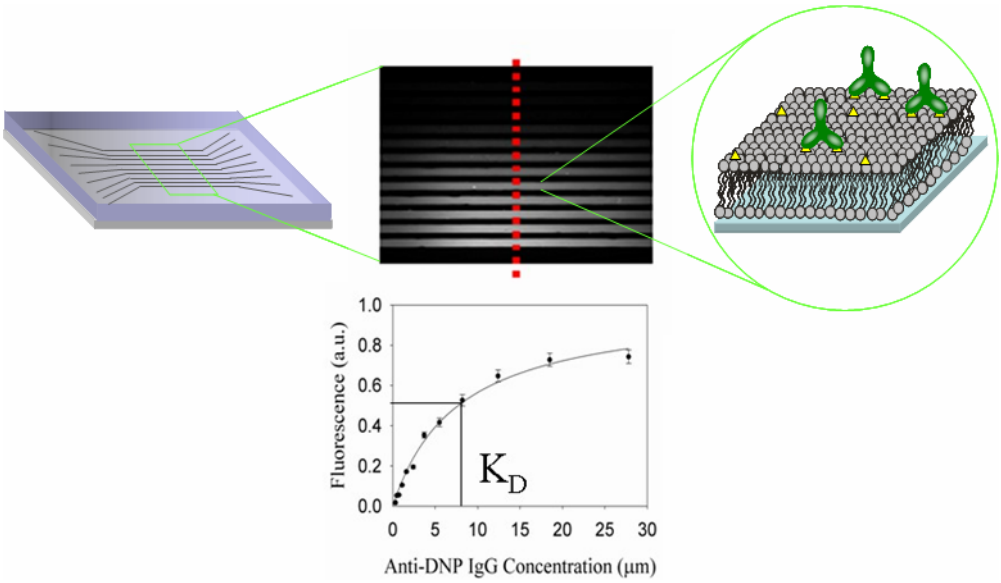

Figure 2.7. Schematic drawing of a microfluidic device used to perform one-shot binding assays (top, left-hand side). (Middle) A total internal reflection microscopy image of the channels in a working microfluidic device. Each channel has a different concentration of fluorescently tagged protein flowing through it. (Right) A schematic representation of a bilayer coated on the surface of the microchannel and the binding of a protein to a ligand presented on it. (Below) The binding curve obtained from the data in the image above it.

2.6. Vibrational Sum Frequency Spectroscopy VSFS

The use of a surface selective spectroscopic technique is crucial in order to elucidate molecular level information of interacting species at an interface. Applications involving linear spectroscopic methods are limited due to their inability to discriminate between molecules at the surface from those in the bulk. Since its advent in the 1980s, VSFS has made it possible to obtain vibrational spectra specific to the interface.[79]

The theory of VSFS has been described in the literature.[92-94] VSFS is a second order nonlinear optical technique that combines a variable infrared laser beam and a visible laser beam which overlap at a surface or interface. The selection rules that govern such processes only allow for molecules present at the surface, (or media that lack inversion symmetry) to produce a polarization at the sum frequency, $P^{(2)}(\omega_{VIS} + \omega_{IR})$ which is the SF signal that is detected. The SF signal is resonantly enhanced as the input IR frequency corresponds to the vibrational modes of the molecular moieties that are properly aligned at the surface; therefore, vibrational spectra of molecules, at an interface or surface under investigation can be obtained. The SF intensity (I_{SFG}) is proportional to the square of the surface nonlinear susceptibility $\chi^{(2)}$ and within the $\chi^{(2)}$ term there exists a resonant $\chi_R^{(2)}$, and a non-resonant $\chi_{NR}^{(2)}$ contribution, which is expressed as follows:

$$I_{SFG} \propto \mathrm{P}_{SFG}^{(2)^2} \propto \left| \chi_{NR}^{(2)} + \sum\nolimits_n \chi_{R_n}^{(2)} \right|^2 I_{VIS} I_{IR} \qquad (2.4)$$

where I_{VIS} and I_{IR} are the intensities of the incident visible and tunable IR beams. The individual resonance $\chi_{R_n}^{(2)}$ are proportional to:

$$\chi_{R_n}^{(2)} \propto \frac{A_n}{\omega_{IR}-\omega_n+i\Gamma_n} \cdot e^{i\varphi_n} \tag{2.5}$$

where A_n is the oscillator strength or intensity, ω_n, Γ_n are the resonant frequency and damping constant of the nth vibrational mode and ω_{IR} is the input IR frequency. The exponential term $e^{i\varphi_n}$, describes the relative phase of the nth vibrational mode and it accounts for interferences between modes that overlap in energy. The oscillator strength A_n, contains the product of both the IR and Raman transition moments, therefore an SF active mode must obey both the IR and Raman selection rules.[94, 95]

The following expression explains that only molecules that obey both IR and Raman selection rules may contribute to the SF signal. This SF selection rule is given by:

$$A_q \propto \frac{\partial \mu_n}{\partial Q}\frac{\partial \alpha_{lm}}{\partial Q} \tag{2.6}$$

in which the A_q term is proportional to the product of the infrared and Raman transition dipole moments and where μ_n and α_{lm} are the dipole moment and polarizability, and Q is the normal coordinate. In other words, the signal arises from the ordering of dipoles at the interface, where centrosymetry is broken.

The scanning SFG spectrometer utilized in this study contains four main components and is illustrated in figure 2.8.[59, 62, 96-99] The source is an Nd:YAG (PY61c, Continuum, Santa Clara, CA) laser, operating at 20 Hz repetition rate and with a peak width of 21 ps, generating a 1064 nm beam. Second, an optical parametric generation/optical parametric amplification (OPG/OPA; LaserVision, Bellevue, WA

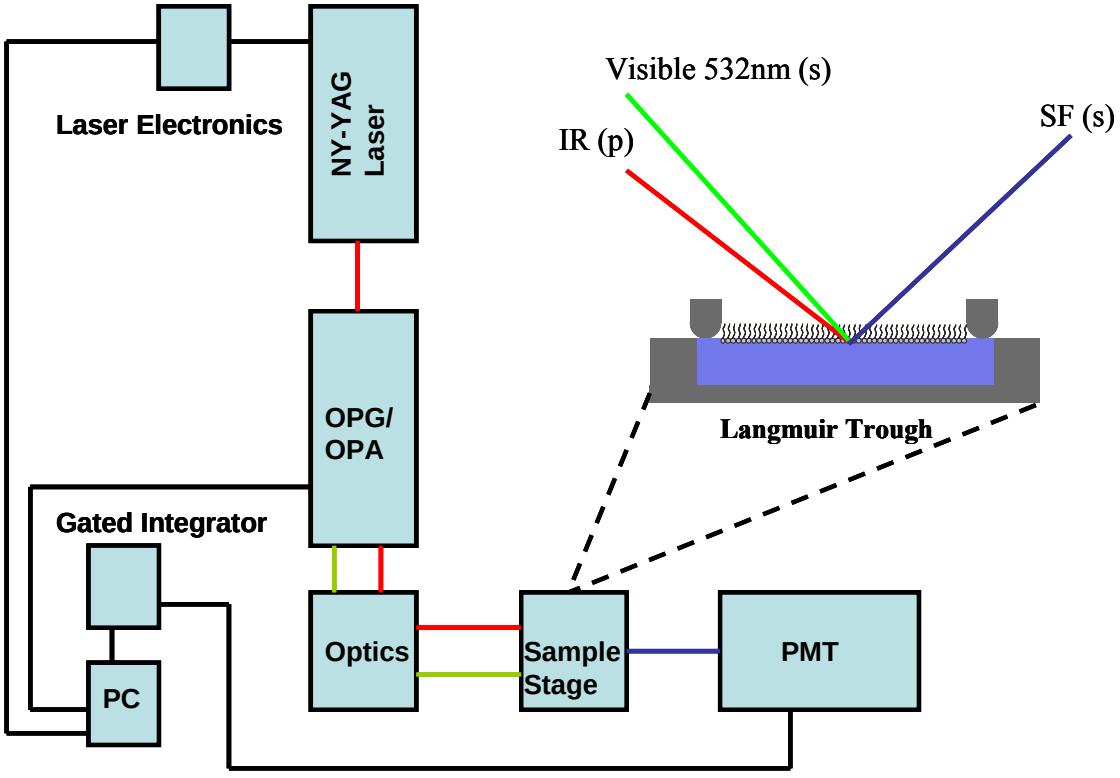

Figure 2.8. The schematic of a scanning vibrational sum frequency spectrometer. The sample stage contains a Langmuir trough which is used to investigate the molecules at the air/water interface.

stage serves to generate the tunable IR beam between 2700 – 4000 cm^{-1} and a visible bean at 532 nm, after which the tunable IR and 532 nm beams are temporally and spatially aligned in the sample stage, the SF signal is detected with a photo-multiplier tube (PMT). The signal is processed through a gated integrator and a PC operating a program written in Lab-View software is used to display the spectra and operate the spectrometer. The polarization combination was ssp, referring to the SF, visible and IR beams respectively.

The acquired SFG spectra can give us information about the aligned chemical species at the interface. Of particular importance is the alignment of interfacial water molecules.[95, 99] The alignment of water molecules is highly dependent on the type of interface. If we consider a solid/aqueous interface, such as SiO_2 or quartz interface, the surface electrostatics will impart differences in the alignment of interfacial water molecules, since SiO_2 is a dielectric material. The pH of the aqueous medium, which affects the surface pH and electrostatics, will also play a mayor role in interfacial water alignment. An example SF spectrum of a quartz/aqueous interface is shown in figure 2.9a. The SF spectrum reveals two important OH spectral features. A peak at 3200 cm^{-1} is attributed to tetrahedrally coordinated water molecules. These are well ordered at the surface and are strongly affected by the surface potential. Another peak at 3450 cm^{-1} is attributed to water molecules with less ordered hydrogen bonding.[99] Figure 2.9b is a cartoon representation of the interfacial water structure. Water molecules closest to the interface are tetrahedrally aligned, followed by water molecules that are less ordered and

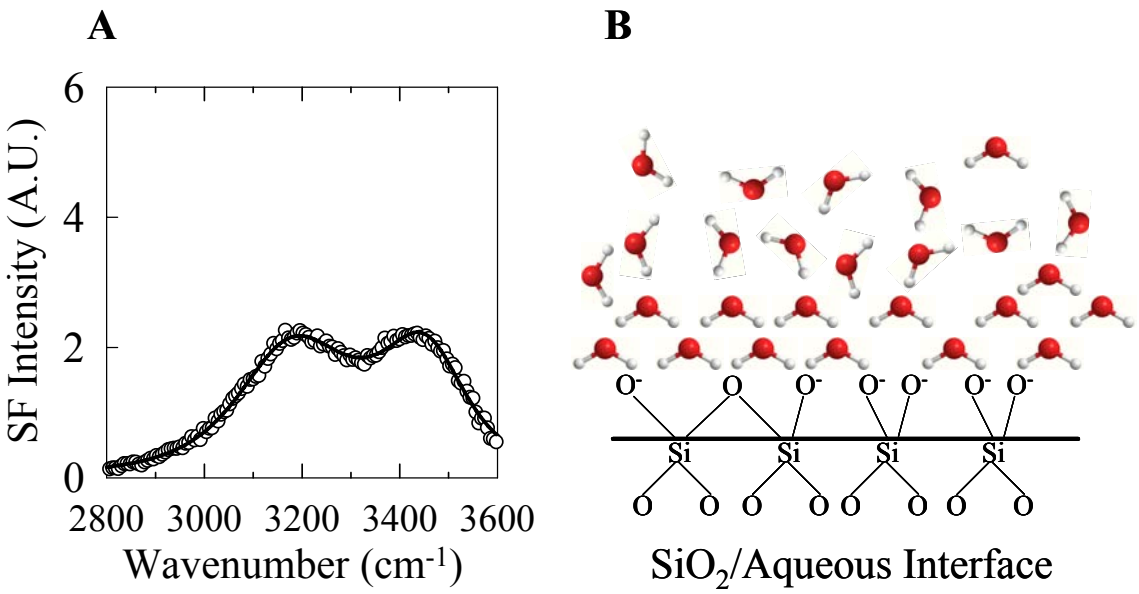

Figure 2.9. The SF spectra of a quartz/aqueous interface at pH 8.0 (A). A cartoon representation of the interfacial water structure (B).

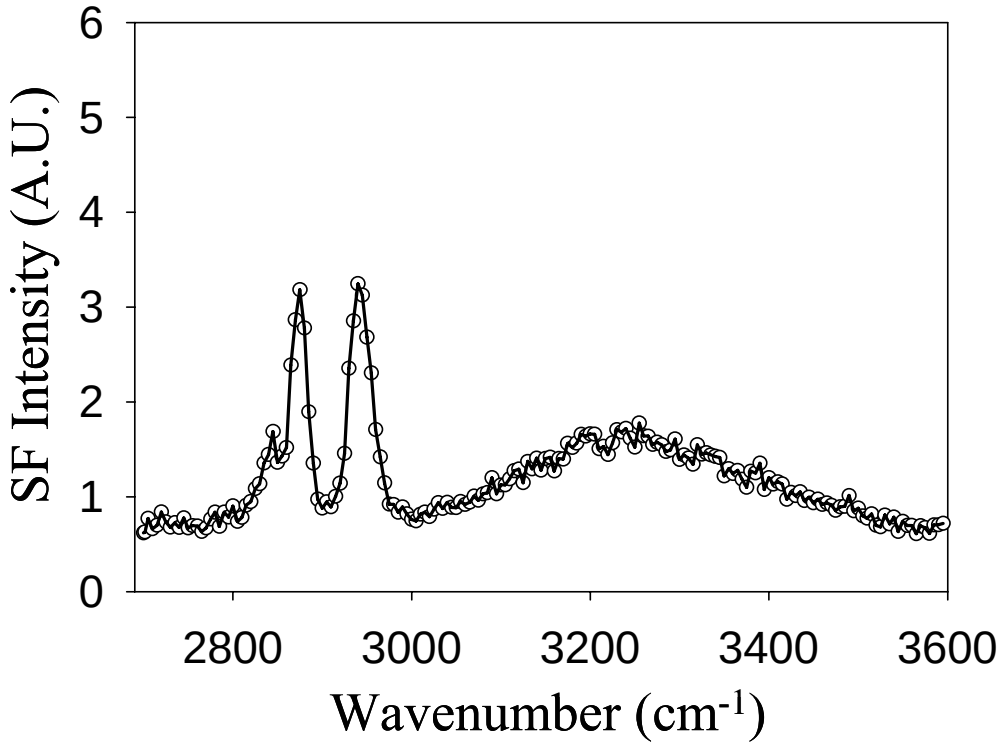

Figure 2.10. An SFG spectrum of a DMPC monolayer at the aqueous/air interface.

have fewer hydrogen bonds as illustrated in figure 2.9b.

The alignment of molecules at the aqueous/air interface can also be interrogated.[80] Using a Langmuir trough, we can obtain SF spectra of a lipid monolayer. Figure 2.10 shows an SFG spectra of dimyristoyl phosphatidylcholine (DMPC) at an water/air interface. The two main spectral features, a peak at ~2875cm^{-1} and ~2940cm^{-1}, are from the CH_3 symmetric stretch and CH_3 asymmetric vibration respectively.[98]

2.7. Atomic Force Microscopy

Since its invention in 1986 by Binnig[81] et. al., scanning probe microscopy (SPM) has become one of the more prevalent surface analytical techniques to gain morphological information of a sample at the sub-micrometer and nanometer level. Herein we will focus on Atomic Force Microscopy (AFM), which detects surface topography and roughness, as shown in figure 2.11.[100] AFM has the potential to obtain high resolution images (~1nm^2 to 250 μm^2), without adversely affecting the structure of sensitive bio-molecules such as proteins, since the imaging can be obtained under environmental or physiological conditions.[47, 101]

A typical AFM consists of four main components, a probe, piezoelectric scanner, photodiode detector and a controller to provide a feedback loop mechanism for the instrument.[102] The probes utilized for AFM consist of either a silicon nitride (Si_3N_4) pyramidal tip (for contact mode) or etched silicon (for tapping mode) which is attached to a flexible cantilever.[20] The resolution of this technique depends on the sharpness of

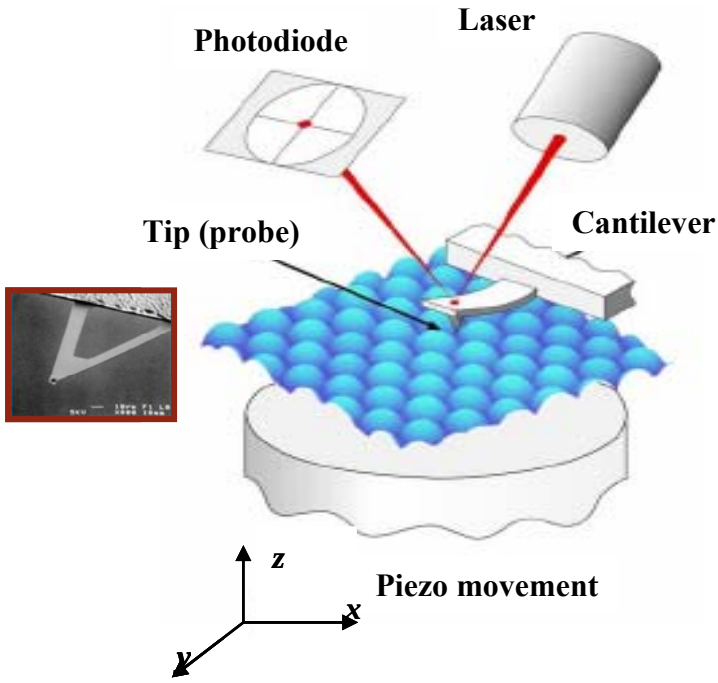

Figure 2.11. The schematics of an atomic force microscope. The insert shows an electron micrograph of a silicon nitride cantilever and tip.

the tip, which range from 5-20 nm in diameter. In contact mode AFM data are obtained by scanning the tip under constant height (z-constant) or force (F-constant). Tapping mode AFM consists of scanning the tip attached to an oscillating cantilever across the sample surface. The cantilever is oscillated at or near its resonant frequency, which ranges from 100-500 kHz in air and 5-10 kHz in fluid, with an amplitude ranging from 20–100 nm from the surface.[20] Since the tip-sample interaction is constant, higher lateral resolution is achieved with lower forces and less damage to the sample. The piezo scanner allows for the precise movement of the sample in x, y and z coordinates when a voltage is applied to the piezoelectric material. The PZT scanner consists of a lead zirconate titanate piezo electric ceramic.[20, 103] The photodiode detector, located in the scan-head, is divided into four sections or quadrants (A, B, C, and D). The signal is detected for each quadrant as well as a sum signal (A+B+C+D). The signal arises from a diode laser beam that is reflected off of the cantilever. As the probe samples the surface features, the cantilever is deflected, which in turn causes a deflection of the laser. The change in deflection of the laser is detected by the photodiode, while at the same time the controller provides the feedback loop in order to adjust the z position of the piezo scanner such that the vertical deflection voltage, defined as (A+B)-(C+D), of the photodiode is (A+B) = (C+D) or in other words, the laser is at the center of the photodiode quadrants.

The imaging of biological samples is best done under fluid conditions employing tapping mode.[47] This is due to in part by the forces experienced by the tip during the imaging process. The main forces experienced are coulombic and attractive van der

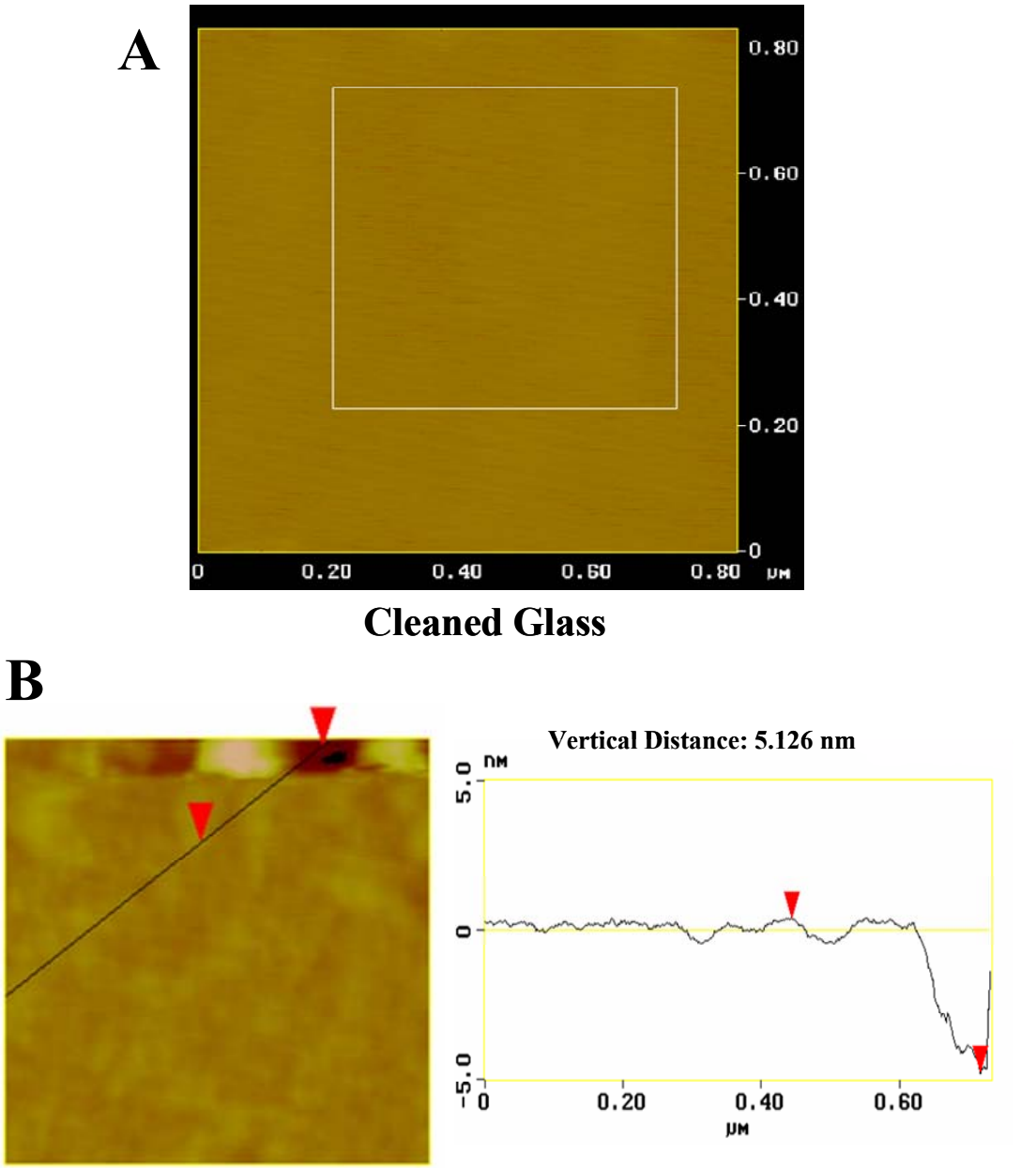

Figure 2.12. The atomic force micrograph of an anealled borosilicate microscope slide (A) and (B) of a supported phosphatidylcholine bilayer.

Waals forces between the tip and the sample surface. Surface tension, electrostatic and fluid damping or capillary forces also have an affect on the tip-surface interactions.[100, 104] This is especially evident in soft samples, such as biologicals materials.

In order to circumvent these problems, the AFM imaging is best performed under water for biological specimens, and the tapping mode provides less tip-sample interactions that can lead to denaturation of biomolecules or other artificial effects. Figure 2.12a shows a typical liquid tapping mode AFM for an annealed borosilicate microscope slide. Borosilicate microscope slides serve as the support for the phospholipid membranes employed in this study. It is important to verify the surface roughness of the substrate, and AFM is an excellent tool to ascertain such morphological information. The RMS of this sample is 0.100 nm for 1μm x 1μm area. Figure 2.12b is a liquid tapping mode AFM image of a supported phophatidylcholine bilayer. A line scan through a defect within the lipid membrane shows a height of ~5.0 nm, which is in good agreement with published results for the thickness of a supported lipid membrane.[47, 105] In general, the image shows a uniform lipid bilayer and further confirms the existence of a phospholipid membrane on top of a borosilicate microscope slide.

CHAPTER III

FLUID AND AIR-STABLE LIPOPOLYMER MEMBRANES FOR BIOSENSOR APPLICATIONS

3.1. Synopsis

The behavior of polyethylene glycol (PEG) conjugated lipids was investigated in planar supported egg phosphatidylcholine bilayers as a function of lipopolymer density, chain length of the PEG moiety, and type of alkyl chains on the PEG lipid. Fluorescence recovery after photobleaching measurements verified that dye-labeled lipids in the membrane as well as the lipopolymer itself maintained a substantial degree of fluidity under most conditions that were investigated. PEG densities exceeding the onset of the mushroom-to-brush phase transition were found to confer air-stability to the supported membrane. On the other hand, substantial damage or complete delamination of the lipid bilayer was observed at lower polymer densities. The presence of PEG in the membrane did not substantially hinder the binding of streptavidin to biotinylated lipids present in the bilayer. Furthermore, above the onset of the transition into the brush phase, the protein binding properties of these membranes were found to be very resilient upon removal of the system from water, rigorous drying, and rehydration. These results indicate that supported phospholipid bilayers containing lipopolymers show promise as rugged sensor platforms for ligand-receptor binding.

3.2. Introduction

Supported phospholipid bilayers[22, 45, 83, 106] could potentially serve as highly selective sensor devices for a variety of biological analytes.[1, 22, 44, 77] Phospholipid membranes are attractive because of their two-dimensional fluidity[29, 61, 107, 108], which allows the individual molecular constituents to rearrange laterally just as they would on the surface of a cell membrane.[28, 66, 109-111] Moreover, supported bilayers are quite resistant to non-specific protein adsorption and biofouling.[66] Unfortunately, such platforms have not been widely exploited for practical biosensors. One problem stems from their instability upon exposure to air, which causes the fluid lipid membrane to reorganize and/or delaminate from the surface.[29, 37, 64, 66, 68, 70, 71, 112] Since the lipids are only held to the substrate by van der waals forces[46], the thin film can curl up and peal away from the aqueous/solid interface as air is introduced.[63] Moreover, any bilayer segments remaining behind at the solid/air interface probably reorganize to have their hydrophobic alkyl chains face toward the air as shown in figure 3.1a.

In an effort to overcome these limitations we recently designed a supported membrane containing a close packed protein layer linked to its outer surface[63] as illustrated in figure 3.1b. This modification increased the bending elastic modulus[44, 113] of the bilayer and thereby substantially raised the barrier to delamination. Also, the presence of the hydrophilic protein layer inhibited lipid reorientation after air exposure. When the system was pulled through the air/water interface, the bilayer remained intact on the surface and a thin water film could be visibly seen above the patterned bilayer

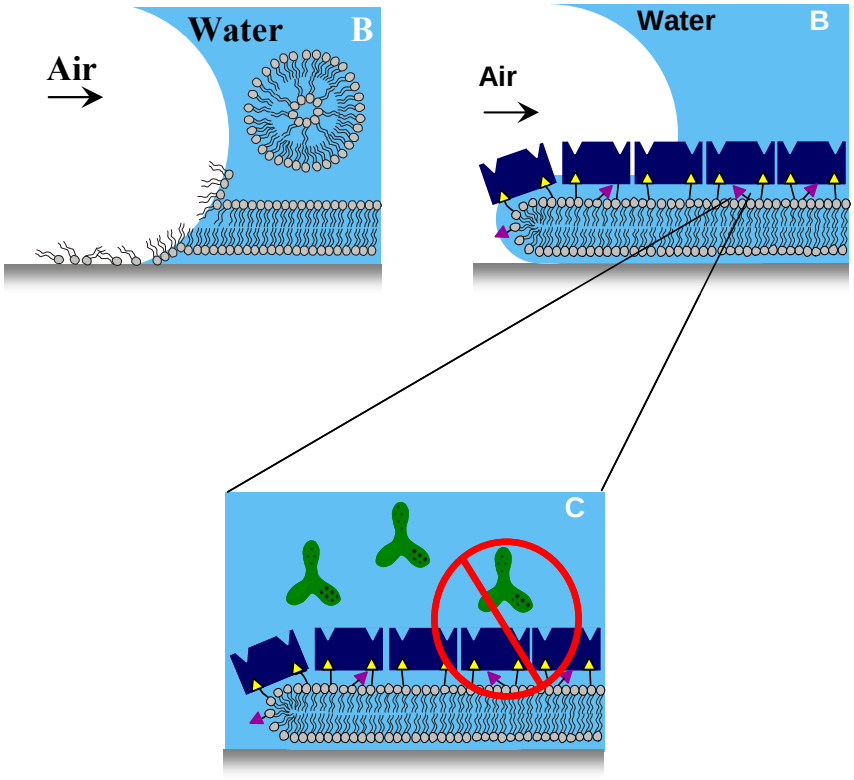

Figure 3.1. Initial strategy to preserve a solid supported lipid membrane. (A) The stability of a phospholipid membrane exposed to air. (B) Protection of the lipid bilayer with a protein coating. (C) The protein coating leaves no room to undergo facile ligand-receptor binding, therefore limiting the systems biosensing capabilities.

regions. Furthermore, the supported membrane was not destroyed even when dried under a stream of flowing nitrogen. In fact, it remained two-dimensionally fluid in the presence of humid air as well as when it was reintroduced to bulk water. Unfortunately, such a system is unsuitable for sensor design because the tightly packed proteins leave no room for the binding of additional analyte species from aqueous solution when binding ligands are incorporated into the membrane (Figure 3.1c). It would therefore be desirable to design a protective coating for the supported bilayer that would afford air stability while still allowing target analytes to bind to ligands presented in the membrane.

In order to achieve this goal, we[73] have incorporated poly(ethylene glycol) phosphatidylethanolamine (PEG-PE) lipopolymers[114] into supported lipid membranes[115, 116] (Figure 3.2). Poly(ethylene glycol)[117] is an inert, water soluble polymer which has been employed in various areas of surface science as well as biochemical/biomedical research. The size and degree of polymerization of PEG molecules can be easily tailored, and the polymer can be attached to other moieties via a linker.[117] An example of this is the derivatization of phosphatidylethanolamine (PE) lipids via attachment to the free amine on the head group. Such PEG-conjugated lipids are commercially available. Utilizing PEG-PE provides a controlled means of varying the polymer density on a lipid membrane surface by varying the mole fraction of the lipopolymer used to make phospholipid vesicles.[13, 118]

The physical-chemical[114] properties of PEG-PE and PEG lipopolymers including oligomer length (n_p) and surface density have been well characterized for lipid

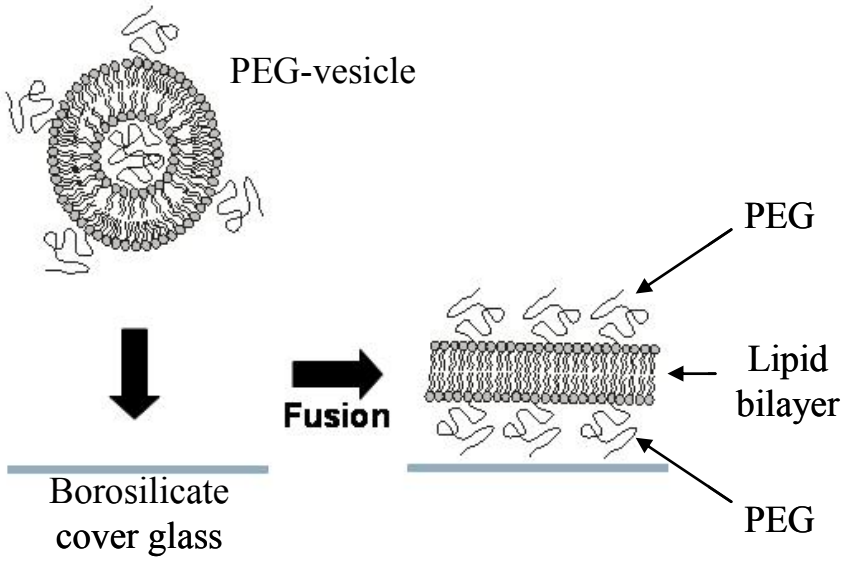

Figure 3.2. The fusion of PEG-lipopolymer vesicles to a borosilicate substrate forms a stable supported lipopolymer membrane.

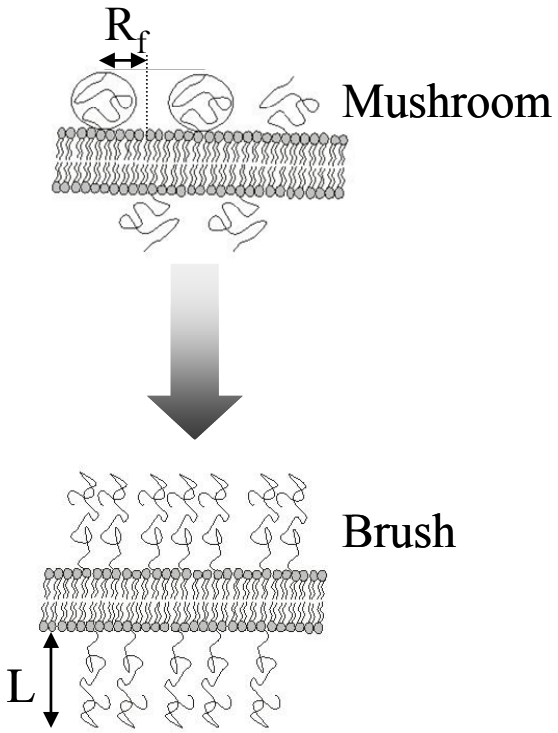

Figure 3.3. Illustration of the mushroom to brush transition of PEG-conjugated lipids at the surface of a phospholipid vesicle as the packing density is increased. The letter D represents the lipopolymer spacing and the circle around the two PEGs shows the Flory radius. When the distance is sufficiently small, the molecules switch from the globular to the elongated brush conformation and protrude further from the membrane surface. This height is designated by the letter L.[119]

vesicles.[120] A unique feature of PEG is its conformation, which is dependent on its mole fraction in the lipid bilayer. This is shown in figure 3.3. At low surface density, PEG exists as a globular conformation, which is referred to as the "mushroom" state. As the density increases, the polymer undergoes a transition from the globular to a brush like conformation.[121] This process is usually called the mushroom-to-brush transition. It is a broad phase transition and depends on the concentration and the chain length of the PEG.[117, 121, 122]

The behavior in the mushroom state can be modeled by Flory-Huggins theory, which describes the characteristic folded radius (R_F) of a random coil as a function of monomer size and chain length.[118] The transition to the more elongated brush phase commences when the spacing between PEG-conjugated lipids is less than $2R_F$. By applying the polymer scaling laws, we can determine the Flory[121] radius for a given PEG-lipopolymer using the following expression:

$$R_f = a_m n_p^{3/5} \qquad (3.1)$$

Where a_m is the monomer size of an ethylene glycol unit which equals 0.39 nm, and n_p is referred to the degree of polymerization. The Flory radius for a PEG polymer in solution was found to be similar within experimental error to the radius of a PEG lipopolymer within a lipid membrane at low density, i.e. in the mushroom conformation. This suggests that the polymer scaling laws can be applied to the PEG polymers attached to a phospholipid membrane. With this information, we can estimate the mushroom-to-brush transition for a PEG lipopolymer of a given size.[118, 123] This is given by the following equation:

$$\chi_p^{m\to b} \geq \frac{A_l}{\pi a_m^{\,2}} n_p^{-6/5} \qquad (3.2)$$

Where $\chi_p^{m\to b}$ is defined as the mole fraction of the onset of the mushroom-to-brush transition, n_p is the degree of polymerization and A_l is the membrane surface area per lipid molecule.[124] The surface area will depend on the phase transition of the individual lipids. For a lipid in the fluid phase, A_l ranges from ~0.60 – 0.70 nm^2, and for a lipid in the gel phase, A_l decreases and ranges from ~0.40 – 0.48 nm^2 due to the close hexagonal packing of the lipids. The approximate length (L_{brush})[125] of the polymer in the brush conformation can be calculated by:

$$L_{brush} = \frac{a_m^{5/3} n_p}{D^{2/3}} \qquad (3.3)$$

Where a_m is the monomer size (0.39 nm) and D is the interpolymer distance or spacing, which is related to the polymer density within the film. As the density increases, the length of the polymer brush increases due to the entropic and repulsive interactions between the PEG moieties.[126, 127]

The mole fraction χ_p of the onset of the mushroom-to-brush transition for PEG polymers of various sizes are calculated in table 3.1. This illustrates the tendency of χ_p to decrease with increasing polymer molecular weight or size. The Flory radius is also shown in this table and according to equation 3.1, the R_F increases with increasing polymer size.

Table 3.1. Application of the Polymer Scaling Laws to PEG Lipopolymers.

PEG MW. (Da)	**Degree of Polymerizatin n_p**	**Flory Radius R_F (nm)**	**Mole% onset of mushroom-to-brush $\chi^{m\rightarrow b}$**
350	8	1.36	11
550	12	1.73	7
750	17	2.13	4.4
1000	22	2.49	3.3
2000	45	3.83	1.4
3000	67	4.86	0.8
5000	114	6.69	0.5

* The A_l = 0.65 nm of phosphocholine lipids in the fluid phase

One use of PEG conjugated-lipids has been in an effort to stabilize lipid vesicles for drug delivery.[128, 129] It was found that introducing the lipopolymer reduces vesicle aggregation and promotes vesicle-vesicle fusion.[130] On the other hand, PEG molecules have been more generally employed at interfaces as a coating to resist non-specific protein adsorption.[131] There are several theories to explain the ability of PEG-coated surfaces to resist biofouling. These include the effects of steric repulsion[132], tightly bound layers of hydration waters[133], and the conformation of the PEG chains. In most of the cases studied, the PEG molecules were covalently anchored to the underlying surface through a linker group. For example, a thiol[115, 116] has been used to attach PEG to Au or Ag surfaces, while a silane was employed when using glass or quartz. The method of grafting PEG to a surface is believed to play a key role in the repulsion of biomacromolecules.[134-136]

In our systems, PEG is linked to a two-dimensionally fluid phospholipid bilayer, rather than grafted to a fixed location. Thus, the polymer chains should have more flexibility to accommodate the introduction of protein molecules from aqueous solution. This is a key point, as we have demonstrated that the density of the lipopolymer can be titrated, according to the scaling laws, in order to render the lipid film air stable while allowing for facile ligand-receptor interaction. In other words, proteins may indeed be able to diffuse through the PEG film and specifically bind with ligands that are presented in the membrane.

The choice of pegylated bilayers for stable biosensor design is inspired by the cell glycocalix[74], which is a thick carbohydrate film consisting of oligosaccharides,

polysaccharide chains, and adsorbed proteoglycans that can rise tens of nanometers above the plasma membrane.[75] There is some evidence in the literature that these sugar layers play a role in stabilizing the cell membrane in the dry state.[137-139] On the other hand, when cells are fully hydrated, the carbohydrate films are presumably flexible enough to allow external proteins to diffuse through them and bind to the underlying membrane constituents.[140] It has been proposed that a PEG coating can serve as a simple mimic of a glycocalix on a supported phospholipid membrane[141], since such a system is lacking in the literature.

Herein we demonstrate that the surface density and chain length of PEG-PE are critical parameters in affording air-stability. Specifically, the lipopolymer protects the membrane in the more tightly packed brush conformation while delamination and damage occur in the mushroom state. Furthermore, PEG coatings allow proteins such as streptavidin to bind with biotinylated lipids (biotin-PE) within the membrane under all surface densities tested. The results indicate that the binding behavior is not greatly affected by the presence of the lipopolymer coating and that a biotinylated membrane above the onset of the mushroom to brush transition is able to bind streptavidin after it has been removed from bulk solution, rigorously dried, and reintroduced to water.

3.3. Experimental

Materials. Chemicals described herein are used without further purification unless indicated. The lipid 1,2-dipalmitoyl-sn-glycero-3-phosphoethanolamine-N-[methoxy(polyethylene glycol)] (PEG-DPPE), 1,2-disearoyl-sn-glycero-3-

phosphoethanolamine-N-[methoxy(polyethylene glycol)] (PEG-DSPE) and 1,2-dioleoyl-sn-glycero-3-phosphoethanolamine-N-[methoxy(polyethylene glycol] (PEG-DOPE) were purchased from Avanti Polar Lipids (Alabaster, AL) with PEG molecular weights of 550 and 2000 Da. 1,2-Dioleoyl-sn-glycero-3-phosphoethanolamine-N-(cap biotinyl) (sodium salt) (biotin cap-PE), 1,2-distearoyl-*sn*-glycero-3-phosphoethanolamine-N-[amino(polyethylene glycol)2000] (ammonium salt) (NH_2-PEG^{2000} DSPE) and L-α-phosphatidylcholine from egg (egg PC) were also purchased from Avanti Polar Lipids. *N*-(Texas Red sulfonyl)-1,2-dihexadecanoyl-sn-glycero-3-phosphoethanolamine (Texas Red DHPE), Alexa Fluor-488 labeled streptavidin, and Alexa Fluor-594 succinimidyl ester were obtained from Molecular Probes (Eugene, OR). Purified water, which was acquired from a NANOpure Ultrapure Water System (Barnstead, Dubuque, IA), had a minimum resistivity of 18.2 MΩ·cm. This water was used in the preparation of all buffer solutions. Phosphate buffer saline (PBS) was prepared using 10.0 mM sodium phosphate with the addition of 150 mM NaCl (Sigma-Aldrich). The pH was adjusted to 7.4 by the addition of NaOH (EM Science). Poly(dimethylsiloxane) (PDMS) was used to fabricate PDMS wells and microfluidic devices. The polymer and crosslinker were purchased from Dow Corning (Sylgard Silicone Elastomer-184, Krayden Inc.). Glass microscope slides were purchased from VWR International and were cleaned and annealed according to established procedures.

Preparation of Pegylated Unilamellar Vesicles and Bilayer Formation. Small unilamellar vesicles[106] were prepared from egg PC, PEG-PE lipopolymer, and 0.5 mol% Texas Red DHPE, which was incorporated as a fluorescence probe. The desired

mole fraction of PEG^{550}-DOPE or PEG^{2000}-DOPE was mixed with egg PC and dye-conjugated lipid in chloroform. The solvent was then evaporated under a stream of nitrogen followed by desiccation under vacuum for 4 hours. Rehydration of the lipids was performed in PBS solution at pH 7.4. After 10 freeze-thaw cycles the large vesicles were extruded through a polycarbonate filter, which had an average pore size of 50 nm. Small unilamellar vesicles prepared by this method were 70 ± 10 nm in diameter as determined by dynamic light scattering using a 90Plus Particle Size Analyzer from Brookhaven Instruments Corporation.

All PEG-PE containing vesicles were delivered to the surface of planar glass microscope slides in a PDMS/glass microfluidic device format using previously described techniques.[76, 77, 86] After a 30 minute incubation period, the microchannels and microwells were thoroughly rinsed with the appropriate buffer or purified water. The samples were placed under an inverted epifluorescence Nikon Eclipse TE2000-U microscope and observed with a 10x objective. Images were obtained using a MicroMax 1024b CCD camera (Princeton Instruments) and data analysis was performed with MetaMorph software (Universal Imaging).

PEG-labeling. Dye labeling of NH_2-PEG^{2000} DSPE was accomplished by first preparing small unilamellar vesicles of egg PC with various quantities of this molecule (0.5 to 5 mol%). The labeling reaction was carried out by incubating the SUVs with Alexa Fluor-594 succinimidyl ester for 2 hours at room temperature. The succinimidyl ester reacted with the primary amine to form a covalent linkage between the amine PEG chain and the fluorescent dye. Any unreacted dye was separated from the labeled

vesicles via size exclusion chromatography. It should be noted that this procedure will label about half the amines present in the vesicles.

Fluorescence Recovery after Photobleaching (FRAP). FRAP[78] curves, which have been previously utilized to assay the lateral fluidity of polymer tethered[142] bilayer systems, were obtained herein by exposing the sample to laser irradiation from a 2.5 W mixed gas Ar^+/Kr^+ laser (Stabilite 2018, Spectra Physics). Planar bilayer samples were irradiated at 568.2 nm with 100 mW of power for times not exceeding 1 sec. A 17.7 μm full-width at half-max bleach spot was made by focusing the light onto the bilayer through the 10x objective. The recovery of the photobleached spot was monitored by time-lapse imaging. The fluorescence intensity of the bleached spot was then determined as a function of time after background subtraction and intensity normalization. All fluorescence recovery curves were fit to a single exponential to obtain both the mobile fraction of dye-labeled lipids and the half-time of recover, $t_{1/2}$, following standard procedures.[29]

Drying Procedures for Bilayers. Before drying, the pegylated bilayers were thoroughly rinsed with purified water in order to remove salt from the buffer solutions. The excess water and the PDMS stamp were removed and the supported membrane was dried under a stream of nitrogen. Subsequently, the bilayers were imaged in order to access damage caused by drying. The bilayers were stored for time periods up to 24 hours in a dust-free container before rehydration. Rehydration was performed with either purified water or PBS buffer at pH 7.4. A FRAP curve was obtained to ascertain whether the lipid bilayers regained lateral mobility.

Ligand-receptor Binding. Biotin-streptavidin binding was employed as a model of ligand-receptor interactions in the presence of the lipopolymer. Vesicles were prepared by adding 1 mol% biotin-cap-PE to a given lipid mixture. Binding was assayed by flowing 0.20 mg/ml Alexa Fluor-488 streptavidin over a biotinylated membrane and incubating the protein solution for 30 minutes followed by copious rinsing with PBS buffer at pH 7.4. The bilayers were imaged under a 10x objective and the fluorescence intensity of the bound streptavidin was determined after background subtraction and image normalization.

3.4. Results and Discussion

Vesicle Fusion with PEG-PE. Supported phospholipid bilayers containing various concentrations of PEG-PE in egg PC with 0.5 mol% Texas Red DHPE were characterized in a first set of experiments. The bilayers contained lipopolymer with either 12 (PEG^{550}-DOPE) or 45 (PEG^{2000}-DOPE) ethylene oxide repeat units. All supported bilayers appeared to be uniform down to the diffraction limit under fluorescence microscopy using a 100x objective. FRAP data were obtained for each system and an example with 5 mol% PEG^{550}-DOPE is shown in Figure 3.4a. In this case the mobile fraction of Texas Red DHPE was 98 ± 1% and the $\tau_{1/2}$ value was 23 sec. As discussed in Chapter II, the diffusion constant, D, can be obtained from the $\tau_{1/2}$ value by employing the following equation:

$$D = \frac{w^2}{4t_{1/2}}\gamma_D \qquad (3.4)$$

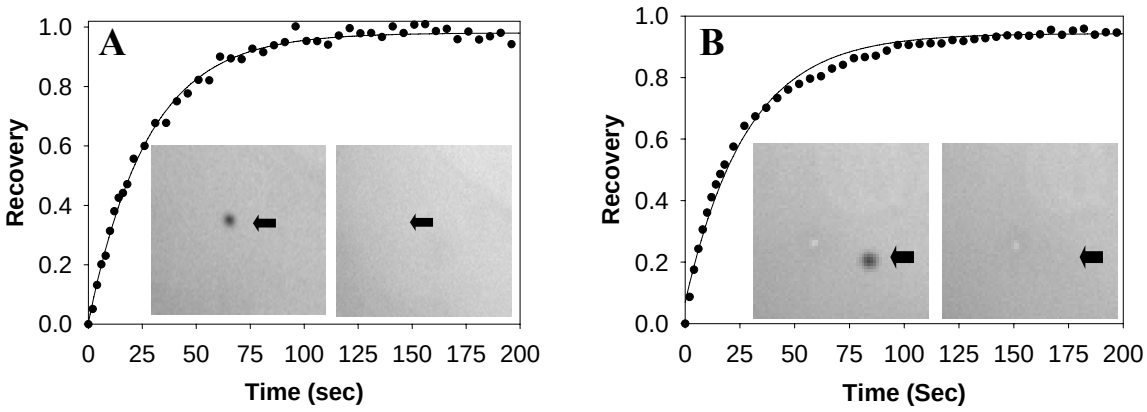

Figure 3.4. FRAP curves of PEG bilayers on planar borosilicate substrates. **(a)** The recovery curve for a membrane containing 5 mol% PEG^{550}-DOPE in egg PC with 0.5 mol% Texas Red DHPE. **(b)** The same conditions as **(a)**, but with 5 mol% PEG^{2000}-PE. The mobile fraction of the dye moiety in the bilayers is 96 ± 1% in both cases.

w is the full width at half max of the Gaussian profile of the focused beam and γ_D is a correction factor that depends on the bleach time and the geometry of the laser beam.[78] For the data in Figure 3.4a the value of the diffusion constant, D = 3.7 ± 0.2 x 10^{-8} cm^2/sec, was obtained by using *w* = 17.7 μm and γ_D = 1.1. In the case of 5 mol% PEG^{2000}-DOPE (Figure 3.4b), the diffusion constant was 4.0 ± 0.2 x 10^{-8} cm^2/sec with 98 ± 1% recovery. Both values were identical within experimental error to data obtained with pure egg PC bilayers (D = 4.0 ± 0.2 x 10^{-8} cm^2/sec with 98 ± 1% recovery).

The effect of the lipopolymer density on the diffusion constant of the Texas Red labeled lipids is shown in Figure 3.5. As can be seen, there is little if any dependence of the measured value of this constant on the PEG^{550}-DOPE density. Moreover, the mobile fraction of the probe remained at ~98% for all concentrations employed. Analogous experiments were performed with PEG^{2000}-DOPE (Figure 3.5). In contrast to the case with PEG^{550}, the results for the highest lipopolymer densities did show a slowing of the diffusion constant. However, this only occurred at lipopolymer concentrations of at least 10 mol%. By contrast, the onset of the mushroom to brush phase transition occurs at 1.4 mol% for a PEG^{2000}-PE in a lipid membrane. Therefore, the initial drop in the diffusion constant occurred well into the brush transition. Additional FRAP experiments were performed with egg PC membranes containing various concentrations of PEG^{2000}-DPPE, PEG^{2000}-DSPE, and PEG^{550}-DPPE. The results showed that the absence of double bonds and the lengthening of the alkyl chains had no noticeable effect on either the diffusion constants or mobile fractions measured within experimental error.

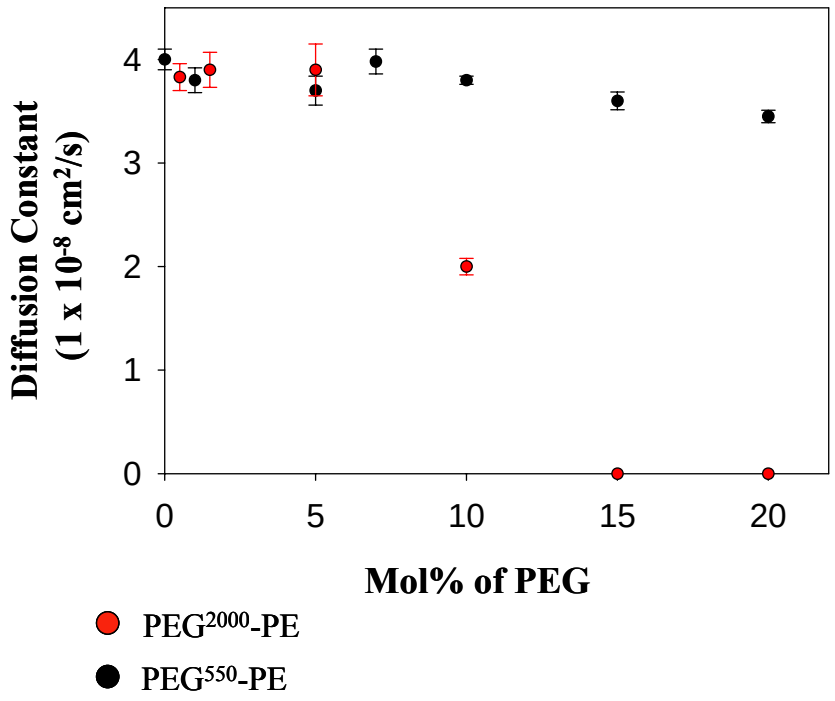

Figure 3.5. Texas Red DHPE diffusion constants in egg-PC bilayers with various concentrations of PEG^{550}-PE bilayers (black dots) and PEG^{2000}-PE bilayers (red dots).

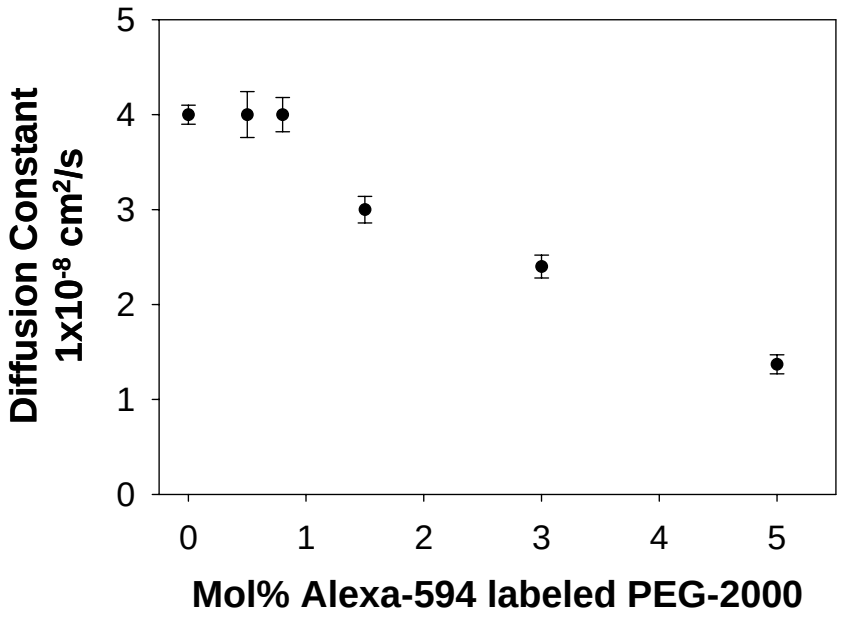

Figure 3.6. The diffusion constant of Alexa-594 Labeled PEG^{2000} DSPE in egg-PC bilayers as a function of the lipopolymer density.

In order to further characterize membrane fluidity, we investigated the diffusion of the PEG lipopolymer itself within the egg PC bilayer. This was accomplished by employing amine terminated PEG^{2000}-DSPE (NH_2-PEG^{2000}-DSPE) that was labeled with Alexa Fluor-594. Supported lipid bilayers were formed on glass in the same fashion described above. Diffusion constants for the dye labeled PEG^{2000}-DSPE were obtained as a function of its density in the egg PC membranes and the values obtained are plotted in Figure 3.6. At PEG densities below the onset of the mushroom-to-brush transition (1.4 mol% for a PEG^{2000}), uniform diffusion constants were observed that closely matched those of the dye labeled lipids. At 1.5 mol% lipopolymer, however, a slight decrease in D to $3.0 \pm 0.2 \times 10^{-8}$ cm^2/s was seen. This corresponds almost exactly to the onset of the mushroom-to-brush transition. The mobile fraction of the Alexa Fluor 594 labeled PEG^{2000} DSPE decreased to 60% ± 5% at this PEG density. At higher PEG concentrations, the decrease in the diffusion constant continued. Such behavior is expected as the polymer molecules have increasing interactions with their neighbors as they are brought into ever closer proximity.[142]

Air-stability of Pegylated Supported Bilayers. In the next set of experiments we wished to determine the ligand densities and oligomer repeat lengths of PEG that would confer air-stability to the supported bilayers. A typical example of bilayer delamination in the absence of PEG-PE is shown on the left side of Figure 3.7. Much of the lipid material is transferred to the aqueous solution as the water phase retreats. This was verified by fluorescence analysis of the remaining solution. Additional

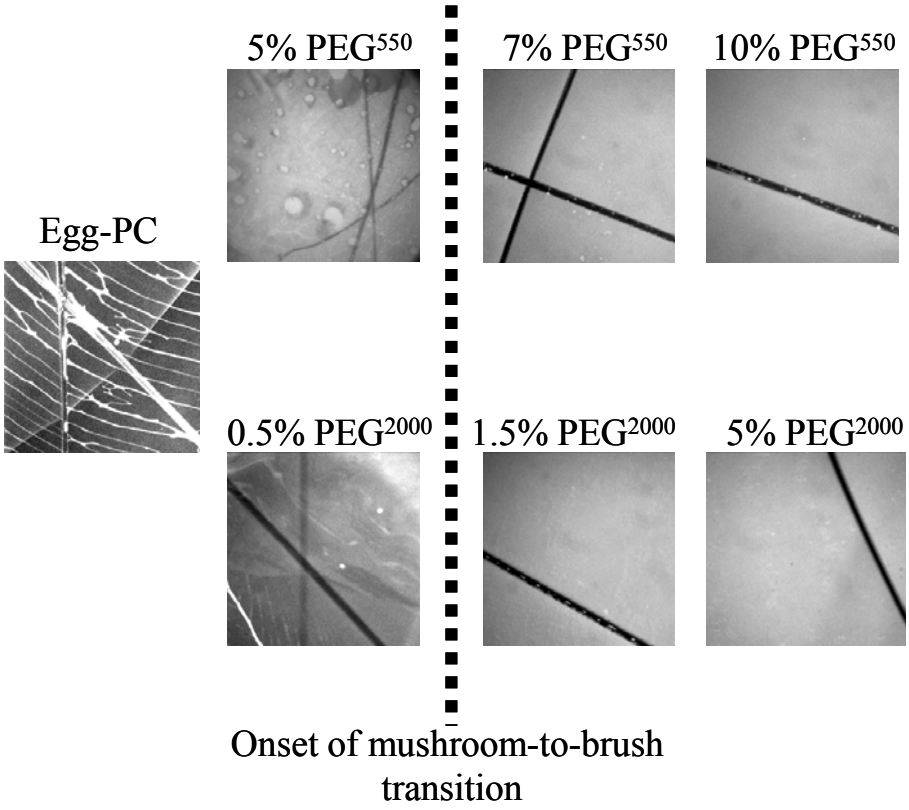

Figure 3.7. Fluorescence micrographs of planar supported phospholipid bilayers containing various concentrations of PEG-PE. The bilayers were imaged after removal from bulk aqueous solution and rigorous drying by blowing dry nitrogen over the sample.

Table 3.2. The diffusion constants and percent recovery of Egg-PC supported membranes before and after dehydration.

	Diffusion Control ($x10^{-8}$ cm^2/s)	**% Recovery Control**	**Diffusion Dry/Rehydrated ($x10^{-8}$ cm^2/s)**	**% Recovery Dry/Rehydrated**
egg-PC	4.0 ± 0.2	98 ± 1	___	___
5% PEG^{550}-PE/egg-PC	3.7 ± 0.2	98 ± 1	3.3 ± 0.2	93 ± 4
5% PEG^{2000}-PE/egg-PC	4.0 ± 0.2	98 ± 1	3.4 ± 0.2	95 ± 1

fluorescently labeled material was left on the glass surface and formed a patterned which reflected the direction in which the cover slip was removed from solution. The introduction of either PEG^{550}-DOPE or PEG^{2000}-DOPE changed this situation remarkably. Indeed, even at low concentrations, the lipopolymer caused most of the bilayer to remain at the interface. As long as the PEG chain was in the mushroom state, however, significant damage to the bilayer could be clearly observed. Taking FRAP images after drying in air and subsequent rehydration confirmed the idea that some areas retained fluidity, while others did not. For the case of 5 mol% PEG^{550} in egg PC, the fraction of the bilayer that returned to full fluidity after rehydration was ~40 to 50%. By contrast with the above results, performing experiments at lipopolymer concentrations above the onset of the mushroom to brush transition yielded supported membranes that showed excellent air-stability and lacked any obvious signs of damage or stress (Figure 3.7). This markedly improved air stability was imparted precisely at the onset point of the mushroom to brush transition, which is known to be 7 mol% for PEG^{550}-DOPE and 1.4 mol% for PEG^{2000}-DOPE as stated above. Furthermore, table 3.2 demonstrates the effect of the presence of the PEG-lipopolymer on the two-dimensional diffusion constants before and after dehydration.

Control experiments were performed to test whether PEG containing membranes in the brush phase could withstand many cycles of drying and rehydration. This is shown in figure 3.8. The results indicated that as long as the membranes were not rigorously blown dry, they could easily withstand multiple cycles of removal from bulk

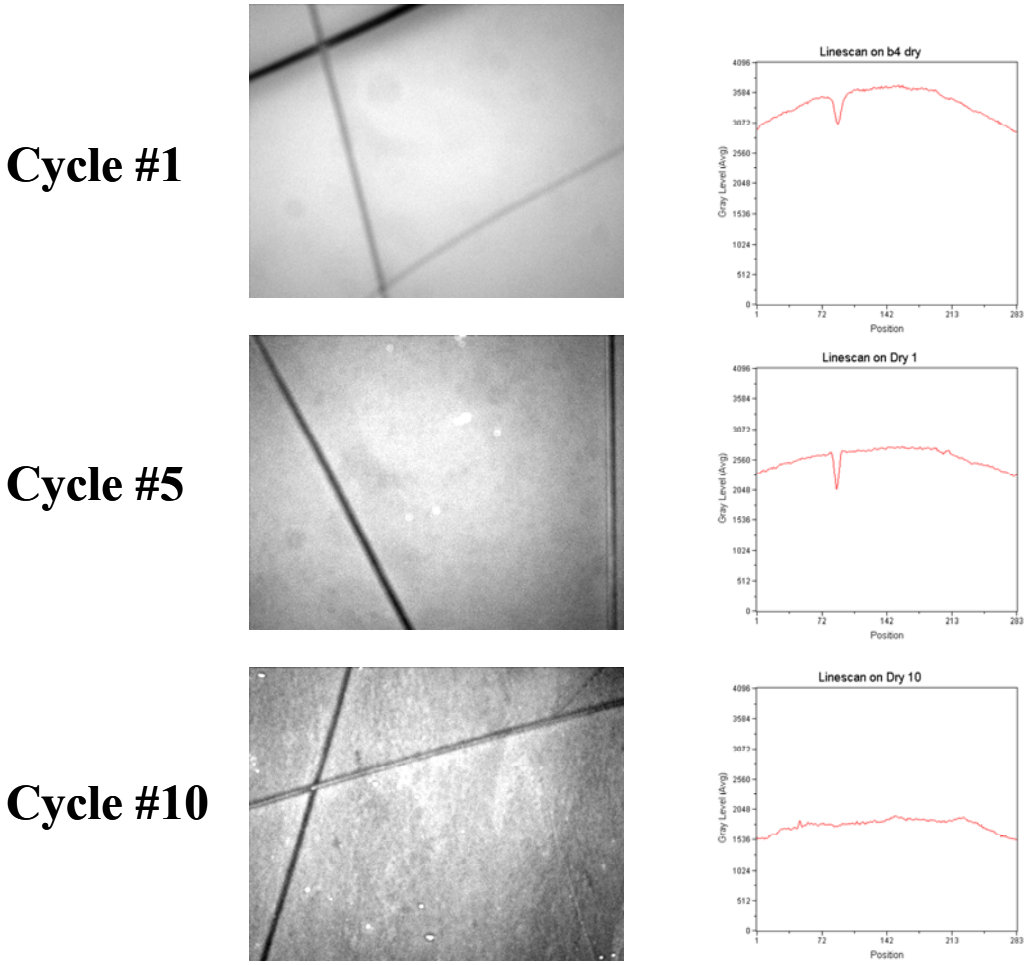

Figure 3.8. Dehydration/rehydration cycles of PEG-lipopolymer membranes.

water. On the other hand, membranes containing 5 mol% PEG^{2000}-DOPE showed evidence for modest damage after 10 cycles of rigorous drying and rehydration. In fact the first indications of stress were noted after 5 drying cycles and the fluorescence intensity began to drop as well. This indicates that the bilayers, while well protected by the PEG layer, nevertheless probably still sustain some finite damage upon each drying cycle. Such damage, however, is almost impossible to note by fluorescence microscopy after just one cycle. This is significant because most remote sensing applications would probably require fabricating a supported lipid bilayer device in one location, drying the platform for shipment, and rehydrating of the system at a second location for use as a sensor. Thus only one drying cycle should be typically necessary.

The Effects of Poly(ethylene glycol) on Ligand-receptor Binding. In a final set of experiments the ability of the pegylated membranes to bind proteins from the aqueous solution was determined when appropriate binding ligands were incorporated. To achieve this, supported membranes were prepared with biotin-cap-PE. Next, fluorescently labeled streptavidin was introduced into the bulk solution at 0.2 mg/ml and allowed to incubate for 30 min before being rinsed away with PBS solution. Three different membrane compositions were investigated: egg PC, egg PC with 5 mol% PEG^{550}-DOPE, and egg PC with 5 mol% PEG^{2000}-DOPE. For each of these cases the binding of Alexa 488-streptavidin was tested in the presence and absence of 1 mol% biotin-cap-PE in the membrane (Figure 3.9). As can be seen from the fluorescence micrograph of the microfluidic channels, the level of non-specific adsorption of streptavidin was quite low in all cases in the absence of biotinylated lipids. On the other

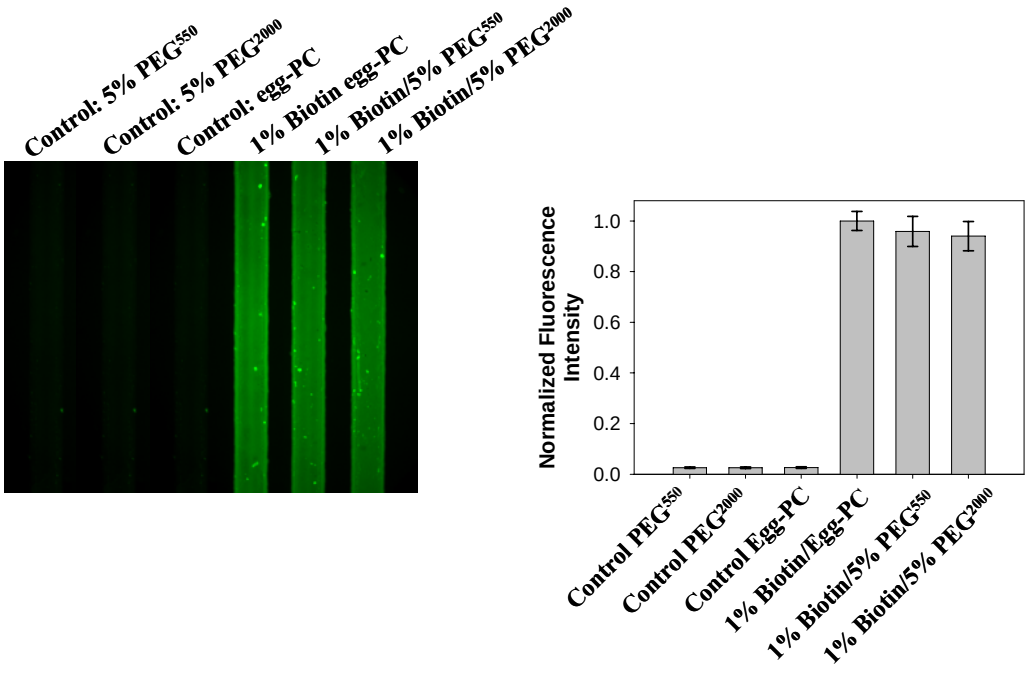

Figure 3.9. The effects of PEG-PE on streptavidin binding to supported membranes containing biotin-cap-PE. **(A)** Fluorescence micrograph of the microfluidic device containing various membrane chemistries. Alexa Fluor 488 labeled streptavidin was flowed over the bilayer coated microchannels, incubated for 30 min, and rinsed away with PBS buffer before imaging. **(B)** A bar graph of the relative fluorescence intensity in each channel of the device. The intensity for streptavidin binding to the channel containing 1 mol% biotin-cap-PE in egg PC was normalized to 1.0.

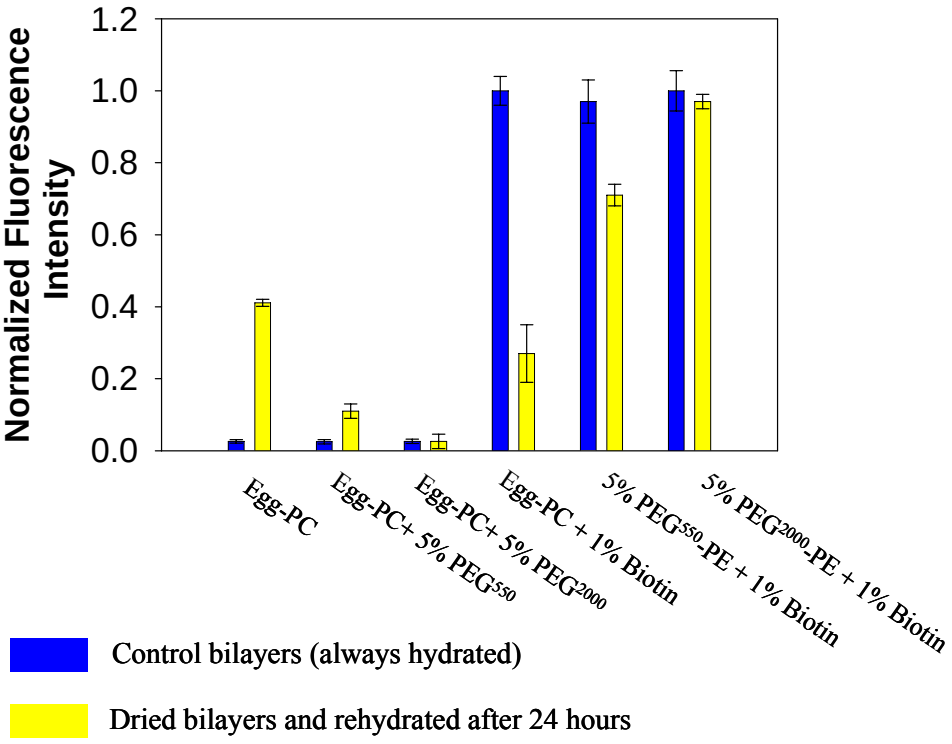

Figure 3.10. Bar graph of streptavidin binding in lipid bilayers containing biotin-cap-PE. A comparison is made between bilayers in which Alexa Fluor 488 labeled streptavidin is introduced over freshly prepared bilayers (blue bars) and after the bilayers have been dried in nitrogen, allowed to sit 24 hours in air, and rehydrated with bulk water (yellow bars).

hand, streptavidin binding was substantially greater in those membranes where biotin was incorporated. Significantly, the presence of the pegylated lipids seemed to have little influence on the extent of protein binding under these conditions. This was the case for both the 5 mol% PEG^{550}-DOPE membrane as well as the membrane containing 5 mol% PEG^{2000}-DOPE. The polymer should be in the mushroom state in the former membrane, while it is well into the brush transition in the latter.

The experiments described above were repeated on membranes with the same six lipid chemistries, but after the supported bilayers were exposed to air, dried under nitrogen, left in ambient air for 24 hours, and reintroduced to bulk PBS. This time only the membranes containing 5 mol% PEG^{2000} showed the same extent of streptavidin binding within experimental error as the corresponding membranes that were not exposed to air (Figure 3.10). The membrane that contained biotin and 5 mol% PEG^{550} showed roughly 75% as much binding, while the membrane that contained only egg PC (either with or without biotin) showed an amount of streptavidin binding that was consistent with non-specific adsorption.

3.5. Summary and Conclusions

Previous investigators have shown that the incorporation of PEG into bilayers increases the bending elastic modulus of the membrane.[143, 144] This PEG induced stiffening varies as a function of grafting density and chain length.[145] Other reports indicate that the degree of hydration (n_h) of PEG molecules increases significantly when

PEG is in the brush conformation.[123, 146] A PEG^{550}-PE molecule is associated with ~36 water molecules in the mushroom state, whereas a PEG^{2000}-PE can bind ~138 water molecules under similar conditions. In the brush conformation, the degree of hydration increases by ~30% for both molecules. On the other hand, phosphatidylcholine in a lipid bilayer has only ~2.5 – 6 water molecules per lipid head group. The incorporation of PEG increases the degree of hydration of the membrane even when the larger footprint size of the PEG vs. a regular phosphatidylcholine headgroup is taken into account.[118] This, of course, occurs because the PEG thickens the hydrophilic layer. It is almost certainly this increase in the hydration layer thickness in combination with the increase in the bending elastic modulus which imparts stability upon air exposure. Such effects are reminiscent of the behavior of amorphous sugar glasses that can trap water at the surface of cell membranes as well as rigidify them.[147]

It should be noted that polyethylene glycol moieties are commonly employed at interfaces to resist non-specific protein adsorption.[148] In the present work, however, these molecules had little if any effect on the extent of streptavidin binding to the lipid membranes (Figures 3.9 & 3.10). The key difference is that the PEG chains employed here were linked to a two-dimensionally fluid phospholipid bilayer, rather than grafted to a fixed location on the surface.[149] Thus, the polymer chains are more flexible and able to reorganize to accommodate incoming protein molecules at least up to the size of streptavidin (66 kD). On the other hand, the PEG film might alter the kinetics and thermodynamics of biotin-streptavidin binding.[150] In particular, it is possible that the k_{on} and k_{off} values could be somewhat suppressed in the presence of the lipopolymer film.

Furthermore, the size of the protein species may play a significant role in whether these physical constants are altered. In fact, it has been previously shown that particles of very large size, such as streptavidin immobilized on 2.8 μm polystyrene beads, do not readily bind to biotin moieties presented on pegylated bilayers in a rolling type assay.

In summary, pegylated phospholipid bilayers on planar solid supports can be employed as air-stable platforms for binding proteins. The lipopolymer layer remained flexible enough to accommodate protein binding, while dye labeled lipid molecules were generally unaffected by the presence of PEG-PE up to moderate densities. It would therefore seem that polyethylene glycol can imitate a cell glycocalix in a key respect. It protects the lipid bilayer from substantial damage upon exposure to air. It may also be the case that such films can act as size selective filters. Thus they might allow binding of smaller proteins, while preventing the binding of larger complexes. On going studies in our laboratory will now determine whether such size restrictions in these model systems can be correlated with the *in vivo* behavior of the cell glycocalix.

CHAPTER IV

A POLY(ETHYLENE GLYCOL) SIZE-SELECTIVE FILTER FOR LIGAND-RECEPTOR BINDING ON SOLID SUPPORTED LIPID MEMBRANES

4.1. Synopsis

A technique for size selective, on-chip discrimination of proteins analytes was developed using poly(ethylene glycol) (PEG) lipopolymers incorporated into supported lipid membranes. By employing various PEG lipopolymer in supported lipid membranes at mole fractions corresponding to the onset of the mushroom-to-brush transition, we observed a protein size-dependent effect on the levels of binding of three protein analytes: streptavidin, IgG and biotinylated IgM, to membrane-bound biotin-PE receptors. When the PEG lipopolymer is well into the brush conformation, complete exclusion occurs for the larger proteins (IgG and IgM), while streptavidin is still able to penetrate through the PEG layer and bind to the surface-bound ligands. This method integrates microfluidics with nanoscale size size-exclusion films for separation of protein mixtures even if all species recognize the identical ligand.

4.2. Introduction

The ability to selectively discriminate between analytes, while performing multiple tasks ‘on-chip’, is a highly desirable property for the next generation of biosensors that will be used to study such things as multivalent ligand-receptor binding,

viral infections of cells, and as monitors of toxins in our environment. To meet the requirements of such surface-based bioanalytical applications, these new devices must be capable of selective detection of analytes while minimizing nonspecific interactions from species that may arise from the environment or the bulk.[14] Nonspecific interactions lead to surface fouling, which compromises the selectivity, sensitivity, and life-time of the device.[131]

Solid supported phospholipid membranes[21, 22, 33, 106] are an ideal biomimetic analytical platform that is receiving much attention in the area of biosensing because they are easily incorporated into microfluidic devices[77], and more importantly, for their ability to mimic real cell surface properties.[24, 30, 45, 151] A fundamental property of supported lipid bilayers (SLBs) is the two dimensional lateral fluidity of the lipids within the thin film.[24, 29] SLBs can mimic the same lateral rearrangements that take place within the cell biomembrane that in turn, allows for processes such as multivalent ligand-receptor binding[26], pathogen attack, inflammatory response, and cell[152] signaling to take place.[25, 28, 111] However, current SLB devices suffer from several drawbacks that hinder their use as robust platforms for the above mentioned applications. These drawbacks include fragility of the thin membranes[46], lack of air stability[63], fouling by nonspecific adsorption[54], and the inability to discriminate between different-sized analytes that can block target ligands in the membrane.[27]

The goal of our current work is to incorporate other aspects of the native biomembrane architecture that might aid in the prevention of biofouling and aggregation as well as discriminate between different proteins that can bind to the same ligands. In

particular we mimic the cell surface glycocalyx[74] structure using poly(ethylene glycol) PEG incorporated lipopolymers.[1, 39] This polymer coating is inspired by the elaborate chemistries found on bacterial and eukaryotic cell surfaces. The cell surface glycocalyx consists of glycosylated proteins, glycolipids, proteoglycans that can extend tens of nanometers above the plasma membrane. It affords membrane stability, plays a role in cell signaling, cell-cell interactions, and may possibly function as a macromolecular filter.[140] PEG has been proposed as a mimic[141] of the cell surface glycocalyx in artificial bilayer systems, and its incorporation within supported membranes has allowed for the air-stabilization of SLBs while providing a porous architecture for facile ligand-receptor interactions.[73] Since the size, density, and structural conformation of the PEG lipopolymer can be tailored within lipid membranes, the accessibility of a variety of ligands, i.e. proteins, antibodies and toxins, to surface bound receptors can be controlled.

The interactions of various proteins with grafted PEG polymers have been well studied for an assortment of PEG sizes and polymer conformations.[132] Both theoretical[122] and *in vitro* studies have shown a conformation-dependent ability of PEG to avoid nonspecific protein adsorption and affect ligand-receptor binding using a variety of techniques, including surface force measurements[153, 154], micropipette techniques[118], surface plasmon resonance[131] (SPR), fluorescence microscopy[155], among other surface analytical methods[136]. At low surface density, the polymer chains avoid each other and consequently assume discrete mushroom-like conformations on the surface, allowing proteins to interact with the uncovered surface.[117] At high PEG densities, the polymer chains are forced to interact with each other, forming a brush-like structure that creates a

higher steric repulsion from the surface for the proteins that encounter the polymer brush.[122, 156] The net effect of steric repulsion, van der waals attraction, and hydrophobic interactions are dependent on the degree of polymerization (n_p) and grafting density of the PEG, which in turn also affects the length and thickness of the polymer network.[127] These tunable parameters also affect how easily a protein or analyte can pass through the polymer meshwork.[120]

Here we present results for PEG lipopolymers incorporated into supported membranes that perform 'on-chip' filtering of protein analytes of various sizes. An important aspect of our system is that the PEG lipopolymer experiences similar two-dimensional lateral diffusion[73, 142] to that of the fluid lipid film and does not adversely affect either the lipid or ligand mobility in the membrane. Another unique aspect of PEG is the ability to control polymer grafting density, and thus conformation. Therefore, we can tailor the repulsive interactions that proteins of various sizes will encounter for a given PEG coating. By combining microfluidic technology with fluorescence detection, we demonstrate selective, 'on-chip' screening of three proteins: streptavidin, IgG, and the much larger protein, IgM, to surface-bound biotin lipids.

4.3. Experimental

Vesicle Preparation. Small unilamellar vesicles (SUVs) were prepared according to an established procedure[42] by mixing appropriate amounts of 1-Palmityol-2-Oleyol-sn-Glycero-3-Phophocholine (POPC) lipids and 1,2-Dioleyol-sn-Glycero-3-Phosphoethanolamine-N-[Methoxy(polyethylene glycol)] lipids of molecular weights:

350, 550, 750, 1000, 2000, 3000, and 5000 Da with 1 mole % 1,2-Dipalmityol-sn-Glycero-3-Phosphoethanolamine-N-(Biotinyl) (sodium salt) Biotin-PE lipids (Avanti Polar Lipids, Alabaster, AL). In the first set of experiments, the mole fraction of each PEG-lipopolymer (with degree of polymerization ,n_p = 8, 12, 17, 22, 45, 67, and 114 respectively) was adjusted to the onset of the mushroom-to-brush transition ($\chi^{m\rightarrow b}$), where the polymer grafting distance (D) is less than $2R_F$ according to scaling theory[118]. For the second set of experiments, vesicles were made containing PEG^{2000} or PEG^{5000} in the brush conformation, approximately 3 times $\chi^{m\rightarrow b}$ (see table 4.1). The sizes of SUVs were determined to be 100 ± 5 nm by dynamic light scattering (90 Plus Particle Sizer, Brookhaven, CA).

Microfluidic Device and Microwell Preparation. PDMS microfluidic devices and microwells were fabricated according to established procedures of Yang[45] and Albertorio[73] et al using Polydimethylsiloxane acquired from Dow Corning (Sylgard, silicone elastomer-184). The devices were bonded to clean and anealled borosilicate glass coverslips. Bilayers were formed inside microchannels and microwells via vesicle fusion.[36] Finally, the excess unfused vesicles were rinsed out with phosphate buffer saline solution (PBS: 10 mM $Na_2HPO_4^-$, 5mM $NaH_2PO_4^{2-}$, 150 mM NaCl) at pH 7.4.

Protein Labeling. Texas Red-conjugated Streptavidin, Alexa-fluor-488 labeled streptavidin, unlabeled streptavidin and Alexa-fluor-594 succinimidyl ester were purchased from Molecular Probes (Eugene, OR). Anti-biotin IgG and biotinylated IgM were acquired from Rockland Immunochemicals (Gilbertsville, PA) and were

Table 4.1. Properties of PEG Lipopolymers.

PEG MW. (Da)	**Degree of Polymerizatin n_p**	**Flory Radius R_F (nm)**	**Mole% onset of mushroom-to-brush $\chi^{m\rightarrow b}$**
350	8	1.36	11
550	12	1.73	7
750	17	2.13	4.4
1000	22	2.49	3.3
2000	45	3.83	1.4
3000	67	4.86	0.8
5000	114	6.69	0.5

* The flory radius (R_F) and $\chi^{m\rightarrow b}$ were calculated according to Marsh[118]

Table 4.2. Protein Molecular Weights and Sizes.

Protein	Streptavidin	IgG	IgM
Molecular Weight (kD)	52.8	150	900
Size (nm)	5.5	17	36

* The size and molecular weight for these proteins were acquired from Needham[114] et.al. and Roberts[157] et.al.

conjugated to Alexa-fluor-594 succinimidyl ester and purified by size exclusion chromatography. All protein solutions were 1 μM in PBS buffer, pH 7.4. Properties such as molecular weight and size for each protein[89, 120, 157] are summarized in table 4.2.

Fluorescence Microscopy. Ligand-receptor binding experiments were carried out either inside microfluidic devices or in microwells and the protein binding was detected via fluorescence microscopy using an inverted epifluorescence Nikon Eclipse TE 2000-U microscope with a Sensys CCD (Photomatrics, Roper Scientific). 1 mole% biotin-PE was employed as the membrane bounded receptor for all experiments. After bilayers were formed and rinsed with PBS buffer, the surfaces were incubated with a 1mg/ml solution of fibrinogen (Sigma-Aldrich) for 30 minutes in order to reduce the nonspecific background binding. Afterwards, the fibrinogen was rinsed out with PBS buffer and the protein analyte solution (either streptavidin, IgG or IgM) was injected and incubated for 1 hour followed by copious rinsing with PBS buffer. Fluorescence imaging was carried out under either 4X or 10X magnification. The levels of protein binding and background correction are analyzed using Meta-Morph software (Universal Imaging) and always normalized to the control bilayer (POPC + 1mole% Biotin-PE).

4.4. Results and Discussion

The aim of the first set of experiments was to measure the effect of PEG size on ligand-receptor binding. Specifically, we tested the ability of three proteins, spanning a range of several orders of magnitude in molecular weight (table 4.2), to penetrate through the various PEG lipopolymers and bind to membrane-bound biotin ligands. The

mole fraction of the PEG lipopolymers was held at the onset of the mushroom-to-brush transition in order to ensure maximum packing of the polymer, thus allowing for a sufficiently porous network for proteins to diffuse through. The results are shown in figure 4.1, where the fluorescence intensity is normalized to the control bilayer (POPC + 1 mole% biotin-PE) and plotted against the molecular weight of the PEG lipopolymers.

In the case of streptavidin, we observed that the protein is indeed able to diffuse through the polymer network and bind to the surface-bound biotin molecules at all PEG molecular weights within experimental error. Overall, the lipopolymer is unable to sterically hinder streptavidin from penetrating the PEG layer, even though we expect the packing of the PEG moieties at the mushroom-to-brush transition to coat nearly the entire membrane surface. For the antibiotin IgG, the levels of binding progressively drop with increasing PEG size and seem to plateau at ~75%. Even for the largest PEG lipopolymer, PEG^{5000}, some IgG is able to pass through the polymer layer and bind to the surface biotins.

A similar binding effect was observed for the biotinylated IgM, however, here the experiment was carried out in a slightly different way using a biotinylated IgM since antibiotin IgM was not readily available. In this case, the bilayers are first exposed to unlabeled streptavidin for one hour to ensure complete binding to the biotinylated membrane, as our results above indicate. Streptavidin, having four biotin-binding pockets (two on each side), is able to penetrate the PEG layer, bind, and irrespective of orientation, present at least two available binding sites for the biotinylated IgM to attach to. The biotinylated IgM solution was injected into the microfluidic channels, allowed to

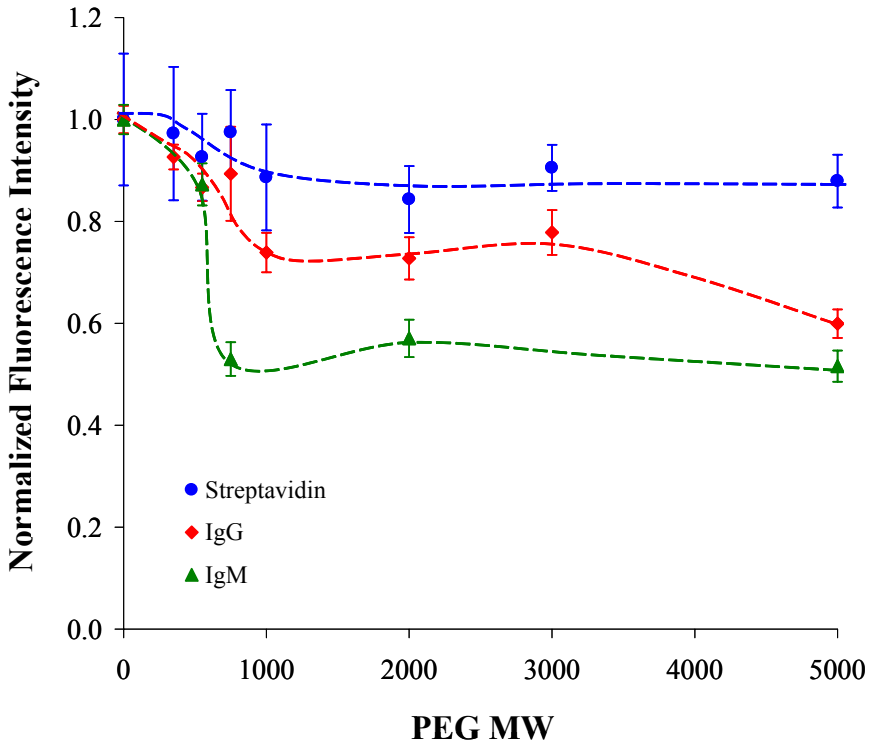

Figure 4.1. The effect of PEG size on protein binding. Peg-lipopolymer incorporated bilayers are prepared at the onset of the mushroom-to-brush transition. The level of binding of each protein: streptavidin (blue), IgG (red), and biotinylated IgM (green) to 1 mole% biotin-PE surface bound receptor is normalized to the control channel (POPC+1 mole% biotin-PE). The dashed lines are guides for the eye.

incubate for one hour followed by rinsing with PBS buffer and then subsequently imaged. The levels of binding are again normalized to the control, 1 mole % biotin in POPC. Interestingly there is an almost immediate drop in binding at an intermediate PEG size (PEG^{750}) which plateaus to a level of ~50%.

A similar filtering effect was observed for avidin-biotin binding in giant unilamellar vesicles (GUVs) in the presence of PEG^{750}.[114] However, in that case the binding was only allowed to proceed for 2 minutes, raising the question as to whether the system reached thermodynamic equilibrium. The affinity binding constant of streptavidin-biotin has a ($K_a \sim 10^{15}$ $mole^{-1}$)[150] and it is typical to wait about 1 hour[28, 89] during binding experiments before quantifying results; therefore, in our experiments, we incubated our chips with each protein solution for one hour to ensure thermodynamic equilibrium and complete binding.

Figure 4.1 shows that there is definitely a protein-size effect when it encounters the polymer in the mushroom-to-brush state, indicating that, up to a certain degree, the proteins are able to diffuse through the porous network and encounter the surface bound receptors. This data corroborates findings of several studies reported in the literature. First, similar size-exclusion effects have been modeled, typically for higher grafting densities, in which mean field theory was employed to estimate the change in binding affinity of a protein as a function of lipopolymer density and size.[129, 149] A similar effect was also modeled for proteins of various sizes as they encountered a particular lipopolymer brush.[120, 158, 159] Furthermore, the repulsion interactions of PEG were demonstrated experimentally by the surface force apparatus.[160]

In the second set of experiments, we aimed to achieve complete filtering of the proteins by titrating the polymer density to the brush conformation, where the interpolymer distance is less than the flory radius ($D < R_F$), which causes more interaction between polymer chains as well as chain elongation. The brush configuration increases the steric repulsions that proteins will encounter at the polymer/aqueous interface. We chose to work with PEG^{2000} and PEG^{5000} at mole% of 5 and 1.5 respectively, which is ~3 times greater than the corresponding mole % for the onset of the mushroom-to-brush ($\chi^{m\rightarrow b}$) transition (table 4.1). The data are summarized in figure 4.2. The streptavidin case, in blue, shows statistically no affect on binding due to the polymer brush, compared to both the control and mushroom-brush case at PEG molecular weights 2000 and 5000 Da. IgG binding, shown in red, already dropped to ~75% at 1.5 mole% PEG^{2000} ($\chi^{m\rightarrow b}$ for PEG^{2000}). By increasing the mole% of PEG^{2000} to 5% (brush state), the level of binding drops to ~20%, thus the lipopolymer brush filters out ~80% of the incoming IgG. The size exclusion effect is more pronounced for the larger PEG^{5000} in the brush state, at 1.5 mole% PEG^{5000}, where nearly 100% of the incoming IgG are filtered out. Figure 4.3 illustrates how the polymer brush might hinder the binding of IgG to surface-bound receptors.

A similar trend is observed for the largest protein, IgM, shown in green. At 1.5 mole% PEG^{2000}, the level of binding is ~50%, thus filtering out half of the biotinylated IgM. At 5 mole%, the same polymer decreased binding to ~10%, blocking ~90% of the protein from reaching the surface ligands. The effect is similar for the largest PEG^{5000} lipopolymer, in which the polymer mushroom only excludes ~50% of the IgM, while at

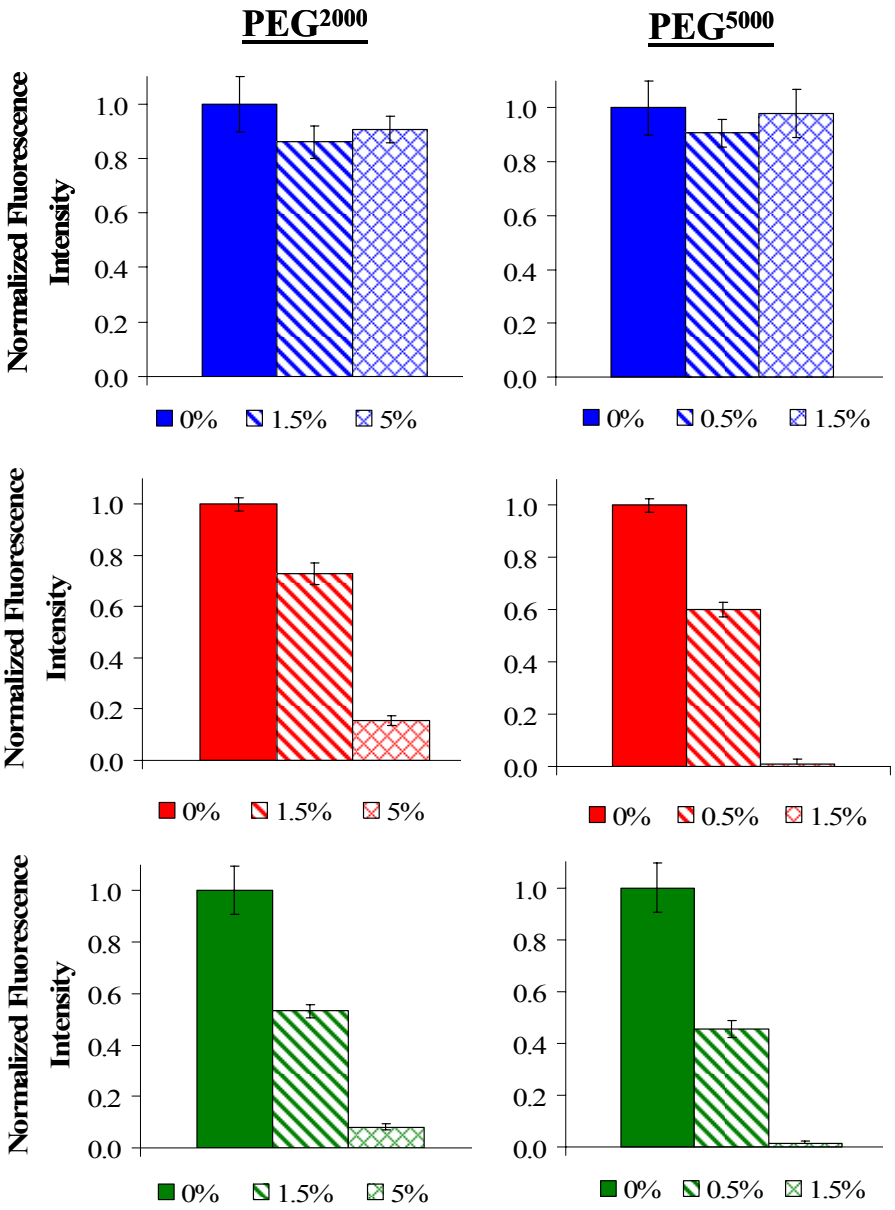

Figure 4.2. Protein filtering induced by the presence of a polymer brush at the surface. The levels of binding of streptavidin (blue), IgG (red) and biotinylated IgM (green) are compared for PEG^{2000} and PEG^{5000} at a mole fraction of the onset of their respective mushroom-to-brush transition and at 3 times higher, in the brush conformation.

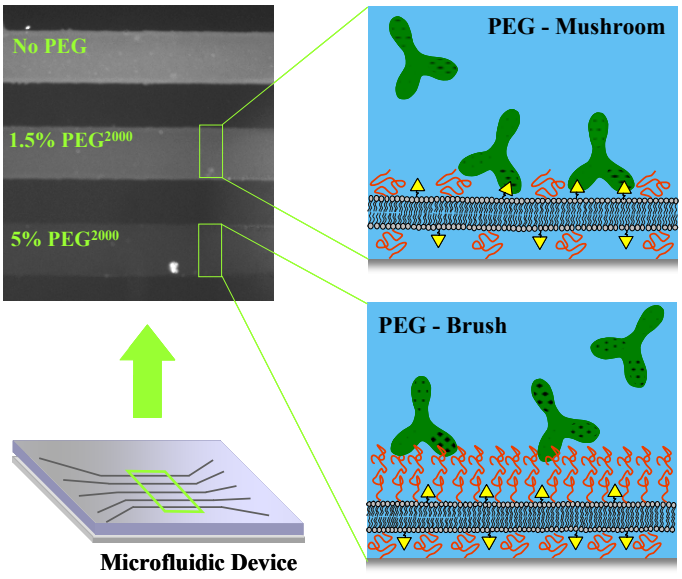

Figure 4.3. The 'on-chip' filtering of IgG using PEG^{2000} incorporated supported bilayers. Bilayers are formed inside a microfluidic device (left side). The levels of IgG binding are compared and normalized to the control channel (uppermost channel). The protein is able to penetrate the polymer layer at low polymer densities corresponding to the mushroom conformation (middle channel), while at high densities, or brush conformation, (lowest channel) the protein is filtered. The process is schematically represented in the right side.

1.5 mole% the brush completely filters out the incoming protein. In this particular case there could be another plausible explanation for the reduction in binding of biotinylated IgM, instead of a size-exclusion effect. It is possible that the streptavidin bound to the biotinylated membrane may not be properly oriented for subsequent binding of biotinylated IgM. However, our data indicate that the polymer brush does not affect the levels of streptavidin binding (Figure 4.2) compared to the control and mushroom-to-brush regime, as it might if the protein was not able to align properly to the surface because of the presence of the dense lipopolymer layer. Furthermore, the data in figure 4.1 show a similar trend for the drop in binding of biotinylated IgM compared to the antibiotin IgG. Since the size of an IgM (~36 nm) is roughly twice as large as an IgG (~17 nm), one would expect a decrease in the level of binding by half to be reasonable and this coincides with the data presented in figure 4.2.

These data illustrate that the mushroom state of PEG lipopolymers does not afford sufficient steric repulsion to block or filter proteins from the surface even at maximal coverage at the onset of the mushroom-to-brush transition. On the other hand, the polymer brush provides sufficient repulsion that results from a balance of steric effects, van der waals attraction, and hydrophobic interactions that leads to either almost or complete filtering of the protein analytes. However, these effects are mitigated for a sufficiently small-sized proteins, as demonstrated by the streptavidin data. These types of size exclusion effects have been modeled using mean field[118, 122] and scaling theory[127, 153, 160] for protein adsorption[132] and ligand-receptor binding[161], as mentioned above, and we provide additional supporting evidence to these theories.

A major advantage of combining size-selective filtering with microfluidic transport on 'lab-on-a-chip' devices is that it could possibly lead to assays that use complex mixtures of analytes, such as crude cell extracts for proteomics applications, and even whole blood serum samples for medical diagnostics, without having to purify the serum or extracts first. There are microfluidic devices that are capable of carrying out cell cytometry on chip to analyze cellular chemical contents.[162] Such a device consists of a complex series of channels and valves, usually a cell manipulation channel, reagent introduction channel, a reaction chamber, and a separation channel. Capillary electrophoresis separates discrete cellular components, which can then be identified and analyzed, or possibly sent to another area of the chip for subsequent experiments, perhaps for ligand-receptor binding studies.[162] The new type of on-chip screening device presented here is different from the latter in that it is not necessary to have a complex series of channels and a discrete separation chamber within the chip but rather separation can occur simultaneously within the binding channel. We demonstrate a simplified version of such an experiment in figure 4.4, where we used a mixture of streptavidin and antibiotin IgG to prove that we can screen for proteins with an affinity towards the same receptor. Figure 4.4 shows a microfluidic device in which the first two channels (from left-to-right) contain control bilayers (POPC + 1 mole% biotin-PE) and the third channel contains 1.5 mole% PEG^{5000} + 1 mole% biotin-PE. Alexa-488 labeled streptavidin and Alexa-594 labeled IgG were respectively introduced into the first two channels (control bilayers), while a 1:1 mixture of the two proteins was introduced into

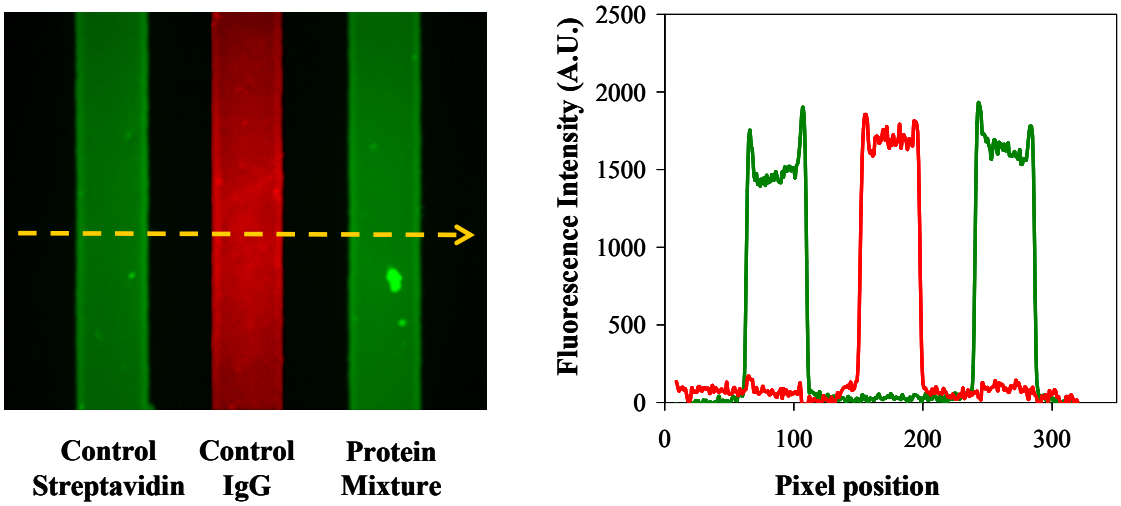

Figure 4.4. The size selective filtering of protein mixtures inside a microfluidic device. Shown on the left is a microfluidic device in which the first two channels (from left-to-right) contain POPC + 1 mole% biotin-PE. The third channel contains 1.5 mole% PEG^{5000} + 1 mole% biotin-PE. Fluorescence micrographs were acquired and overlaid after the bilayers were exposed to Alexa-488-streptavidin (green) and Alexa-594-IgG (red). Shown on the right is the line scan of the fluorescence intensity (A.U.) for each channel. In channel 3, in which the protein mixture was introduced, the binding of streptavidin (green line) is similar to that of the control channel while the level of binding for IgG (red line) is depressed.

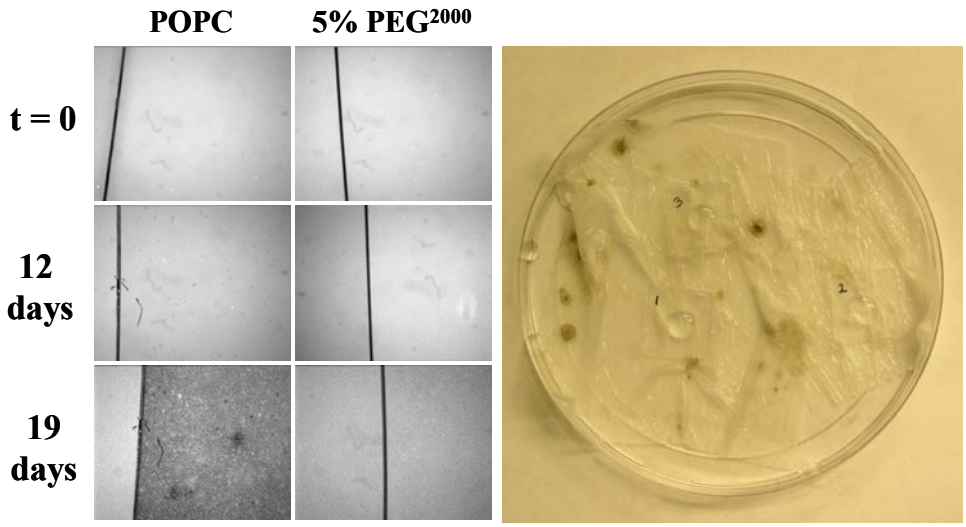

Figure 4.5. SLB biofouling induced by the growth of mold. Left: An unprotected POPC supported bilayer exposed to mold spores in a Petri dish (right-most image) initially appeared normal, but after 12 days, mold and/or bacteria seemed to infiltrate the bilayer. After 19 days, the growth was quite substantial and whole quadrants became destroyed. Middle: A POPC bilayer protected by 5 mol% PEG-conjugated lipids. This bilayer showed complete growth inhibition even after 19 days. Note: the dark lines were scratches purposely made in the bilayer to determine the background fluorescence level and identify different chip regions.

the third channel. According to the data presented in figure 4.2, we should observe a complete filtering of the IgG in the presence of the polymer brush. After collecting fluorescence images in both the green channel (streptavidin-Alexa-488) and the red channel (IgG-Alexa-594), and subsequent overlay of the images, we indeed observe that in the third microfluidic channel a selective filtering can be achieved for the protein mixture as indicated by the line scan shown on the right side of figure 4.4.

Finally, we have tested the ability of PEGylated bilayers to resist bacterial and mold growth. Resistance to such contamination is especially important for bilayer devices that will be used continuously in water or humid environments where the possibility of biofouling by mold, algae, and bacteria is quite high. The results are shown in figure 4.5. Supported POPC lipid bilayers, with 0.1 mole% Texas Red DHPE as a fluorescence probe, containing either 5 mole% PEG^{2000} or 1.5 mole% PEG^{5000} were formed inside PDMS microwells. The membranes were subsequently imaged under 10X magnification and left in a humid environment for a period of 2 weeks. We observed that bilayers without lipopolymer constituents did not resist the growth of mold after two weeks, while bilayers that contained a dense coating of lipopolymers were found to be very resistant to mold growth (figure 4.5).

4.5. Summary and Conclusions

Size selective filtering using poly(ethylene glycol) lipopolymer incorporated into supported lipid membranes allows further enhancement of rapid, on chip screening of protein analytes. By controlling the size and density of the PEG polymer we are able to

provide an ‘on chip’ method for the discrimination of complex mixtures of protein analytes; that in turn will lead to better devices for a variety of applications that exhibit a superior resistance towards biofouling. Furthermore, we show that sensing devices that aim to mimic the cellular membrane should incorporate more of the complex architecture of a native membrane to improve its overall performance (selectivity) and lifetime by reducing fouling caused by large contaminants.

CHAPTER V

ON THE MECHANISM OF CRYPROTECTION: THE INTERACTIONS OF TWO ANALOG SUGARS TREHALOSE AND MALTOSE WITH PHOSPHATIDYLCHOLINE SUPPORTED LIPID MEMBRANES

5.1. Synopsis

A study of biopreservation using solid supported phospholipid membranes as a model system is presented. A cryoprotection mechanism for two analog sugars, trehalose and maltose is proposed. Herein, we present the effects of trehalose and maltose on the main phase transition temperature of DMPC supported phospholipid bilayers by employing temperature controlled fluorescence recovery after photobleaching. Trehalose is observed to lower the main phase transition temperature T_m, while maltose increases it. We observe the occurrence of buckling of the thin film which seems to coincide with the ripple phase in the gel state of the supported DMPC bilayer and a suppression of such phase by the addition of trehalose. Trehalose is observed to maintain lipid phase segregation and avoid lipid mixing, while maltose does not. The interaction of each sugar at the air/water and monolayer/aqueous interface was probed with vibrational sum frequency spectroscopy (VSFS). Finally, the effectiveness of cryoprotection for each sugar is presented. We observe that trehalose is the most effective preservation agent compared to maltose and poly(ethylene glycol) PEG-

lipopolymer incorporated bilayers. Our findings suggest that because of the 'clam shell' type structure of trehalose, due to its C1α-C1α linkage, it is more effective at penetrating further into the lipid membrane, thus replacing interfacial water via H-bonding within the headgroups, and henceforth, reducing lipid packing and van der waals interactions of the acyl chains.

5.2. Introduction

Achieving long-term stability of 'biologicals' is an important goal of the pharmaceutical and food industry, and medical research.[163, 164] For example, the preservation of proteins[165], cells, tissues, and vaccines is usually done under cryogenic or freeze-dried conditions in the presence of additives.[166] However, in most instances, only short-term preservation is accomplished. An understanding of biopreservation at the molecular level would provide a means in which to create better synthetic mimics that work as well as natural preservants. Biopreservation involves the ability of an organism to protect itself from an external stress in order maintain physiological function.[137, 167] Such external stress may be caused by an anhydrobiotic[168] (dry) or a cryogenic[169] environment where the biomembrane is most vulnerable to damage. Many organisms may employ specialized proteins or synthesize a large amount of di- and tri-saccharides, which upon synthesis, are relocated to the extracellular side of the biomembrane.[170] Among these, are small non-reducing sugars such as trehalose[171], and other sugars such as sucrose[172], glucose and larger fructans[173] that function as lipopreservatives. Even though *in vivo* and *in vitro*[174] experimentation have yielded some information about the

molecular species involved in preservation, a molecular level mechanism as to why some lipopreservatives work better than others is still unclear.

Trehalose, a non-reducing disaccharide has proven to be the most effective lipo-preservative within anhydro- or cryobiotic conditions.[175] Simple model systems, such as liposomes[176, 177], have been employed to study the interactions of trehalose and other sugars with the lipid membrane.[178] These studies generally consist of determining the extent of liposome fusion and leakage upon dehydration/rehydration or during freeze fracture.[179, 180] The morphological effects are also observed by assaying for lipid phase segregation[176, 181] since irreversible phase segregation of lipids and membrane constituents is an inherent consequence during these events.[182, 183] Results indicate that trehalose is the best at preventing lipid phase segregation[181], liposome fusion and leakage.[179, 180] Formation of an amorphous sugar glass, direct interaction of trehalose with the lipid molecules and the physiochemical aspects of water-sugar interaction are observations that have lead towards two main proposed hypotheses. The first hypothesis, 'water replacement'[184], proposes that the direct interaction of trehalose with the lipid head groups via hydrogen bonding replaces water molecules at the lipid/aqueous interface.[185, 186] This water replacement model suggests that the direct interaction of trehalose with the lipids is responsible for preservation of the membrane.[187] Fourier transform infrared spectroscopy (FTIR) results indicate a change in the H-bonding environment of the phosphoryl group in the presence of trehalose.[188] Neutron diffraction experiments indicate that trehalose has a high affinity towards disrupting tetrahedrally coordinated water molecules known as 'ice-like' water.[189, 190] A

second hypothesis, 'vitrification'[191], suggests that there is a formation of an amorphous sugar glass at the lipid/aqueous interface where the osmotic and volumetric properties of the sugar lowers the phase transition temperature (T_m) of the lipid molecules within the membrane.[192, 193] Most observations are obtained by differential scanning calorimetry (DSC) of dried liposomes.[181] An increase in the phase transition temperature occurs when liposomes are desiccated due to the decreased headgroup spacing of the lipids, which in turn allows for stronger van der waals interactions of the lipid acyl chains. However this increase in T_m is suppressed in the presence of not only trehalose, but to various degrees, other sugars.[192, 193] This leads to the question of why there is a natural preference towards trehalose than other sugars, and even more interesting is the comparison with its analog sugar, maltose, which is a reducing sugar.

Our focus has been to investigate the cryobiotic preservation mechanism by directly comparing trehalose and maltose utilizing a solid supported lipid membrane system. Solid supported lipid bilayers[1, 21, 22, 29] have proven to be an ideal system in which to mimic the biomembrane.[77, 84] Properties such as the lateral fluidity of the individual lipid molecules and membrane constituents are preserved in these membrane mimics.[24, 29, 40, 46, 61, 194] Lateral fluidity is essential to membrane function, as it facilitates a variety of processes such as ligand-receptor binding[26, 28, 90], cell signaling[195] and trafficking, and exocytosis among others. An advantage of the SLB format is that we can study the function of the membrane in terms of the lateral fluidity of the lipids and how this is affected, for example, by a cryogenic stress. Under low temperature conditions, the lateral diffusion of lipids is suppressed. This is primarily due to that most

of the lipids are undergoing their liquid-to-gel main phase transition and other pre-phase transitions.[105, 196, 197] In the gel state, a decrease in headgroup spacing leads to an increase in van der waals interactions of the acyl chains, thus ordering the hydrophobic tails.[80, 198] This may also have an effect on the morphology and lipid phase segregation of the membrane due in part to the formation of ice at the membrane interface. Therefore, we hypothesize that a lipoprotectant should have an effect on the lipid phase transitions, and that therefore a direct interaction with the lipid moiety is needed.

Herein, we employ lipid bilayers supported on a borosilicate substrate of either POPC or DMPC in combination with fluorescence microscopy to compare the effects of the analog sugars, trehalose and maltose, on the DMPC main phase transition temperature (T_m). We used fluorescence recovery after photobleaching[58, 78] (FRAP) to study the phase transition temperature change by measuring the diffusion constant of the lipid bilayer as a function of temperature. We observed that trehalose suppressed the liquid-to-gel transition temperature of DMPC while maltose appeared to slightly increase it. We also observed cracking and buckling of the supported lipid bilayer a few degrees lower than the main transition which coincides with the ripple phase transition. As a consequence, an effect of the presence of the sugars is observed. The morphological effect of cryogenic temperature, by exposing POPC lipid bilayers to -80 ^{o}C, was also probed. A difference in the ability of each lipopreservative in membrane protection is reported.

Vibrational sum frequency spectroscopy[79, 80, 95] VSFS was used to study the chemical nature of the interaction of each sugar at the air/water and monolayer/aqueous

interfaces.[98] Finally, we compared the ability of each sugar to avoid lipid phase segregation at low temperatures utilizing a Langmuir monolayer system. This study reveals differences in how trehalose and maltose interact with a supported lipid membrane.

5.3. Experimental

Materials. 1-Palmitoyl-2-Oleoyl-*sn*-Glycero-3-Phosphocholine (POPC), 1,2-Dimyristoyl-*sn*-Glycero-3-Phosphocholine (DMPC) and 1,2-dioleoyl-sn-glycero-3-phosphoethanolamine-N-[methoxy(polyethylene glycol] (PEG-DOPE) with a PEG molecular weight of 350, 550 and 2000 Da were purchased from Avanti Polar Lipids (Alabaster, AL). *N*-(Texas Red sulfonyl)-1,2-dihexadecanoyl-sn-glycero-3-phosphoethanolamine (Texas Red DHPE) were obtained from Molecular Probes (Eugene, OR). Purified water acquired from a NANOpure Ultrapure Water System (Barnstead, Dubuque, IA), had a minimum resistivity of 18.2 MΩ·cm, and was used in the preparation of all buffer solutions. Phosphate buffer saline (PBS) was prepared using 10.0 mM sodium phosphate with the addition of 150 mM NaCl (Sigma-Aldrich). The pH was adjusted to 7.4 by the addition of NaOH (EM Science). Solutions of D(+)-trehalose (99.5%, Fluka Biochemika, CH) and D(+)-maltose monohydrate (90%, Acros Organics, NJ) were prepared in deionized water at 20% or 2.0% w/w. The chemical structure of trehalose and maltose are illustrated in figure 5.1. Poly(dimethylsiloxane) (PDMS) was used to fabricate PDMS wells devices. The polymer and crosslinker were purchased from Dow Corning (Sylgard Silicone Elastomer-184, Krayden Inc.). Glass

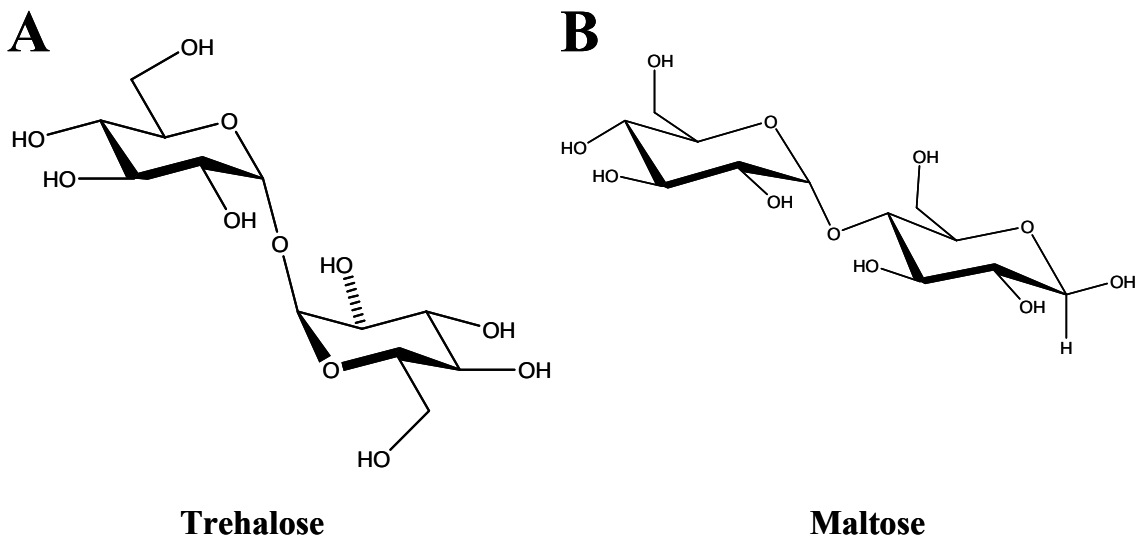

Trehalose **Maltose**

Figure 5.1. The chemical structure of trehalose (A) and maltose (B).

microscope slides were purchased from VWR International and were cleaned and annealed according to established procedures.[45]

Preparation of Small Unilamellar Vesicles and Bilayer Formation. Small unilamellar vesicles[42] were prepared from either POPC or DMPC and 0.1 mol% Texas Red DHPE, which was incorporated as a fluorescence probe. PEG lipopolymer incorporated vesicles were prepared as previously described.[73] Briefly, the solvent was then evaporated under a stream of nitrogen followed by desiccation under vacuum for 4 hours. Rehydration of the lipids was performed in PBS solution at pH 7.4. After 10 freeze-thaw cycles the large vesicles were extruded through a polycarbonate filter, which had an average pore size of 50 nm. Small unilamellar vesicles prepared by this method were 80 ± 10 nm in diameter as determined by dynamic light scattering using a 90Plus Particle Size Analyzer from Brookhaven Instruments Corporation.

Vesicles were delivered to the surface of planar glass microscope slides in a PDMS/glass microwell device. After a 10 minute incubation period, the microwells were thoroughly rinsed with the appropriate buffer or purified water. The samples were placed under an inverted epifluorescence Nikon Eclipse TE2000-U microscope and observed with a 10x objective. Images were obtained using a MicroMax 1024b CCD camera (Princeton Instruments) and data analysis was performed with MetaMorph software (Universal Imaging).

Fluorescence Recovery after Photobleaching (FRAP). FRAP curves were obtained by exposing the sample to laser irradiation from a 2.5 W mixed gas Ar^+/Kr^+ laser (Stabilite 2018, Spectra Physics). Planar bilayer samples were irradiated at 568.2

nm with 100 mW of power for times not exceeding 1 sec. A 17.0 μm full-width at half-max bleach spot was made by focusing the light onto the bilayer through the 10x objective. The recovery of the photobleached spot was monitored by time-lapse imaging. The fluorescence intensity of the bleached spot was then determined as a function of time after background subtraction and intensity normalization. All fluorescence recovery curves were fit to a single exponential to obtain both the mobile fraction of dye-labeled lipids and the half-time of recovery, $t_{1/2}$, following standard procedures.[73, 78] The diffusion constant, D, could be obtained from the $\tau_{1/2}$ value by employing the following equation:

$$D = \frac{w^2}{4\tau_{1/2}}\gamma_D \qquad (5.1)$$

Where *w* is the full-width-at-half-max of the Gaussian profile of the focused beam and γ_D is a correction factor that depends on the bleach time and the geometry of the laser beam. Herein w = 17.0 μm and the value of γ_D is 1.2. The diffusion constant for a POPC bilayer and DMPC bilayer, above its T_m was 4.0 ± 0.2 x 10^{-8} cm^2/sec with 98 ± 1% recovery.

Determination of the Main Phase Transition Temperature T_m. The T_m of DMPC lipid bilayers supported on borosilicate was acquired using a 'homebuilt' temperature controlled system illustrated in figure 5.2a. Briefly, this consisted of two square brass tubes (1/8"x1/8", K&S Engineering, IL) spaced ~1mm apart that have been expoxy glued to a metal ring. The brass tubes are fitted to rubber hoses that in turn are connected to a temperature controller (VWR Scientific). The spacing between the brass

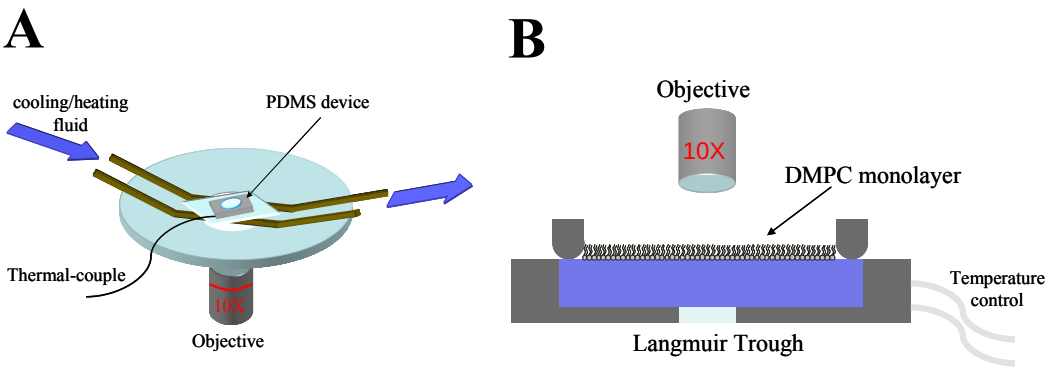

Figure 5.2. (A) Temperature control device for fluorescence recovery after photobleaching experiments. (B) Langmuir trough set-up for an upright-fluorescence microscope.

tubes allows for a more precise control of the temperature by avoiding temperature drift. After calibration, the error in the temperature system was found to be 0.2 ^{o}C. A PDMS microwell system is place on top of the brass tubes, while the temperature of the PDMS system is monitored by a thermocouple (Omega Engineering, CT). FRAP measurements are taken as a function of temperature starting at 35 ^{o}C to 11 ^{o}C. The diffusion constant is plotted as a function of temperature (^{o}C) and the data are fit to the following equation in order to obtain T_m:

$$y = \frac{a}{1 + e^{\frac{-(T - Tm)}{b}}} \tag{5.2}$$

Vibration Sum Frequency Spectroscopy VSFS. VSFS relies on second order nonlinear optical process by which two incident lasers: a tunable infrared ω_{IR} and fixed visible beam (ω_{vis}) are both focused temporally and spatially upon an interface. The resulting output is a signal generated at the sum of the incident frequencies $\omega_{SF} = \omega_{IR} + \omega_{VIS}$. In the dipole approximation the process is forbidden for centrosymetric media. However, at an interface, where centrosymetry is broken, oscillators that are aligned to the incoming polarizations will generate a sum frequency signal. Therefore, as the tunable IR beam reaches a vibrational mode for of an aligned species, its sum frequency signal is increased, thus generating an IR spectrum of the interface.

Our[62, 96, 98, 99] VSFS experiments are performed using an Nd:YAG laser (PY61; Continuum, Santa Clara, CA) operating at 20 Hz repetition rate with a peak width of 21 ps producing an output at 1064 nm. The 1064 nm beam is pumped through an optical parametric generation/amplification OPG/OPA stage (Laser Vision; Belleview, WA).

This produces the tunable IR (2700 cm^{-1} – 3700 cm^{-1}) and the fixed visible beam a 532 nm. The polarization used in our experiments was $S_{SF}S_{VIS}P_{IR}$. SF spectra were acquired using a Langmuir trough from 2700 cm^{-1} – 3700 cm^{-1} in which solutions of 2% w/w trehalose and maltose were probed at the air/water interface. DMPC monolayers with 2% and 20% trehalose and maltose sub phases were also investigated.

Langmuir Monolayer Fluorescence Microscopy. Monolayers of DMPC lipids with 0.05 mole% Texas Red DHPE were spread on a Langmuir trough (Nima, France) mounted on the stage of an upright fluorescence microscope (Eclipse E800, Nikon) as shown in figure 5.2b. The monolayers were spread from a 1μM lipid solution in chloroform at 27 ^{o}C on either a pure water subphase or a 2 % w/w trehalose or maltose aqueous solution. After the solvent was allowed to evaporate, the pressure was adjusted to 20.0 mN/m. The temperature was lowered and images were acquired every 1 ^{o}C using a 10X long working distance objective.

Cryogenic Freezing of Lipid Bilayers. POPC and PEG-containing POPC lipid bilayers made inside PDMS microwells are first assayed by FRAP, followed by freezing at -80 ^{o}C for 24 hours. The frozen membranes are imaged under 10X magnification to verify surface uniformity and morphology. They bilayers are re-imaged after they have been thawed and FRAP measurements are acquired to verify the function of the lipid membranes.

5.4. Results and Discussion

An important property of phosphatidylcholine (PC) lipids is their temperature dependent ability to undergo phase transitions between various states.[79, 196, 199] The main phase transition is the fluid-to-gel transition[199], which is associated to the ordering of the lipid acyl chains or the transition from liquid disordered to liquid order (gel) phase. Other gel/gel transitions can exist below the main phase transition.[199] These phase transitions depend on the lipid type and chemical structure, such as length of the acyl chains and head group.[200] An intriguing phase is the ripple phase transition[201], which is dependent on thermal hysteresis of the system and is characterized by nanometer size corrugations in the lipid film.[202]

Different techniques have been employed to study lipid phase transitions[203-205]. Typically differential scanning calorimetry (DSC) is performed using a liposome preparation and the main phase transition is typically a sharp transition. DSC and fluorescence anisotropy[206, 207] have been the preferred methods in which to study the effects of trehalose and other sugars on the T_m of various lipids. Atomic force microscopy has been employed to study the main phase transition of supported DMPC bilayers on mica. A broadening as well as a shift of the main phase transition has been observed for the mica supported bilayers.[103] Herein, the method of temperature controlled fluorescence recovery after photobleaching (FRAP) provides the advantage of monitoring the changes in lipid diffusion in a supported bilayer as it undergoes the main phase transition. Figure 5.3 illustrates how the two-dimensional lateral diffusion of a

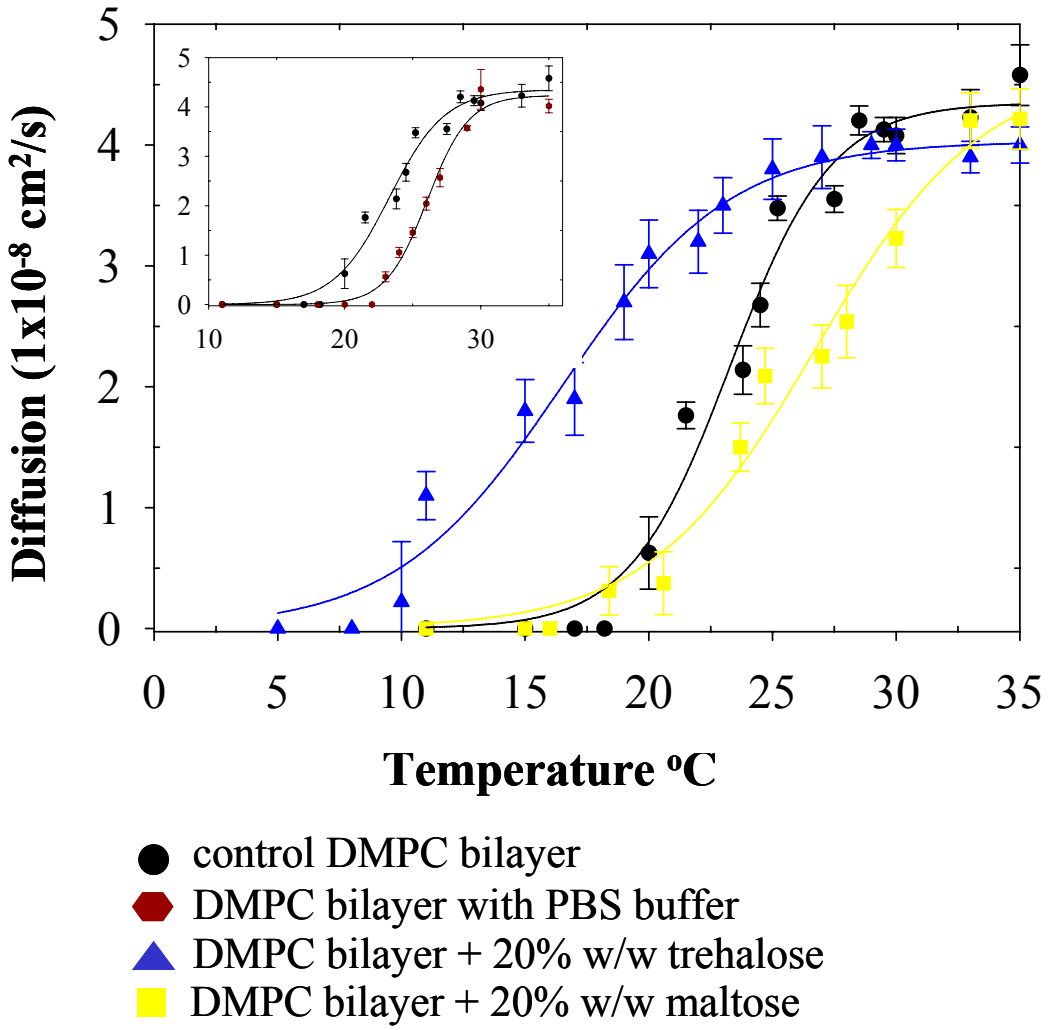

Figure 5.3. DMPC main phase transition determination by temperature controlled fluorescence recovery after photobleaching (FRAP).

DMPC bilayer supported on borosilicate is affected as it undergoes the main fluid/gel transition. Our data indicate that the T_m for the control DMPC bilayer (in the absence of salts) is 23.3 ± 0.5 ^oC. The insert illustrates the effects of salts in the main phase transition temperature for DMPC. We observed an increase in T_m to 26.1 ^oC in the presence of PBS buffer (10 mM sodium phosphate, 150 mM NaCl at pH 7.40). The effect of salts on the main transition temperature has been observed.[208] However, when 20% w/w of trehalose dissolved in deionized water is added, we noticed a shift and broadening of the main phase transition. In this case, the suppression of the fluid-to-gel transition is accompanied by a shift in the T_m to a lower temperature of 16.5 ± 0.5 ^oC. We also observed that for the case of 20% w/w maltose, dissolved in deionized water, the converse effect. The main phase transition was shifted to a slightly higher temperature T_m of 26.7 ± 0.8 ^oC. This indicates differences in the interaction of the two sugars with the underlying lipid membrane.[193]

We also observed an effect on the lipid film morphology as the temperature was lowered below the phase transition temperature. Cracking and corrugations of the control DMPC lipid films were observed to occur at ~ 18 ^oC. Fluorescence micrographs acquired under 10X magnification are depicted in figure 5.4 for all three cases. At 27 ^oC, above the main phase transition, the lipid bilayer films appear to be uniform. When the temperature is lowered passed the T_m for DMPC (23.7 ^oC), features that appear like cracks and larger corrugations are present in the control lipid film as well as in the 20% w/w maltose bilayers. Although the pre-transition seems to be suppressed in supported

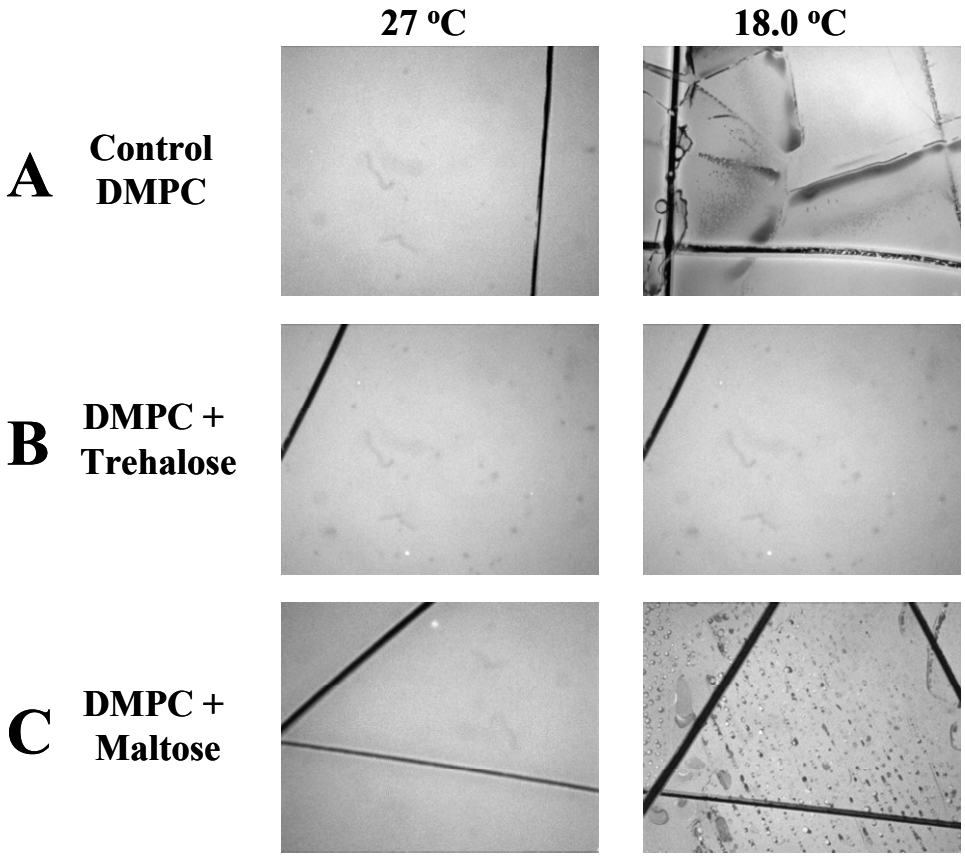

Figure 5.4. Observation of cracking and corrugations within DMPC solid supported lipid bilayers below the main phase transition. (A) control DMPC membrane, (B) 20% w/w trehalose treated bilayer and (C) 20% w/w maltose treated bilayer. Scratches were intentionally made with metal tweezers for focusing purposes.

lipid bilayers, this phenomena seems to coincide with a metastable ripple phase formation. Ripple phases have been rarely observed in a single supported lipid bilayer. When they are observed, they appear as nanometer size periodic corrugations, as studied by AFM and EM. Some models suggest that ripple phases are formed by periodic spontaneous curvature in the lipid bilayer. It has been suggested that this originates from an electrostatic coupling of water molecules with the polar lipid headgroups.[209] Another hypothesis suggests that the ripples form in order to relieve packing frustration within the gel state, because of the close packing of headgroups and acyl chains exceed some osmotic threshold.[210, 211]

Our results with trehalose show that these cracking or corrugations are suppressed within bilayers exposed to 20% w/w solutions of this sugar. This result, in addition to the broadening and shifting of the main phase transition temperature of DMPC supported bilayers may suggest that trehalose is changing the local H-bonding environment of the lipid head groups, by perhaps hydrogen bonding to the phosphoryl group and to some extent the carbonyl groups of the fatty acid chains.[212] This has been shown by FTIR[188] and computational modeling[213-215]. Furthermore, the close interaction of trehalose with the polar headgroups in turn will replace water molecules at the lipid/aqueous interface.[216] This interaction increases the headgroup spacing and thus minimizes the van der waals interactions of the acyl chains, which is evident by the shift of the T_m to a lower temperature. A change in the local water environment at the lipid headgroup will induce changes in the packing density of the polar heads and acyl chains,

thus minimizing or eliminating the packing frustration experienced by the lipid membrane in the gel state.

In the case of maltose, cracking and buckling of the lipid film was observed. These results hint at that the intercalation of maltose within the lipid headgroups has to be less than that of trehalose, since maltose appears not to be reducing the lipid packing in the gel phase, as demonstrated in our T_m measurements

Phase Segregation in DMPC Monolayers. We studied the main phase transition of DMPC monolayers using a Langmuir trough on an inverted fluorescence microscope, as depicted in figure 5.2b. We aimed to study the phase segregation that occurs below the liquid-to-gel transition and determine if trehalose and maltose maintain or suppresses phase segregation. A good lipoprotectant should avoid lipid mixing and maintains phase segregation, since it is important for biomembrane structure and function.

Fluorescence micrographs using 10X magnification were acquired for DMPC monolayers spread at 27 ^{o}C on a water subphase (control monolayer), or either on a 2% w/w trehalose or 2% w/w maltose aqueous solution. Images were taken as a function of temperature while the monolayer was cooled to ~10 ^{o}C. Figure 5.5 illustrates the progression of the DMPC monolayer as it transitions through the liquid-to-gel phase. At 27 ^{o}C, in the liquid phase, all the monolayers appear to be uniform. At 23 ^{o}C the control DMPC monolayer begins to exhibit phase segregation in the form of small domains, while the 2% trehalose and 2% maltose monolayers appear to remain uniform. As the temperature is lowered, the control monolayer exhibits an increasing phase segregation

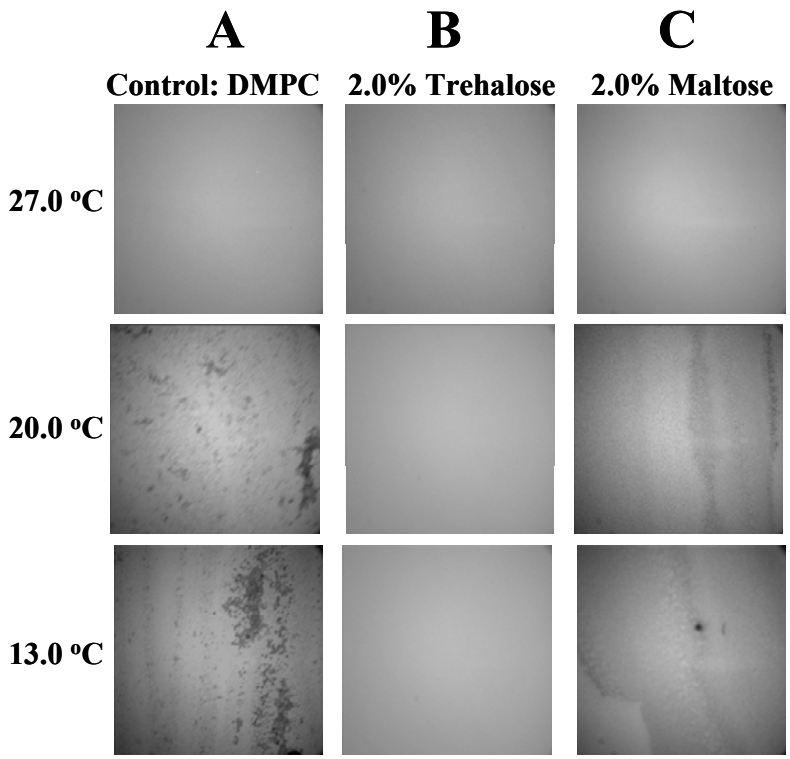

Figure 5.5. Phase segregation in DMPC monolayers as the main phase transition is crossed. (A) control DMPC monolayer, (B) DMPC monolayer with 2% w/w trehalose subphase. Trehalose maintains phase segregation and avoids lipid mixing. (C) DMPC monolayer with 2% w/w maltose subphase. All DMPC monolayers contain 0.05 mole% Texas Red DHPE as a fluorescent probe.

while the 2% trehalose monolayer remains uniform and the 2% maltose monolayer begins to show small 'domain-like' features. At 13 ^{o}C, well into the gel phase, the control monolayer shows a high surface coverage of domains. The 2% maltose monolayer also exhibits a high surface density of domains, however, qualitatively they appear to be much smaller than those found in the control monolayer. Interestingly, the 2% trehalose monolayer shows no domains and is uniform even well into the gel state.

This illustrates and supports the observations the trehalose maintains phase segregation and avoids lipid mixing.[217] The intercalation of trehalose within the lipid headgroups may consequently lower the van der waals interactions among acyl chains, which could make it harder for lipids to reorganize or phase separate.

Vibrational Sum Frequency Spectroscopy. To further test our previous observations we have investigated the interfacial alignment of both sugar molecules by VSFS. In the first set of experiments, we tested the interaction of trehalose and maltose at the air/water interface using solutions of 2% and 20% w/w of each compound. The SF spectrum is shown in figure 5.6. Interestingly, trehalose (at 2% and 20%) shows a high tendency towards the air/water interface as indicated by the alignment of (-CH) moieties present our SF spectra at ~2875 and 2940 cm^{-1}. However, in the case of maltose, no such spectral features are present for both 2% and 20% w/w sugar solution. To rule out contamination from our sample, we also tested for glucose, ethylene glycol and other possible trace contamination and found no such spectral features. Indeed, the

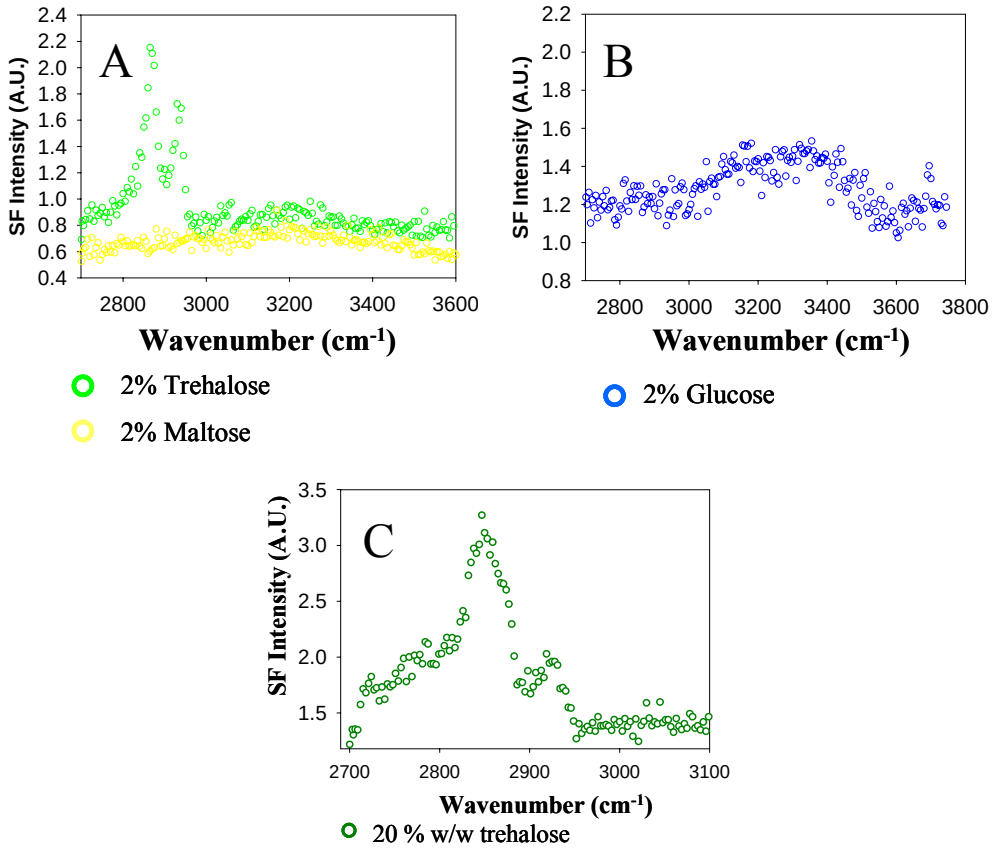

Figure 5.6. The SF spectra of trehalose, maltose and glucose. Shown in (A) is the SF spectra of 2% w/w solutions of trehalose and maltose. (B) is the spectra of glucose. The bottom panel shows the spectra for a 20% w/w solution of trehalose (C). The SF spectra indicate that trehalose preferentially partitions towards the air/water interface.

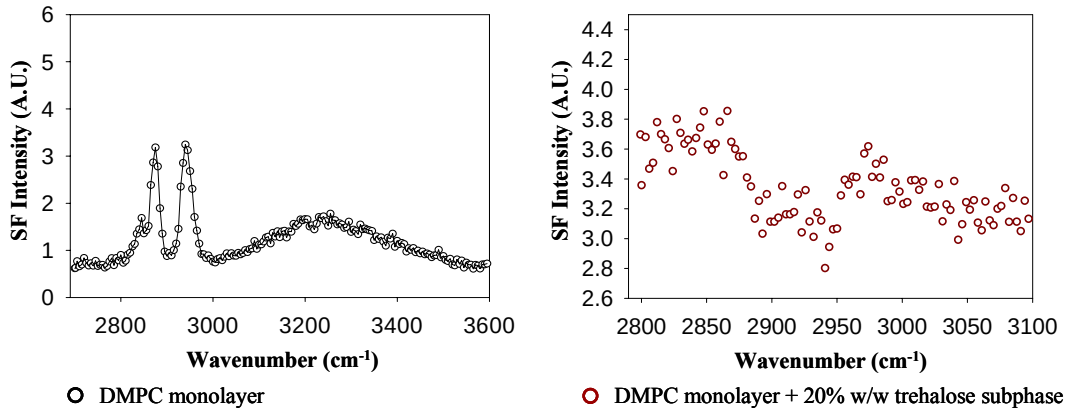

Figure 5.7. The SF spectra of the interaction of trehalose with a DMPC monolayer. Shown on the left is the SF spectra of a DMPC monolayer on a water subphase. The right hand spectra is of a DMPC monolayer with 20% w/w trehalose subphase.

chemical assignment of these peaks and identification of the specific moieties from the sugar giving rise to the spectral features is not a trivial task.

Another key observation that hints at the preferential partitioning of trehalose towards the air/water interface and its interaction with the hydrophobic medium is its depression of the water surface tension as measured by a Wilhelmy balance (data not shown). This effect was not observed for other sugars that were tested.

To further probe the interfacial behavior of trehalose, we acquired SFG spectra of this sugar at the DMPC monolayer/aqueous interface to test if trehalose will preferentially partition towards the air/water interface in the presence of a lipid monolayer or remain in the bulk. To this end we employed deuterated DMPC lipids since the (-C^2H or -CD) mode is shifted towards a lower frequency and there are no spectral features in the range of 2800 – 3100 cm^{-1}. The SFG spectra are shown in figure 5.7. We first acquired a spectrum of hydrogenated DMPC monolayer in a water subphase. There are two major spectral features. A peak at 2875 cm^{-1} and 2940 cm^{-1}, are indicative of the CH_3 moiety of the lipid molecules. A broad peak at 3200 cm^{-1} is due to interfacial water molecular alignment.

The right hand spectra of figure 5.7 is of the deuterated DMPC monolayer with a 20% w/w trehalose subphase. Shown is the region of 2800 – 3100 cm^{-1}, in which the bare deuterated monolayer does not yield any spectral features as explained above. However, in the presence of trehalose, we observe (-CH) moieties at ~2950 cm^{-1} that originate from the sugar molecules. This indicates that in the presence of a lipid monolayer, a fraction of the trehalose molecules try to partition closer the air interface.

The lower signal-to-noise in this spectrum is due to a lower density (or number) of molecules that are aligned at the interface compared to the bulk. The SFG intensity depends on the number of interfacial aligned moieties (β), to the polarization employed in the measurement.

Cryoprotection of Supported Lipid Bilayers. POPC bilayers have been employed to test the cryopreservation properties of both sugars. In these experiments bilayers were exposed to either 20% w/w or 2% w/w solutions of both sugars. We also aimed to test the following hypothesis: the freezing of interfacial water at -80 ^{o}C will also cause substantial membrane damage; thus if trehalose is replacing interfacial water molecules it will provide the best protection under these conditions. In order to help answer this question, we also employed PEG-containing lipopolymer bilayers.[73] The PEG moiety is known to bind ~3 water molecules per monomer repeat unit.[218] Therefore, by using PEG-lipopolymers of various sizes, we aim to increase the localization of water molecules at the lipid headgroups. The preparation of PEG-lipopolymer bilayers was previously demonstrated.[73] We have used three different PEG-lipopolymers, PEG^{350}, PEG^{550}, and PEG^{2000} at mole percents equal to 11%, 7% and 1.5% respectively, which is at the onset of the mushroom-to-brush transition.[118] Diffusion measurements were taken before freezing. After which the samples were frozen at -80 ^{o}C for 24 hours. The samples were then thawed and imaged at 10X magnification and diffusion measurements were acquired.

The results are summarized in figure 5.8. For simplicity, we have divided the figure into three main groups, trehalose and maltose treated, and PEGylated bilayers.

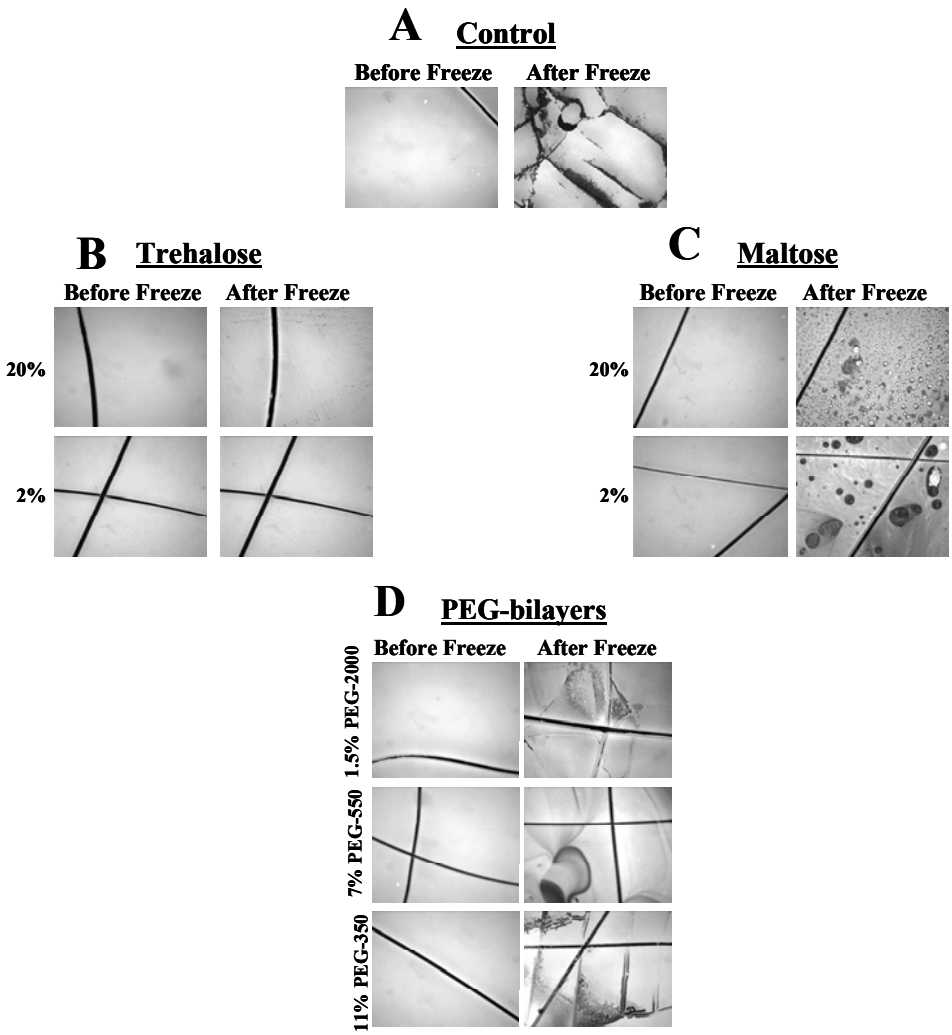

Figure 5.8. The cryoprotection of supported POPC membranes. (A) control POPC membrane, (B) trehalose treated, (C) maltose treated and (D) PEG-lipopolymer membranes. Scratches were intentionally made with a tweezers for focusing purposes and background correction.

The control POPC bilayer exhibits extensive damage due to cracking and buckling of the two dimensional film. However, it should be noted in areas where we acquired diffusion data, the diffusion constant was similar within experimental error, to the before freezing case ($4.0\pm0.2 \times 10^{-8} cm^2/s$). The 20% w/w trehalose treated bilayer exhibited no damage followed by the 2% w/w trehalose bilayer which showed very minimal damage. The diffusion constants of these bilayers after freezing were similar to the initial diffusion. Both maltose treated bilayers (20% and 2% w/w) exhibited substantial cracking and buckling, but their diffusion constants were similar to the control bilayers. The PEG-bilayers were interesting because they also exhibited damage during freezing. Although their diffusion constants were similar to the control diffusion within experimental error, the PEG-lipopolymer was unable to afford protection to the membrane. This may suggests that the increase localization of water at the lipid headgroup causes damage upon freezing, thus hinting at that in order to achieve cryoprotection of the lipid membrane, water replacement may be an important issue.

5.5. Summary and Conclusions

We propose that the effective cryopreservation of trehalose, as a lipopreservative, can be explained in that trehalose is able to further partition deeper into the lipid headgroups. There is an important difference between trehalose and maltose which rests within their respective chemical structure. In the maltose molecule, the two glucose rings are linked via a C1α-C4α linkage, which a typical glycosilic linkage for most disaccharides. However, in the trehalose molecule, the glucose rings are linked via a

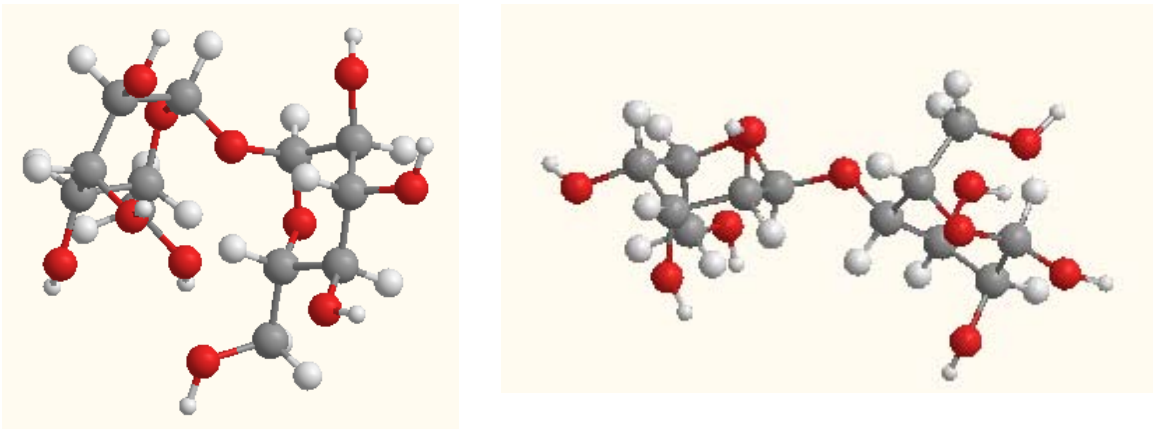

Trehalose **Maltose**

Figure 5.9. The 3D structure of trehalose and maltose.

C1α-C1α bond. This linkage yields a more 'clam shell' or bi-dentate type structure. By comparison, maltose exhibits a more open structure. This has been shown by X-ray diffraction. The structure of each sugar is illustrated in figure 5.9. Our SFG data suggest that it may be this difference in the structure of trehalose compared to maltose which allows it to preferentially partition closer towards the hydrophobic medium. Furthermore, SFG of selectively deuterated trehalose may provide a better means by which to identify the SF peaks present in the trehalose spectra.

We hypothesize that it is due to this unique structure of trehalose that allows for this sugar to penetrate further into the lipid headgroup space compared to maltose and possibly other sugars. This offers an explanation of other studies that have shown that trehalose alters the H-bonding environment of the phosphoryl group. To achieve this, intercalation of the sugar in between the polar heads replaces water molecules. This in turn changes the packing environment of the lipid molecules in the gel phase by lowering the van der waals interactions among acyl chains, resulting in a lowering of packing frustration and improving the film stability. Consequently, such an environment makes it difficult for lipid mixing and phase segregation is maintained as evidenced by our data.

Furthermore, the comparison of trehalose to its analog, maltose, can shed more light into the effectiveness of other sugars. Differences in the stabilization of proteins[219, 220] have been observed for these sugars in which the presence of trehalose prevented amyloid formation while maltose had little effect on protein stability.[221]

Finally, we have demonstrated the utility of supported lipid bilayers as a model system in which to study the mechanism of cryopreservation and anhydrobiosis under physiological conditions.[222]

CHAPTER VI

CONCLUSIONS

The conclusions of this study further support the proposition solid supported phospholipid membranes are useful cell biomembrane mimics. In combination with microfluidic technology, this lab-on-a-chip platform is a powerful system to study biochemical processes such as ligand-receptor binding, model pathogen attach, inflammatory response, model lipid rafts, micro domain, and other membrane biophysical phenomena.

Nature's general solution for generating both high sensitivity and specificity at the membrane surface has been to employ multivalency. Lateral diffusion of the recognition components allows more sensitive detection. Indeed, the organism's immune system can detect the presence of foreign elements at much lower concentrations than possible with monovalent binding and therefore induce a faster immunoresponse. Indeed, multivalent binding can be especially critical for viruses like influenza for which each individual interaction is quite weak and by employing a multivalent approach, only a few interactions are required to trigger infection. A cartoon representation of a generic virus binding via multivalent interaction is shown in figure 6.1.

Supported membranes within lab-on-a-chip type devices could be used for monitoring multiple toxins in parallel by having each species bind to its own surface-

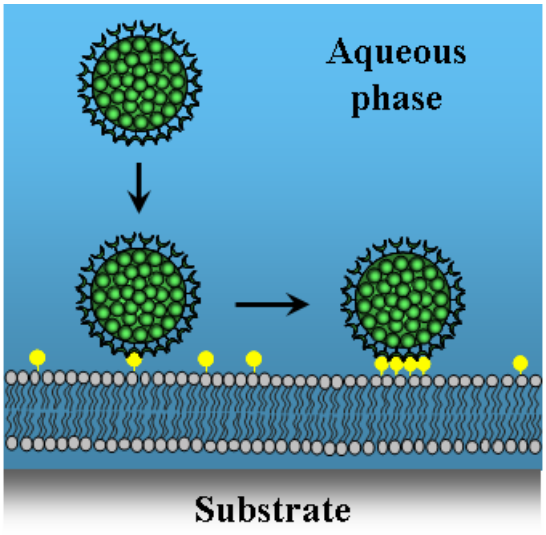

Figure 6.1. An illustration of a generic virus (in green) binding initially to one membrane-associated ligand (in yellow) on a solid-supported lipid bilayer, followed by the lateral rearrangement of other ligands and their subsequent binding to receptors on the particle surface.

associated ligand or combination of ligands. Since it is easy to create spatially addressed arrays of lipid bilayers on a single chip, one could even create platforms for screening applications in a clinical setting. There are, however, several requirements for early-warning detection devices to function in real world environments. First, the device must be robust enough to survive rough transport and storage conditions, that is, the lipid bilayer film must resist mechanical and thermal stresses associated with transit to point of use, as well as possible prolonged storage before implementation. Second, to protect them in both shipping and storage, they should be able to withstand current preservation techniques, such as dehydration or freezing. Once at the point of use, they must recover full function upon rehydration or, ideally, be permanently air stable. Third, they should be exceedingly resistant to contamination outside the laboratory setting to avert environmental fouling or bacterial growth during long term monitoring. Finally, the devices must be highly sensitive and specific to the intended analytes.

A notable drawback to the solid supported lipid bilayer system has been their inherent lack of stability in air as shown in figure 6.2a and 6.2b and discussed in Chapter I. This limits their applicability as 'real world' sensing devices to the laboratory environment. An initial strategy to coat the membrane with a streptavidin layer yielded an air-stable bilayer platform, as illustrated in figure 6.2c, but was incapable of subsequent interactions as a sensing device.

My contribution towards enhancing the stability of phospholipid membranes in air is achieved by employing poly(ethylene glycol) PEG incorporated lipopolymer membranes. Shown in figure 6.2d, this strategy was inspired by mimicking the similar

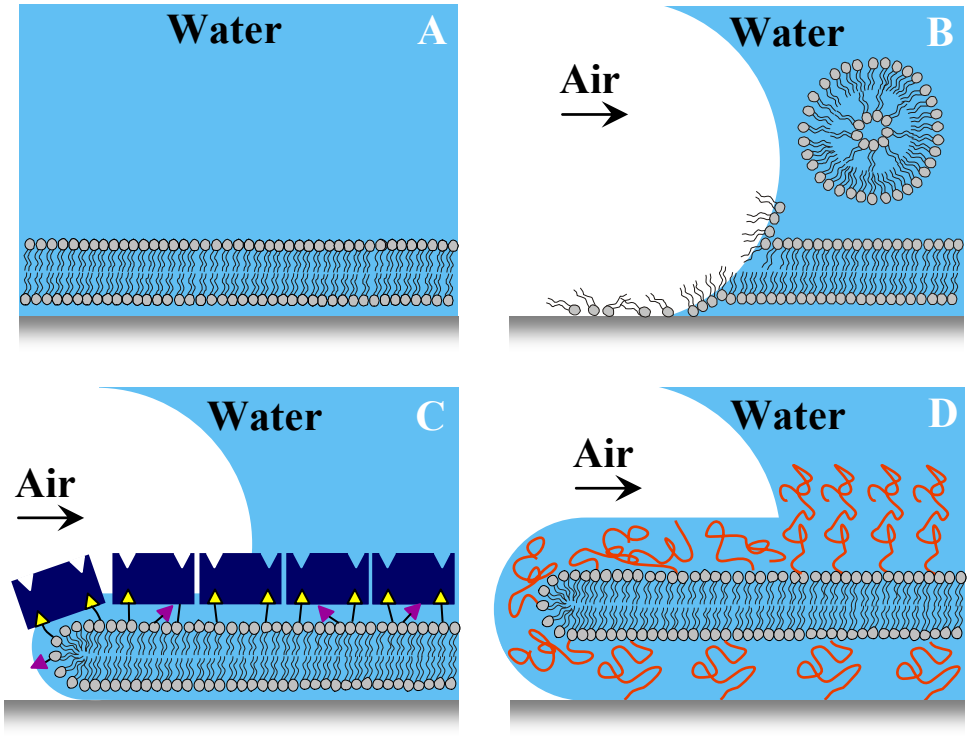

Figure 6.2. A bilayer formed on a solid substrate submerged in an aqueous environment (A). A thin water layer beneath the bottom leaflet and the substrate preserves the lipid mobility. (B) The introduction of an air interface destroys the solid supported bilayer by peeling it away from the surface in vesicle sections. Some lipids may also form patches of monolayers at the air surface. (C) Protein coatings, such as Streptavidin (dark blue rectangles) bound to biotinylated lipids (yellow triangles), help to reduce delamination, but also cover other ligands (purple triangles) so that they are unavailable for binding with the target antigens. (D) PEGylated lipids protect the bilayer from delamination and provide more space between the bottom leaflet and the support.

polymeric architectures found in real cells. By choosing the size of PEG and controlling the polymer density and thereby the conformation of the lipopolymer, the property of air-stability may be conferred. This phenomena precisely occurs at the onset of the mushroom-to-brush transition, where the surface density of polymer is high. From this point onward, complete protection is afforded to the lipopolymer incorporated supported membrane. The lipopolymer functions by trapping interfacial water and stiffening the underlying membrane as shown in figure 6.3.

This work opens up a variety of opportunities for supported membranes as biosensing devices that are more robust and can even function in air. The incorporation of PEG lipopolymers further mimics the biomembrane by acting as a cell surface glycocalyx. The cell glycocalyx, as discussed in Chapters III and IV, is composed of glycosylated proteins, glycolipids, and transmembrane proteoglycans, which can be viewed as polymeric structures that extend tens of nanometers above the plasma membrane. The PEG layer, acting as a glycocalyx mimic, can be used to filter or size discriminate among incoming protein analytes as described in Chapter IV. This strategy, employed with microfluidic technology, can be used to perform multiple tasks 'on chip', thus making it possible to analyze complex mixtures of analytes. For example, be titrating the PEG size, surface density and conformation, would prove useful in the area of proteomics, whereby crude cell extracts can be sorted 'on chip' and for clinical diagnostics of whole blood serum, as depicted in a cartoon representation shown in figure 6.3. The method has proven handy in discriminating between two protein

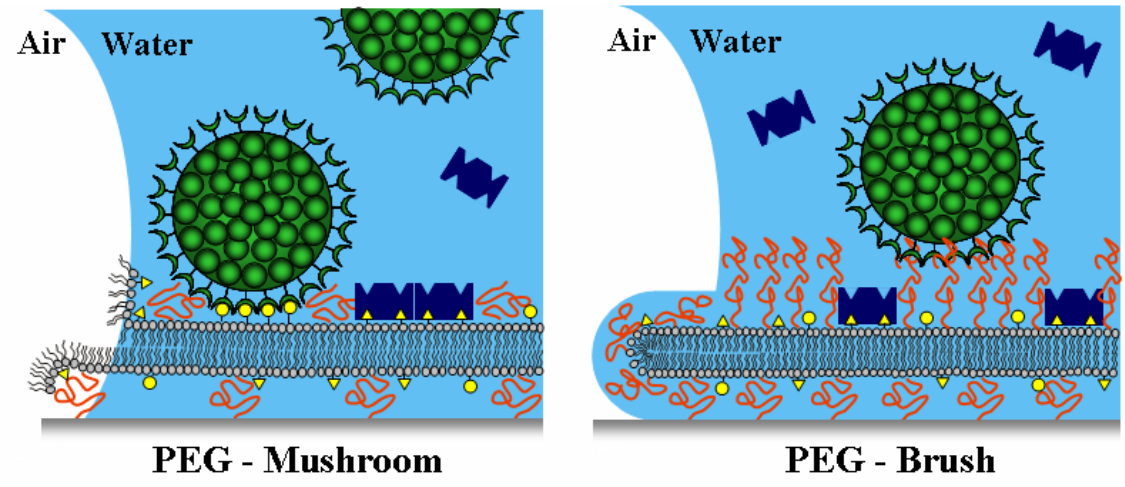

Figure 6.3. Left: PEG at low surface densities (red) assumes a mushroom configuration that does not protect from delamination upon air exposure, prevent large particles (in green) from fouling the surface, or prohibit aggregation of bound moieties (in dark blue). Right: PEG at higher surface densities assumes a brush configuration that protects well from air exposure and acts as a filter for larger particles (green) so that they do not interrupt the sensing of smaller target analyte (dark blue rectangles), which are still able to pass through the meshwork of the lipopolymers and bind to the membrane surface.

analytes (streptavidin and antibiotin IgG) that exhibit similar affinity towards the same surface bound receptor. Furthermore, the PEG layer can also act as a cytoskeleton network, further separating the artificial membrane from the underlying support, which may aid in the incorporation of transmembrane proteins and increase the range of substrates that can be used to form supported membranes.

Supported phospholipid bilayers can be used as models for the chemistry of biopreservation. As discussed in Chapter V, SLBs were employed to elucidate the molecular mechanism of the interaction of trehalose, a known lipopreservative, with the phospholipid membrane. The interactions of sugar molecules with the biomembrane has been proposed to be a key factor in the preservation of biological organisms during a stress event, such as anhydrobiosis (desiccation) or cryobiotic conditions. These events have been studied by *in vivo* and *in vitro* experimentation, but only until recently, solid supported lipid bilayers were used as a stage specific system in which to model these environmental conditions.

I accomplished the goal of proposing a mechanism to explain the natural preference towards trehalose as the best lipopreservative compared to other disaccharides. Particularly, the study focused on comparing the activity of trehalose and its analog, maltose. Differences in their interactions with phosphatidylcholine membranes were found. For example, trehalose seems to depress the liquid-to-gel or main phase transition of a supported DMPC bilayer, while maltose exhibited the converse effect. Trehalose was also found to prevent damage of the underlying film

when exposed to temperatures below the main phase transition and even at lower cryogenic temperatures, whereas maltose was unable to afford protection.

A key breakthrough was achieved by VSFS, where the interactions of both sugars at the air/water and lipid monolayer/aqueous interface were studied. A slight difference in the chemical structure of both sugars became increasingly important. Specifically, the difference lies in the glycosilic bond. In maltose, the two glucose rings are bound by a C1α-C4α linkage. Interestingly, trehalose presents a C1α-C1α glycosilic bond. This bond confers a more compact or bi-dentate structure to the sugar molecule in which the two rings are closer together than in the case of maltose. The model presented in this study suggests that it is this difference in the structure of trehalose compared to other common disaccharides, that allows this sugar to penetrate further into the lipid membrane. This local interaction within the headgroup space causes changes in the H-bonding environment and leads to changes in the van der Waals interactions of the aliphatic tails. Therefore the interaction of trehalose can induce an effect on physical properties such as phase transition temperature of the lipid bilayer, film stability at lower temperatures than the main phase transition temperature, and maintain lipid phase segregation. These affects are what we propose is the reason why trehalose is naturally preferred as a lipopreservative among other disaccharides.

REFERENCES

(1) Sackmann, E.; Tanaka, M. *TIBTECH* **2000**, *18*, 58-64.

(2) Bayley, H. *Curr. Opin. Biotech.* **1999**, *10*, 94-103.

(3) Bayley, H.; Braha, O.; Gu, L. Q. *Adv. Mater.* **2000**, *12*, 139-142.

(4) Cremer, P. S. *Nature* **2004**, *22*, 172-173.

(5) Danielli, J. F. In *Cell Membranes: Biochemistry, Cell Biology and Pathology*; Weissmann, G., Clairborne, R., Eds.; New York Hospital Practice: New York, 1975, pp 3-11.

(6) Tanford, C. *Ben Franklin, Stilled the waves: An Informal History of Pouring Oil on Water with Reflections on the Ups and Downs of Scientific Life in General*; Duke University Press: Durham, NC, 1989.

(7) Langmuir, I. *J. Am. Chem. Soc.* **1917**, *39*, 1848-1906.

(8) Gorter, E.; Grendel, F. *J. Exp. Med.* **1925**, *41*, 439-443.

(9) Danielli, J. F.; Davson, H. *J. Cell. Comp. Physiol.* **1935**, *5*, 495-508.

(10) Hendler, R. W. *Physiol. Rev.* **1971**, *51*, 66-97.

(11) Singer, S. J.; Nicolson, G. L. *Science* **1972**, *175*, 720-731.

(12) Voet, D.; Voet, J. G. *Biochemistry*, 2 ed.; John Wiley & Sons: New York, 1995.

(13) Marsh, D. *Handbook of Lipid Bilayers*; CRC Press: Boca Raton, FL, 1990.

(14) Mammen, M.; Choi, S.-K.; Whitesides, G. M. *Angew. Chem. Int. Ed.* **1998**, *37*, 2754-2794.

(15) Leito, A. M.; Cush, R. C.; Thompson, N. L. *Biophys. J.* **2003**, *85*, 3294-3302.

(16) Wetzer, B.; Pum, D.; Sleytr, U. B. *J. Struct. Biol.* **1997**, *119*, 123-128.

(17) Xu, L.; Frederick, P.; Pirollo, K. F.; Tang, W. H.; Rait, A.; Xiang, L. M.; Huang, W. Q.; Cruz, I.; Yin, Y. Z.; Chang, E. H. *Hum. Gene. Ther.* **2002**, *13*, 469-481.

(18) Muller, P.; Rudin, D. O.; Tien, H. T.; Wescott, W. C. *Nature* **1962**, *194*, 979-980.

(19) Muller, P.; Rudin, D. O.; Tien, H. T.; Wescott, W. C. *J. Phys. Chem.* **1963**, *67*, 534-535.

(20) Muller, D. J.; Engel, A.; Amrein, M. *Biosens. Bioelectron.* **1997**, *12*, 867-877.

(21) McConnell, H. M.; Watts, T. H.; Weis, R. M.; Brian, A. A. *Biochim. Biophys. Acta* **1986**, *864*, 95-106.

(22) Sackmann, E. *Science* **1996**, *271*, 43-48.

(23) McConnell, H. M.; Owicki, J. C.; Parce, J. W.; Miller, D. L.; Baxter, G. T.; Wada, H. G.; Pitchford, S. *Science* **1992**, *257*, 1906-1912.

(24) Groves, J. T.; Boxer, S. G.; McConnell, H. M. *Proc. Natl. Acad. Sci. USA* **1997**, *94*, 13390-13395.

(25) Tamm, L. K. *Biochemistry* **1988**, *27*, 1450-1457.

(26) Tamm, L. K.; Bartoldus, I. *Biochemistry* **1988**, *27*, 7453-7458.

(27) Kalb, E., Engel, J., Tamm, L.K. *Biochemistry* **1990**, *29*, 1607-1613.

(28) Yang, T.; Baryshnikova, O. K.; Mao, H.; Holden, M. A.; Cremer, P. S. *J. Am. Chem. Soc.* **2003**, *125*, 4779-4784.

(29) Cremer, P. S.; Boxer, S. G. *J. Phys. Chem. B* **1999**, *103*, 2554-2559.

(30) Cremer, P. S.; Groves, J. T.; Ulman, N.; Boxer, S. G. *Biophys. J.* **1998**, *74*, A311-A311.

(31) Graneli, A.; Rydstrom, J.; Kasemo, B.; Hook, F. *Langmuir* **2003**, *19*, 842-850.

(32) Groves, J. T.; Ulman, N.; Boxer, S. G. *Science* **1997**, *275*, 651-653.

(33) Groves, J. T.; Ulman, N.; Boxer, S. G. *Science* **1997**, *275*, 651.

(34) Kam, L.; Boxer, S. G. *J. Am. Chem. Soc.* **2000**, *122*, 12901-12902.

(35) Plant, A. L. *Langmuir* **1999**, *15*, 5128-5135.

(36) Kalb, E.; Frey, S.; Tamm, L. K. *Biochim. Biophys. Acta* **1992**, *1103*, 307-316.

(37) Conboy, J. C.; Liu, S.; O'Brien, D. F.; Saavedra, S. S. *Biomacromolecules* **2003**, *4*, 841-849.

(38) Plant, A. L. *Langmuir* **1999**, *15*, 5128-5135.

(39) Wagner, M. L.; Tamm, L. K. *Biophys. J.* **2000**, *79*, 1400-1414.

(40) Tamm, L. K.; McConnell, H. M. *Biophys. J.* **1985**, *47*, 105-113.

(41) Hamai, C.; Yang, T.; Kataoka, S.; Cremer, P. S.; Musser, S. M. *Biophys. J.* **2006**, *90*, 1241-1248.

(42) Barenholtz, Y.; Litman, B. J.; Goll, J.; Thompson, T. E.; Carlson, F. D. *Biochemistry* **1977**, *16*, 2806-2810.

(43) Harrigan, P. R.; Madden, T. D.; Cullis, P. R. *Chem. Phys. Lipids.* **1990**, *52*, 139-149.

(44) Sackmann, E. *FEBS Lett.* **1994**, *346*, 3-16.

(45) Cremer, P. S.; Yang, T. L. *J. Am. Chem. Soc.* **1999**, *121*, 8130-8131.

(46) Groves, J. T.; Ulman, N.; Cremer, P. S.; Boxer, S. G. *Langmuir* **1998**, *14*, 3347-3350.

(47) Seantier, B.; Breffa, C.; Felix, O.; Decher, G. *Nanoletters* **2004**, *4*, 5-10.

(48) Hook, F.; Rodahl, M.; Fredriksson, C.; Brzezinski, P.; Keller, C. A.; Voinova, M.; Krozer, A.; Kasemo, B. *Faraday Discuss* **1997**, *107*, 229-246.

(49) Keller, C. A.; Kasemo, B. *Biophys. J.* **1998**, *75*, 1397-1402.

(50) Richter, R. P.; maury, N.; Brisson, A. R. *Langmuir* **2005**, *21*, 299-304.

(51) Leibau, M.; Hildebrand, A.; Neubert, R. H. H. *Eur. Biophys. J.* **2001**, *30*, 42-52.

(52) Keller, C. A.; Glasmastar, K.; Zhdanov, V. P.; Kasemo, B. *Phys. Rev. Lett.* **2000**, *23*, 5443-5446.

(53) Reimhult, E.; Hook, F.; Kasemo, B. *Langmuir* **2003**, *19*, 1681-1691.

(54) Glasmastar, K.; Larsson, C.; Hook, F.; Kasemo, B. *J. Colloid Interface Sci.* **2002**, *246*, 40-47.

(55) Efremov, A.; Mauro, J. C.; Raghavan, S. *Langmuir* **2004**, *20*, 5724-5731.

(56) Larsson, C.; Rodahl, M.; Hook, F. *Anal. Chem.* **2003**, *75*, 5080-5087.

(57) Rossi, C.; Homand, J.; Bauche, C.; Hamdi, H.; Ladant, D.; Chopineau, J. *Biochemistry* **2003**, *42*, 15273-15283.

(58) Lopez, A.; Dupou, L.; Altibelli, A.; Trotard, J.; Tocanne, J. F. *Biophys. J.* **1988**, *53*, 963-970.

(59) Kim, J.; Cremer, P. S. *J. Am. Chem. Soc.* **2000**, *122*, 12371-12372.

(60) Garcia-Manyes, S.; Oncins, G.; Sanz, F. *Biophys. J.* **2005**, *89*, 1812-1826.

(61) Cremer, P. S.; Groves, J. T.; Kung, L. A.; Boxer, S. G. *Langmuir* **1999**, *15*, 3893-3896.

(62) Kim, J.; Kim, G.; Cremer, P. S. *J. Am. Chem. Soc.* **2002**, *124*, 8751-8756.

(63) Holden, M. A.; Jung, S.-Y.; Yang, T.; Castellana, E. T.; Cremer, P. S. *J. Am. Chem. Soc.* **2004**, *126*, 6512-6513.

(64) Petralli-Mallow, T.; Brigmann, K. A.; Richter, L. J.; Stephenson, J. C.; Plant, A. L. *SPIE* **1999**, *3858*, 25-31.

(65) Ross, E.; Rozanski, L.; Spratt, T.; Liu, S.; O'Brien, D. F.; Saavedra, S. S. *Langmuir* **2003**, *19*, 1752-1765.

(66) Ross, E.; Bondurant, B.; Spratt, T.; Conboy, J. C.; O'Brien, D. F.; Saavedra, S. S. *Langmuir* **2001**, *17*, 2305-2307.

(67) Plant, A. l.; Brighamburke, M.; petrella, E. C.; Oshannessy, D. J. *Anal. Biochem.* **1995**, *226*, 342-348.

(68) Morigaki, K.; Baumgart, T.; Jonas, U.; Offenhäusser, A.; Knoll, W. *Langmuir* **2002**, *18*, 4082-4089.

(69) Morigaki, K.; Baumgart, T.; Offenhäusser, A.; Knoll, W. *Angew. Chem. Int. Ed.* **2001**, *40*, 172-174.

(70) Morigaki, K.; Kiyosue, K.; Taguchi, T. *Langmuir* **2004**, *20*, 7729-7735.

(71) Morigaki, K.; Schonherr, H.; Frank, C. W.; Knoll, W. *Langmuir* **2003**, *19*, 6994-7002.

(72) Phillips, S. K.; Dong, Y.; Carter, D.; Cheng, Q. *Anal. Chem.* **2005**, *77*, 2960-2965.

(73) Albertorio, F.; Diaz, A. J.; Yang, T.; Chapa, V. A.; Kataoka, S.; Castellana, E. T.; Cremer, P. S. *Langmuir* **2005**, *21*, 7476-7482.

(74) Schneider, M. F.; Lim, K.; Fullor, G. G.; Tanaka, M. *Phys. Chem. Chem. Phys.* **2002**, *4*, 1949-1952.

(75) Hooper, N. M. *Curr. Biol.* **1998**, *8*, R114-R116.

(76) Holden, M. A.; Kumar, S.; Castellana, E. T.; Beskok, A.; Cremer, P. S. *Sensors and Actuators B* **2003**, *92*, 199-207.

(77) Yang, T. L.; Jung, S. Y.; Mao, H. B.; Cremer, P. S. *Anal. Chem.* **2001**, *73*, 165-169.

(78) Axelrod, D.; Koppel, D. E.; Schlessinger, J.; Elson, E.; Webb, W. W. *Biophys. J.* **1976**, *16*, 1055-1069.

(79) Chen, S. C.; Sturtevant, J. M.; Gaffney, B. J. *Proc. Natl. Acad. Sci.* **1980**, *77*, 5060-5065.

(80) Gurau, M. C.; Castellana, E. T.; Albertorio, F.; Kataoka, S.; Lim, S.-M.; Yang, R. D.; Cremer, P. S. *J. Am. Chem. Soc.* **2003**, *125*, 11166-11167.

(81) Binnig, G.; Quate, C. F.; Gerber, C. *Phys. Rev. Lett.* **1986**, *56*, 930-933.

(82) Bowden, N.; Brittain, S.; Evans, A. G.; Hutchinson, J. W.; Whitesides, G. M. *Nature* **1998**, *393*, 146-149.

(83) Groves, J. T.; Boxer, S. G. *Acc. Chem. Res.* **2002**, *35*, 149-157.

(84) Groves, J. T.; Mahal, L. K.; Bertozzi, C. R. *Langmuir* **2001**, *17*, 5129-5133.

(85) Mao, H. B.; Holden, M. A.; You, M.; Cremer, P. S. *Anal. Chem.* **2002**, *74*, 5071-5075.

(86) Holden, M. A.; Kumar, S.; Beskok, A.; Cremer, P. S. *J. Micromech. Microeng.* **2003**, *13*, 412-418.

(87) Soumpass, D. M. *Biophys. J.* **1983**, *41*, 95-97.

(88) Mao, H.; Yang, T.; Cremer, P. S. *J. Am. Chem. Soc.* **2002**, *124*, 4432-4435.

(89) Mao, H. B.; Yang, T. L.; Cremer, P. S. *Analytical Chemistry* **2002**, *74*, 379-385.

(90) Thompson, N. L.; Lagerholm, B. C. *Curr. Opin. Biotech.* **1997**, *8*, 58-64.

(91) Thompson, N. L.; Pearce, K. H.; Hsieh, H. V. *Eur. Biophys. J.* **1993**, *22*, 367-378.

(92) Gragson, D. E.; McCarty, B. M.; Richmond, G. L. *J. Am. Chem. Soc.* **1997**, *119*, 6144-6152.

(93) Shen, Y. R. *Solid State Commun.* **1998**, *108*, 399-406.

(94) Shen, Y. *The Principals of Nonlinear Optics*; John Wiley & Sons: New York, 1984.

(95) Richmond, G. L. *Chem. Rev.* **2002**, *102*, 2693-2724.

(96) Kim, J.; Cremer, P. S. *Chem. Phys. Chem.* **2001**, *8*, 543-546.

(97) Kim, J.; Kim, G.; Cremer, P. S. *Langmuir* **2001**, *17*, 7255-7260.

(98) Gurau, M. C.; Lim, S.-M.; Castellana, E. T.; Albertorio, F.; Kataoka, S.; Cremer, P. S. *J. Am. Chem. Soc.* **2004**, *126*, 10522-10523.

(99) Kataoka, S.; Gurau, M. C.; Albertorio, F.; Holden, M. A.; Lim, S.-M.; Yang, R. D.; Cremer, P. S. *Langmuir* **2004**, *20*, 1662-1666.

(100) Kim, D. T.; Blanch, H. W.; Radke, C. J. *Langmuir* **2002**, *18*, 5841-5850.

(101) Jung, S.-Y.; Lim, S.-M.; Albertorio, F.; Kim, G.; Gurau, M. C.; Yang, R. D.; Holden, M. A.; Cremer, P. S. *J. Am. Chem. Soc.* **2003**, *125*, 12782-12786.

(102) Jandt, K. D. *Mat. Sci. Eng.* **1998**, *21*, 221-295.

(103) Tokumasu, F.; Jin, A. J.; Feigenson, G. W.; Dvorak, J. A. *Ultramicroscopy* **2003**, *97*, 217-227.

(104) Choi, K. H.; Friedt, J. M.; Frederix, F.; Campitelli, A.; Borghs, G. *App. Phys. Lett.* **2002**, *81*, 1335-1337.

(105) Charrier, A.; Thibaudau, F. *Biophys. J.* **2005**, *89*, 1094-1101.

(106) McDonald, R. C.; McDonald, R. I.; Menco, B. P.; Takeshita, K.; Subbarao, N. K.; Hu, L. *Biochim. Biophys. Acta* **1991**, *1061*, 297-303.

(107) Lipowsky, R. *Colloids Surf., A.* **1997**, *128*, 255-264.

(108) Baumgart, T.; Offenhausser, A. *Biophys. J.* **2002**, *83*, 1489-1500.

(109) McConnell, H. M.; Watts, T. H.; Weis, R. M.; Brian, A. A. *Biochim. Biophys. Acta* **1986**, *864*, 95-106.

(110) Kam, L.; Boxer, S. G. *Langmuir* **2003**, *19*, 1624-1631.

(111) Thompson, N. L.; Drake, A. W.; Chen, L.; Broek, W. V. *Photochem. Photobiol.* **1997**, *65*, 39-46.

(112) Phillips, S. K.; Cheng, Q. *Anal. Chem.* **2005**, *77*, 327-334.

(113) Evans, E.; Rawicz, W. *Phys. Rev. Lett.* **1997**, *79*, 2379-2382.

(114) Needham, D.; Kim, D. H. *Colloids Surf., B.* **2000**, *18*, 183-195.

(115) Munro, J. C.; Frank, C. W. *Langmuir* **2004**, *20*, 3339-3349.

(116) Munro, J. C.; Frank, C. W. *Langmuir* **2004**, *20*, 10567-10575.

(117) De Gennes, P. G. *Scaling Concepts in Polymer Physics*; Cornell Univ. Press: Ithaca, NY, 1979.

(118) Marsh, D.; Bartucci, R.; Sportelli, L. *Biochim. Biophys. Acta* **2003**, *1615*, 33-59.

(119) Zdyrko, B.; Varshney, S. K.; Luzinov, I. *Langmuir* **2004**, *20*, 6727-6735.

(120) Needham, D.; McIntosh, T. J.; Lasic, D. *Biochim. Biophys. Acta* **1992**, *1108*, 40-48.

(121) Flory, P. J. *Principals of Polymer Chemistry*; Cornell Univ. Press: Ithaca, NY, 1971.

(122) De Gennes, P. G. *Adv. Colloid Interface Sci.* **1987**, *27*, 189-209.

(123) Marsh, D. *Biophys. J.* **2001**, *81*, 2154-2162.

(124) Harder, P.; Grunze, M.; Whitesides, G. M.; Laibinis, P. E.; Dahint, R. *J. Phys. Chem. B* **1998**, *102*, 426-436.

(125) Jeon, S. I.; Lee, J. H.; Andrade, J. D.; de Gennes, P. G. *J. Colloid Interface Sci.* **1991**, *142*, 149-158.

(126) Jeon, S. I.; Andrade, J. D. *J. Colloid Interface Sci.* **1991**, *142*, 159-166.

(127) Jeon, S. J.; Lee, J. H.; Andrade, J. D.; De Gennes, P. G. *J. Colloid Interface Sci.* **1991**, *142*, 149-158.

(128) Ashok, B.; Arleth, L.; Hjelm, R. P.; Rubenstein, I.; Onyuksel, H. *J. Pharm. Sci.* **2004**, *93*, 2476-2487.

(129) Photos, P. J.; Bacakova, L.; Discher, B.; Bates, F. S.; Discher, D. E. *Journal of Controlled Release* **2003**, *90*, 323-334.

(130) Lentz, B. R.; Lee, J. H. *Molecular Membrane Biology* **1999**, *16*, 279-296.

(131) Prime, K. L.; Whitesides, G. M. *J. Am. Chem. Soc.* **1993**, *115*, 10714-10721.

(132) Michel, R.; Pasche, S.; Textor, M.; Castner, D. G. *Langmuir* **2005**, *21*, 12327-12332.

(133) Tirosh, O.; Barenholz, Y.; Katzhendler, J.; Priev, A. *Biophys. J.* **1998**, *74*, 1371-1379.

(134) Warriner, H. E.; Keller, S. L.; Idziak, S. H. J.; Slack, N. L.; Davidson, P.; Zasadzinski, J. A.; Safinya, C. R. *Biophys. J.* **1998**, *75*, 272-293.

(135) Otsuka, H.; nagasaki, Y.; Kataoka, K. *Langmuir* **2004**, *20*, 11285-11287.

(136) Otsuka, H.; Nagasaki, Y.; Kataoka, K. *Langmuir* **2004**, *20*, 11285-11287.

(137) Crowe, J. H.; Crowe, L. M.; Chapman, D. *Science* **1984**, *223*, 701-703.

(138) Carpenter, J. F.; Crowe, L. M.; Crowe, J. H. *Biochim. Biophys. Acta* **1987**, *923*, 109-115.

(139) Mouradian, R.; Womersley, C.; Crowe, L. M.; Crowe, J. H. *Biochim. Biophys. Acta* **1984**, *778*, 615-617.

(140) Evans, S. V.; MacKenzie, C. R. *J. Mol. Rec.* **1999**, *12*, 155-168.

(141) Albersdorfer, A.; Feder, A. T.; Sackmann, E. *Biophys. J.* **1997**, *73*, 245-257.

(142) Soong, R.; Macdonald, P. M. *Biophys. J.* **2005**, *88*, 255-268.

(143) Bivas, I.; Winterhalter, M.; Meleard, P.; Bothorel, P. *Europhys. Lett.* **1998**, *41*, 261-266.

(144) Laradji, M. *Europhys. Lett.* **2002**, *60*, 594-600.

(145) Hristova, K.; Needham, D. *J. Colloid Interface Sci.* **1994**, *168*, 302-314.

(146) Tirosh, O.; Barenholz, Y.; Katzhendler, J.; Priev, A. *Biophys. J.* **1998**, *74*, 1371-1379.

(147) Rex, S.; Zuckermann, M. J.; Lafleur, M.; Silvius, J. R. *Biophys. J.* **1998**, *75*, 2900-2914.

(148) Mammen, M.; Gomez, F. A.; Whitesides, G. M. *Analytical Chemistry* **1995**, *67*, 3526-3535.

(149) Rex, S.; Bian, J.; Silvius, J. R.; Lafleur, M. *Biochimica et. Biphysica Acta* **2002**, *1558*, 211-221.

(150) Blankenburg, R.; Meller, P.; Ringsdorf, H.; Salesse, C. *Biochemistry* **1989**, *28*, 8214-8221.

(151) Stelzle, M.; Weissmüller, G.; Sackmann, E. *J. Phys. Chem.* **1993**, *97*, 2974-2981.

(152) Groves, J. T.; Mahal, L. K.; Bertozzi, C. R. *Langmuir* **2001**, *17*, 5129-5133.

(153) Jeppesen, C.; Wong, J. Y.; Kuhl, T. L.; Israelachvili, J. N.; Mullah, N.; Zalipsky, S.; Marques, C. M. *Science* **2001**, *293*, 465-467.

(154) Klein, J.; Luckham, P. *Nature* **1982**, *300*, 429-431.

(155) Burridge, K. A.; Figa, M. A.; Wong, J. W. *Langmuir* **2004**, *20*, 10252-10259.

(156) De Gennes, P. G. *Macromolecules* **1980**, *13*, 1069-1075.

(157) Roberts, C. J.; Davies, M. C.; Tendler, S. J. B.; Williams, P. M.; Davies, J.; Dawkes, A. C.; Yearwood, G. D. L.; Edwards, J. C. *Ultramicroscopy* **1996**, *62*, 149-155.

(158) Klein, J.; Luckham, P. *Macromolecules* **1984**, *17*, 1041-1048.

(159) Hansen, P. L.; Cohen, J. A.; Podgomik, R.; Parsegian, A. V. *Biophys. J.* **2003**, *84*, 350-355.

(160) Patel, S.; Tirrell, M. *Colloids and Surfaces* **1988**, *31*, 157-179.

(161) Noppl-Simson, D. A.; Needham, D. *Biophys. J.* **1996**, *70*, 1391-1401.

(162) Wu, H.; Wheeler, A.; Zare, R. N. *Proc. Natl. Acad. Sci. USA* **2004**, *101*, 12809-12813.

(163) Crommelin, D.; Van Bommel, E. *Int. J. Parm.* **1984**, *22*, 299-310.

(164) Crommelin, D.; Van Bommel, E. *Parm. Res.* **1984**, *1*, 159-164.

(165) Cicerone, M. T.; Soles, C. L. *Biophys. J.* **2004**, *86*, 3836--3845.

(166) Crowe, J. H.; Crowe, L. M. *Preservation of Liposomes During Freeze-drying, Liposome Technology*: Boca Raton, Fl., 1993.

(167) Wang, H.-S.; Kang, L. *Cryobiology* **2005**, *51*, 322-329.

(168) Crowe, J. H.; Clegg, J. S. *Anydrobiosis*; Dowden, Hutchinson & Ross: Stroudsburg, PA, 1973.

(169) Yoon, Y.; Pope, J.; Wolfe, J. *Cryobiology* **2003**, *46*, 271-276.

(170) Crowe, J. H.; Crowe, L. M.; Oliver, A. E.; Tsvetkova, N.; Wolkers, W.; Tablin, F. *Cryobiology* **2001**, *43*, 89-105.

(171) Sussman, A. S.; Lingappa, B. T. *Nature* **1959**, *130*, 1343-1346.

(172) Strauss, G.; Hauser, H. *Proc. Natl. Acad. Sci.* **1986**, *83*, 2422-2426.

(173) Hincha, D. K.; Hellwege, E. M.; Heyer, A. G.; Crowe, J. H. *Eur. J. Biochem* **2000**, *267*, 535-540.

(174) Crowe, J. H.; Crowe, L. M.; Carpenter, J. F.; Aurell-Wistrom, C. *Biochem. J.* **1987**, *242*, 1-10.

(175) Crowe, L. M.; Crowe, J. H. *Biochim. Biophys. Acta.* **1988**, *946*, 193-201.

(176) Chiantia, S.; Kahya, N.; Schwille, P. *Langmuir* **2005**, *21*, 6317-6323.

(177) Crowe, J. H.; Hoekstra, F. A.; Crowe, L. M. *Annu. Rev. Physiol.* **1992**, *54*, 579-599.

(178) Sun, W. Q.; Leopold, A. C.; Crowe, L. M.; Crowe, J. H. *Biophys. J.* **1996**, *70*, 1769-1776.

(179) Crowe, L. M.; Womersley, C.; Crowe, J. H.; Reid, D.; Appel, L.; Rudolph, A. *Biochim. Biophys. Acta.* **1986**, *861*, 131-140.

(180) Womersley, C.; Uster, P. S.; Rudolph, A. S.; Crowe, J. H. *Cryobiology* **1986**, *23*, 245-255.

(181) Ohtake, S.; Schebor, C.; Palecek, S. P.; de Pablo, J. J. *Biochim. Biophys. Acta.* **2005**, *1713*, 57-64.

(182) Semmler, K.; Wunderlich, J.; Richter, W.; Meyer, H. W. *J. Microscopy* **1998**, *190*, 317-327.

(183) Ricker, J. V.; Tsvetkova, N. M.; Wolkers, W. F.; Leidy, C.; Tablin, F.; Longo, M.; Crowe, J. H. *Biophys. J.* **2003**, *84*, 3045-3051.

(184) Tsvetkova, N. M.; Philips, B. L.; M., C. L.; Crowe, J. H.; Risbud, S. H. *Biophys. J.* **1998**, *75*, 2947-2955.

(185) Crowe, J. H.; Hoekstra, F. A.; Nguyen, K. H. N.; M., C. L. *Biochim. Biophys. Acta.* **1996**, *1280*, 187-196.

(186) Lee, C. W. B.; Waugh, J. S.; Griffin, R. G. *Biochemistry* **1986**, *25*, 3737-3742.

(187) Lee, S. L.; Debenedetti, P. G.; Errington, J. R. *J. Chem. Phys.* **2005**, *122*.

(188) Wolkers, W. F.; Oliver, A. E.; Tablin, F.; Crowe, J. H. *Carbohydr. Res.* **2004**, *339*, 1077-1085.

(189) Magazu, S.; Migliardo, F.; Mondelli, C.; Vadala, M. *Carbohydr. Res.* **2005**, *340*, 881-887.

(190) Cesaro, A.; Magazu, V.; Migliardo, F.; Sussich, F.; Vadala, M. *Physica B* **2004**, *350*, e367-e370.

(191) Crowe, J. H.; Carpenter, J. F.; Crowe, L. M. *Annu. Rev. Physiol.* **1998**, *60*, 73-103.

(192) Green, J. L.; Angell, C. A. *J. Phys. Chem. B* **1989**, *93*, 2880-2882.

(193) Koster, K. L.; Lei, Y. P.; Anderson, M.; Martin, S.; Bryant, G. *Biophys. J.* **2000**, *78*, 1932-1946.

(194) Groves, J. T.; Boxer, S. G.; McConnell, H. M. *J. Phys. Chem. B* **2000**, *104*, 11409-11415.

(195) Tamm, L. K. *Biochemistry* **1986**, *25*, 7470-7476.

(196) Yang, J.; Appleyard, J. *J. Phys. Chem. B.* **2000**, *104*, 8097-8100.

(197) MacMullen, T. P. W.; Lewis, R. N. A. H.; McElhaney, R. N. *Biochemistry* **1993**, *32*, 516-522.

(198) Cevc, G. *Biochim. Biophys. Acta.* **1991**, *1062*, 59-69.

(199) Enders, O.; Ngezahayo, A.; Wiechmann, M.; Leisten, F.; Kolb, H.-A. *Biophys. J.* **2004**, *87*, 2522-2531.

(200) Koynova, R.; Caffrey, M. *Biochim. Biophys. Acta* **1998**, *1376*, 91-145.

(201) Koynova, R.; Koumanov, A.; Tenchov, B. *Biochim. Biophys. Acta.* **1996**, *1285*, 101-108.

(202) Kaasgaard, T.; Leidy, C.; Crowe, J. H.; Mouritsen, O. G.; Jorgensen, K. *Biophys. J.* **2003**, *85*, 350-360.

(203) Parente, R. A.; Lentz, B. R. *Biochemistry* **1985**, *24*, 6178-6185.

(204) Thulborn, K. R.; Beddard, G. S. *Biochim. Biophys. Acta* **1982**, *693*, 246-252.

(205) Xie, A. F.; Yamada, R.; Gewirth, A. A.; Granick, S. *Phys. Rev. Lett.* **2002**, *89*, 2461031-2461034.

(206) Wolkers, W. F.; Looper, S. A.; McKiernan, A. E.; Tsvetkova, N.; Tablin, F.; Crowe, J. H. *Mol. Membr. Biol.* **2002**, *19*, 201-210.

(207) Wolkers, W. F.; Looper, S. A.; Fontanilla, R. A.; Tsvetkova, N.; Tablin, F.; Crowe, J. H. *Biochim. Biophys. Acta* **2003**, *1612*, 154-163.

(208) Koynova, R.; Brankov, J.; Tenchov, B. *Eur. Biophys. J.* **1997**, *25*, 261-274.

(209) Donaich, S. *J. Chem. Phys.* **1979**, *70*, 4587-4596.

(210) Carlson, J. M.; Sethna, J. P. *Phys. Rev. A.* **1987**, *36*, 3359-3374.

(211) Kirchner, S.; Cevc, G. *Eur. Biophys. J.* **1994**, *28*, 31-36.

(212) Luzardo, M.; Amalfa, F.; Nunes, A. M.; Diaz, S.; Biodi de Lopez, A. C.; Disalvo, A. E. *Biophys. J.* **2000**, *78*, 2452-2458.

(213) Pereira, C. S.; Lins, R. D.; Chandrasekhar, I.; Freitas, L. C. G.; Hunenberger, P. H. *Biophys. J.* **2004**, *86*, 2273-2285.

(214) Sum, A. K.; Faller, R.; de Pablo, J. J. *Biophys. J.* **2003**, *85*, 2830-2844.

(215) Skibinsky, A.; Venable, R. M.; Pastor, R. W. *Biophys. J.* **2005**, *89*, 4111-4121.

(216) Soderlund, T.; Alakoskela, J.-H. I.; Pakkanen, A. L.; Kinnunen, P. K. J. *Biophys. J.* **2003**, *85*, 2333-2341.

(217) Chiantia, S.; Giannola, L. I.; Cordone, L. *Langmuir* **2005**, *21*, 4108-4116.

(218) Heuberger, M.; Drobek, T.; Voros, J. *Langmuir* **2004**, *20*, 9445-9448.

(219) Kaushik, J. K.; Bhat, R. *J. Biol. Chem.* **2003**, *278*, 26458-26465.

(220) Lin, T.-Y.; Timasheff, S. N. *Protein Sci.* **1996**, *5*, 372-381.

(221) Arora, A.; Ha, C.; Park, C. B. *FEBS Lett.* **2004**, *564*, 121-125.

(222) Chapa, V. A.; Albertorio, F.; Diaz, A. J.; Cremer, P. S. *In Preparation*.

VITA

Name: Fernando Albertorio

Address: Department of Chemistry, 3255 TAMU, College Station, TX 77843

E-mail: albertorio@mail.chem.tamu.edu

Education: B.S., Chemistry, Pontifical Catholic University of Puerto Rico - Ponce Puerto Rico